CONTROLS ON POLAR ICE ALGAL COMMUNITIES AND THEIR COUPLING TO SPRING PHYTOPLANKTON COMMUNITIES.

A DISSERTATION SUBMITTED TO
THE DEPARTMENT OF EARTH SYSTEM SCIENCE AND
THE COMMITTEE ON GRADUATE STUDIES OF STANFORD UNIVERSITY
IN PARTIAL FULFILLMENT OF THE REQUIREMENTS
FOR THE DEGREE OF ENVIRONMENTAL EARTH SYSTEM SCIENCE
DOCTOR OF PHILOSOPHY

VIRGINIA SELZ

MAY 2018

This dissertation is online at: http://purl.stanford.edu/xw900vw9938

I certify that I have read this dissertation and that, in my opinion, it is fully adequate in scope and quality as a dissertation for the degree of Doctor of Philosophy.

Kevin Arrigo, Primary Adviser

I certify that I have read this dissertation and that, in my opinion, it is fully adequate in scope and quality as a dissertation for the degree of Doctor of Philosophy.

Karen Casciotti

I certify that I have read this dissertation and that, in my opinion, it is fully adequate in scope and quality as a dissertation for the degree of Doctor of Philosophy.

Leif Thomas

I certify that I have read this dissertation and that, in my opinion, it is fully adequate in scope and quality as a dissertation for the degree of Doctor of Philosophy.

Paula Welander

Approved for the Stanford University Committee on Graduate Studies.

Patricia J. Gumport, Vice Provost for Graduate Education

This signature page was generated electronically upon submission of this dissertation in electronic format. An original signed hard copy of the signature page is on file in University Archives.

Abstract

Sea ice algae, primary producers inhabiting sea ice, are a vital food source for upper trophic levels in spring prior to the development of summer phytoplankton blooms. As ice algae melt out of the sea ice they are eaten by zooplankton, exported to the benthos, or hypothesized to remain in the water column and seed phytoplankton blooms. Over the last few decades, ice conditions have dramatically changed on regional scales in the Arctic and Antarctic. This dissertation work seeks to understand *how these drastic environmental changes impact early spring primary producers.* Even though ice algal measurements have increased in recent years, they are still relatively scarce given the hostile nature of polar regions. In this dissertation, I expand ice algal measurements in the Chukchi Sea pack ice and provide the first measurements of spring ice algae along the west Antarctic Peninsula, while advancing our understanding of the linkages between ice algal and phytoplankton communities in polar oceans using a combination of fieldwork and ecosystem modeling.

In the Arctic, I characterized the biomass, physiology, and community composition of the spring ice algal bloom and identified drivers of bloom decline in the Chukchi Sea. Furthermore, I explored the ice algal seeding hypothesis using multivariate statistical analyses and growth model simulations constrained with paired ice and water column taxonomic composition and algal physiology field data (Chapter 1). To go beyond annual snapshots of ice algal communities, I applied a 1-D sea ice ecosystem state model to the Chukchi Sea region and examined how changing sea ice conditions impacted ice algal production over the 1980 to 2015 period (Chapter 2). Results from these studies suggest that ice algal production has decreased 22% over time due to sea ice melting earlier in the spring season. Ice algal production is likely to continue to decline into the future as ice continues to melt earlier in spring. Our field study suggests that declines in Chukchi Sea ice algal communities will have little effect on the timing of under-ice phytoplankton blooms.

In the Antarctic (Chapter 3), I characterized the taxonomic composition and physiological characteristics of the high biomass slush ice layer and used a combination of experiments to explore the fate of ice algae following ice melt. Combined, results from field samples and experiments suggest that the sea ice environment along the wAP does act as a reservoir and seeds water column populations of certain taxa that are better adapted to both low and high light conditions than their water column counterparts in spring. However, the dominant taxa seeded by

sea ice has a higher sinking rate compared to other phytoplankton groups and therefore sinks following ice melt and does not persist in phytoplankton and contribute to summer phytoplankton blooms.

Comparison of the ice algal communities and the linkages between ice algae and phytoplankton communities of the Arctic and Southern Oceans shows lower trophic level responses to environmental change in polar marine ecosystems are diverse and dependent on the system in question. Understanding how physical and biological drivers impact lower trophic levels is important to advance our knowledge on how continued climatic change will impact regional food web processes as well as broader global biogeochemical cycles.

Acknowledgements

Over the course of my time at Stanford, I have had the pleasure of working with amazing and talented members of the Arrigo Lab and others in the School of Earth, Energy, and Environmental Sciences. I am especially appreciative of the senior Arrigo lab members Gert van Dijken and Matt Mills and former member Anne-Carlijn Alderkamp for their advice and support throughout the course of this dissertation. Hannah Joy-Warren has played an instrumental part in this work contributing her *brainstormy* ideas, her infinite supply of David's Tea and Trader Joes chocolate peanut butter cups, and her endless positive encouragement. Kate Lowry has served as the best senior graduate student mentor anyone could have and I have greatly appreciated her candor in her own graduate research and post-PhD career endeavors. Kate Lewis has elevated the spirit of the office by sharing Murphy with us – sometimes. I am very grateful for all of the support of the past and present Arrigo lab members.

I am especially grateful to my advisor, Dr. Kevin Arrigo, for creating the team-oriented atmosphere that I have worked in over the last 5 years, as well as for giving me the opportunity to work with amazing scientists in some of the most beautiful places on Earth. Kevin has been supportive and encouraging of every idea I have wanted to pursue – *Can I take samples for this? Can I go to Woods Hole? Can we do ice stations?, Can I do this experiment?* and that mentorship has allowed me to advance (which was sometimes sideways or backwards instead of forward) in my own research development. In addition he has led by example in maintaining his ridiculous productivity levels, always working on a paper, while holding academic leadership positions and teaching multiple classes every quarter. I am very thankful of the opportunity I have had to complete my PhD under Kevin's advisorship.

While I have been surrounded by students and professors jazzed about science at Stanford, my family has watched from afar, puzzled as to why I would leave a job to become a student once again and fearful of what would become of me once I did obtain a PhD in Earth System Science. Despite their uncertainties, they have been overwhelmingly supportive throughout the ups and downs of the PhD and I have greatly appreciated their confidence in me. I would not have applied to Stanford, if it weren't for the wise encouraging words of East Coast friends – Dr. Stacy Plum and Monte Plum, and my last year of cross-country commutes at Stanford would have been extremely difficult without the kind and generous support of my in-laws Dr. Lois Gibbs and Stephen Lester. I am very grateful that Ryan Lester migrated West to California with me and continues to figure out how to balance one's own career with that of a significant other.

SuZee has made the most important contribution to maintaining my sanity while at Stanford.

Yes, Stanford has a wealth of resources for students, but none can replace my corgi-spitz mutt SuZee. She has reminded me that it is important to take breaks …. and go to Ft Funston for zoomies time. She has reminded me that there are a lot of other things that are much more stressful than a PhD – like when she eats raisins or a half pound of chocolate – and life can be short, especially for SuZee when she decides to poison herself. She is fine. I am grateful for the constant reminder she gives me to practice balance.

Lastly, I would like to acknowledge my parents who encouraged me from a very young age to ask questions and to be curious. From trips to the public library to vacations focused on education, I grew up in an environment that was centered around learning. I was fortunate enough to have very good teachers at a public school in a small town who cared and encouraged me to continue learning about things that interested me – the ocean. Thank you, I cherish my curious nature and my drive to ask questions and have pursued a career where I can continue to do that.

In addition to the support of lab members, my advisor, my friends, and my family, this work was partially funded by the National Science Foundation (NSF) Office of Polar Programs (ANT-1063592, PLR-1304563), National Aeronautics and Space Administration (Ocean Biology and Biogeochemistry, Cryosphere Science NNX10AF42G), and the McGee and Levorsen research grant (Stanford University, Department of Earth, Energy, and Environmental Sciences) and would not have been possible without the Captain and crew of the R.V. Nathaniel B. Palmer and the USCGC Healy.

Contents

List of Tables

List of Figures

Chapter 0

Introduction

0.1 Background

While the Arctic and Antarctic regions vastly differ, they are both experiencing rapid climate-induced change in first year (FYI) and perennial multi-year ice (MYI) cycles. Globally representing 8 – 13% of the Earth's surface, the sea ice supports a dynamic ecosystem (Tedesco et al. 2012) and impacts broader biogeochemical cycles (Loose et al. 2011). The productivity of the ocean ecosystem is also sensitive to the physical features of sea ice. Broad scale satellite analyses have linked recent sea ice declines to regional changes in annual primary production (Arrigo et al. 2011, Montes-Hugo et al. 2009). While both regions vary in ocean circulation, ice type, and taxonomic composition, multiple studies suggest ice dynamics affect primary production on a broad scale. Most have focused on sea ice and pelagic ecosystems separately; few have investigated the coupling between these two during periods of seasonal ice melt. The objective of this dissertation is to quantify how the physical aspects of sea ice impact its associated algal community, and in turn, explore how the ice algal communities impact the pelagic community. By focusing on areas that are physically and biologically diverse in both the Arctic and Antarctic, this research covers a wide range of potential ice-ocean interactions while advancing understanding on the coupling during transitional periods in the Chukchi Sea and the Western Antarctic Peninsula (WAP).

0.1.1 Seasonal Cycle of Sea Ice

Polar regions share similar connections between the ice and water column throughout the seasonal sea ice cycle. Phytoplankton are incorporated into ice during formation and growth (Garrison et al.1983, Booth et al. 1984) and released back into the water column during ice melt (Riebesell et al. 1991). Convection and surface flooding transport nutrient-rich seawater through brine channels, which support ice algal growth in early spring (Horner et al.1992) when light becomes available (Gosselin et al.1990). During this period, ice algal production is the main food source for both pelagic and benthic consumers (Michel et al. 1996). As the season advances, ice melt creates freshwater-stratified layers beneath the sea ice, cutting off nutrient supply to brine channels (Polashenski et al. 2015). Melt ponds form on the surface of warming ice in the Arctic, whereas in the Antarctic these features are mostly absent. Remaining ice algae either slough off or are flushed from ice during melt and are hypothesized to sink (export), be eaten (respired), or

become phytoplankton and continue to grow in the water column (production)(Michel et al.1996). Thinning ice and melt pond development increase light availability to phytoplankton (Palmer et al. 2014), the mixed layer shoals due to solar heating and ice-melt (Tang et al.1998), ice retreats and pelagic production increases (Mundy et al. 2014). While this seasonal ice algal to phytoplankton bloom progression is well established, the relative importance of the timing and connections between the two ecosystems is still poorly understood.

Comprising both ice that is attached to the coast (land-fast ice) and floating (pack ice) over the surface ocean, polar ice ecosystems are subject to different physical processes, resulting in features unique to the Arctic and Antarctic regions. In the Arctic, a snow covered consolidated ice pack transitions to broken melt pond-covered ice floes due to intense atmospheric solar heating (Perovich et al. 2012, Polashenski et al. 2012). Prior to melt onset, the ice algal community is predominantly located in the bottom few centimeters of the ice. Winter mixing transports nutrient-rich winter water to the surface ocean to support bottom ice algal growth in early spring (Gradinger 2009). In the southern hemisphere, a snow- covered consolidated ice pack transitions to smaller individual pancake-shaped ice floes, which are generally thinner with equal or greater snow cover. Enhanced snow loading on thinner Antarctic ice causes snow or superimposed ice formation, where seawater flooding or snowmelt freezes at the surface. These processes, combined with seasonal internal melting, form gap layers (Jeffries et al. 1997, Ackley et al. 1994). Also referred to as “freeboard” or “infiltration” layers, these sections are characterized by a “honeycomb-like ice matrix filled with seawater below a surface layer of snow and ice” (Ackley et al. 2008, 1994). Because of their porous nature, they can support high concentrations of algal biomass (172-370 μg L^{-1}, Kattner et al. 2004, Fritsen et al. 1998, 2001). Understanding how these differing physical sea ice features in the Arctic and Antarctic impact ice algal blooms will advance knowledge on their potential connections to water column phytoplankton.

0.2 Motivation and Objective

0.2.1 Arctic Ice-Ocean Ecosystem Coupling

Because peak bloom timing in ice precedes the water column, many have hypothesized that sea ice algae “seed” the phytoplankton bloom, and enable the community to go from low to extremely high concentrations over short timescales (Syvertsen 1991, Jin et al. 2007). Previous studies across the Arctic have attempted to address the “seeding” hypothesis by comparing phytoplankton samples to known ice- associated species, ice algae samples to known phytoplankton species, and in very few studies concurrent ice to water column samples. Most of the known ice associated species are pennate diatoms of either benthic or pelagic origin; centric diatoms are less common in sea ice (Horner 1985). Often species are shared between the two

environments, but the concentrations of these shared species are low in the water column (<15%) (Schandelmeier and Alexander 1981, Booth 1984, Tremblay et al. 2006). When ice-originating phytoplankton are dominant, cells are either too unhealthy to contribute to pelagic production (Horner and Schrader 1982) or early spring "seeding" of ice algae is succeeded by centric diatoms (pelagic sp.) prior to bloom initiation (Michel et al. 1996). Other studies have found more similarities in spring compared to summer, supporting seasonal succession prior to phytoplankton bloom development (Szymanski and Gradinger 2016). These observations suggest that when shared species are present, the "seeding" effect is limited in duration because ice and pelagic blooms are separated by dominant species and time. These studies support the historical Arctic view: pennate diatoms dominate the ice in early to late spring while centric diatoms dominate the water column after ice melt (Alexander 1980, Horner and Alexander 1972, Michel 1993).

Many of these studies have focused on the Canadian Archipelago, the Beaufort Sea, or the Eastern Arctic; few have focused on the Chukchi Sea. Of the studies focused on this region, two suggested that ice algae make up a considerable portion of the phytoplankton (Saito and Taniguchi 1978), but their presence is short-lived (Hameedi 1978). Other work found no ice algae present in the water column (Alexander 1980). More recent studies have described *Fragilariopsis oceanica* (pennate diatom)*, Thalassiosira sp*. (centric diatom) (Sukhanova et al. 2009) and *Chaetoceros sp.* (centric diatom)(Laney et al. 2014) as dominant bloom-forming species in the Chukchi, but data addressing potential connections between ice and pelagic communities are lacking. The discovery of massive phytoplankton blooms developing beneath melt-ponded ice (Arrigo 2014, Lowry and Sosik 2014), make these coupling questions especially relevant to the Chukchi Sea. Rather than the traditional view of phytoplankton blooms at the edge of receding pack ice, under-ice blooms develop weeks prior to ice melt (Lowry et al. 2014). If under ice blooms are as widespread as suggested (Lowry et al. 2014), the traditional view of timing between ice and pelagic blooms may not be as temporally separated as once thought. Understanding how ice algal and pelagic blooms are potentially linked will yield insight into the drivers of species composition and bloom timing variability in the Chukchi Sea.

Beyond the role taxonomy plays in ocean-ice coupling, field and modeling studies confirm that ice affects light transmission to the water column (Light et al. 2008, Polashenski et al. 2012) and light availability for arctic phytoplankton (Palmer et al. 2014, Tedesco et al. 2012). Ponded and non-ponded FYI transmit more light than MYI over broad spatial scales (Nicolaus et al. 2012). Snow plays the largest role in blocking light to the water column, reflecting 50-90% of incoming solar radiation back to the atmosphere, depending on melt stage. After snow melt, light transmission through melt pond-covered (>10%) FYI, lacking a dynamic biological community,

is sufficient to support under ice phytoplankton blooms (Palmer et al. 2014). Furthermore, modeling studies by Tedesco et al. (2012) suggest the timing of ice melt will influence the magnitude and timing of both ice and pelagic production.

The Chukchi Sea is a prime area of study for these questions of ice-ocean ecosystem coupling. Primary production in the ecosystem rapidly transitions from one dominated by ice algae in early spring (Gradinger 2009) to one dominated by phytoplankton (Sukhanova et al. 2009, Arrigo et al. 2014) in early summer. A fraction of phytoplankton blooms begin under melt pond-covered ice, prior to break up (Lowry et al. 2014, Arrigo et al. 2014) and production after this initial bloom is fueled by nutrient-rich winter water circulation pathways (Lowry et al. 2015). Given the observed influence of ice on primary production in this region, fully characterizing how both the physical and biological components of ice impact ice algal and phytoplankton communities will improve our knowledge of the impacts of future declines in sea ice.

0.2.2 Antarctic Ice-Ocean Ecosystem Coupling

Unlike the Arctic, shared ice and pelagic species are often dominant bloom-forming taxa in the Southern Ocean. For example, species including, but not limited to, *Phaeocystis antarctica* (Garrison et al. 1987, Lannuzel et al. 2013), *Fraglariopsis cylindrus* and *Chaetoceros sp.* (Mangoni et al. 2009) can be found in both ice and ice-edge bloom communities in early spring, but these observations are inconsistent. Rapid sinking and intense grazing pressure of ice-originating phytoplankton are hypothesized to explain patchy distributions (Kuosa et al. 1992). Community size structure data and mesocosm experiments suggest that small ice algae (<10 μm) are viable to "seed" phytoplankton communities (Lannuzel et al. 2013), but larger cells are subject to aggregation and rapid export (100-500 m d^{-1}, Riebesell 1991), while grazing plays a broader regulatory role in overall ice-edge development (Geisenhagen 1999). Because most studies have focused on the Ross and Weddell Seas, there is a paucity of information on ice algal communities in the west Antarctic Peninsula (WAP), let alone their role in ice-ocean coupling.

Studies specific to the WAP have focused on the relationships between productivity, ice dynamics, and regional circulation. Results indicate processes driving production and species distributions are diverse, reflecting the ecological regimes of the WAP: the permanently open ocean zone (POOZ), seasonal ice zone (SIZ), and coastal continental shelf zone (CCSZ). These biomes are distributed across the coastal (0-300 m deep, 5-10 m MLD), continental shelf (300-1000 m deep, 25-100 m MLD), and continental slope (>1000 m deep, 200 km from coast) regions. Increases in air and sea temperatures (1 and 2°C, respectively) have decreased sea ice duration by 92 days (1979-2013) in the northern WAP and transformed a MYI to FYI cover in the southern WAP (Ducklow et al. 2013). Stratification and mixed layer depth affect both the

composition and total magnitude of phytoplankton blooms, but the type of effect varies regionally (Garibotti et al. 2005, Venables et al. 2013, Montes-Hugo et al. 2009). In a coastal region, heavy ice in winter correlated with larger spring blooms and was explained by reduced mixing, caused by increased water column stability, ultimately increasing light and iron availability (Venables et al. 2013, Annett et al. 2010). In contrast, a similar coastal region and off shelf area (but not mid-shelf) had higher production when MLDs were deeper, rather than shallower, over a 12-year time-series (Vernet et al. 2008). While its still unclear how MLD affects cell size structure or taxonomic composition, in two WAP sections, late ice retreat corresponded with small cell-dominated communities throughout the spring and summer season (Montes-Hugo et al. 2008). On a broader scale along the WAP, satellite analyses show annual production has increased in the South and decreased in the North in response to declining sea ice (Montes-Hugo et al. 2009). Phytoplankton cell size structure also increases from the North (small cryptophytes) to the South WAP region (large diatoms)(Montes-Hugo et al. 2008). Changes are tied to the contrasting ways that declining ice affects light and nutrient availability in these two regions (Montes-Hugo et al. 2009). These studies suggest that complex interactions exist between ice cover, stratification, and resource availability.

Beyond sea ice, atmospheric and oceanographic features influence WAP phytoplankton dynamics. Along the shelf break, the Antarctic Circumpolar Current (ACC) episodically transports upper circumpolar deep water (UCDW) onto the shelf, which supports subsurface productivity maxima (Prezelin et al. 2000, 2004; Dinniman et al. 2004). Observed diatom-dominated blooms correspond to UCDW intrusions (Kavanaugh et al. 2015, Prezelin et al. 2004); however, Serebrennikova and Fanning (2004) found UCDW intrusions diluted silicate rather than enhanced macro-nutrient concentrations. During positive Southern Annular Mode (SAM) years, UCDW intrusions are expected to increase (Dinniman et al. 2011). Montes-Hugo et al. (2009) suggest that these intrusions may explain observed increases in cell size in central WAP continental slope waters. In general, small cells follow an on to offshore gradient; however, this pattern is broken up by areas of unexpected small (coastal) or large (mid-shelf, slope) cells. Production also displays a high (1000 mg C m^2 day^{-1}) to low (100 mg C m^2 d^{-1}) onshore to offshore gradient, averaging 182 +/- 107 g C m^{-2} yr^{-1} that peak in January (15 mg C m^{-3}) (Vernet et al. 2008). Similar to studies focused on sea ice-productivity relationships, these suggest a heterogeneous biological response to varied physical forcing along the WAP (Montes-Hugo et al. 2008).

WAP research has suggested production and species composition are tied to stratification, affecting light and/or nutrient availability and sea ice in this region has been hypothesized to

release iron and/or large algal cells into the water column (Montes-Hugo et al. 2008), yet no spring sea ice data and no assessment of linkages between ice algal and phytoplankton communities exist for this region. Investigating these connections will advance understanding on the coupling between the physical and biological components of the ice and ocean ecosystems along the WAP.

0.2.3 Novel Insights into Coupled Ice-Ocean Ecosystems

The Chukchi Sea and the WAP are relevant regions for ice-ocean coupling questions because sea ice data are scarce and previous studies clearly show ocean biology responds to sea ice, but the type of response is inconsistent. Fully characterizing how both the physical and biological components of ice affect productivity is of utmost importance to understanding current drivers and future changes in polar marine ecosystems.

This dissertation focuses on the Arctic (Chapters 1 and 2) and the Antarctic (Chapter 3) and characterizes the ice algal community and its linkage to the phytoplankton community in these two polar regions. Chapter 1 investigates the controls on spring ice algal blooms using field cruise data and quantifies the impact of ice algal seeding on phytoplankton blooms in the Chukchi Sea using a data-constrained growth model. Chapter 2 elucidates the environmental features that drive declines in ice algal production between 1980 to 2015 in the Chukchi Sea using a coupled biological physical model. Chapter 3 uses a combination of field surveys and shipboard experiments to characterize the ice algal bloom and assess its potential to impact spring and summer phytoplankton blooms following sea ice melt.

Chapter 1

Ice algal communities in the Chukchi and Beaufort Seas in spring and early summer: composition, distributions, and coupling with phytoplankton assemblages.

SELZ V, LANEY S, ARNSTEN AE, LEWIS KM, LOWRY KE, JOY-WARREN HL, MILLS MM, VAN DIJKEN GL, ARRIGO KR

To understand the controls on distributions of ice algal communities in spring and the role of ice algae in under-ice bloom development through possible seeding, we sampled the ice and water column in the Chukchi and Beaufort Seas over spring and summer. Field observations showed that high springtime concentrations of bottom ice algal communities were released from the ice into the water column by summer. Furthermore, during our spring sampling, bottom ice algal concentrations were highly variable. Declines in spring ice algal biomass and physiological state were correlated with ice melt, rather than light or nutrient availability. Nonparametric multivariate data analysis of the seasonal succession of phytoplankton and ice algal community composition illustrated that the loss of algae from the sea ice temporarily elevated water column chlorophyll a (Chl a) levels, as ice-derived taxa dominated the phytoplankton biomass. Model simulations, constrained by field observations from this study, further suggested that seeding by ice algae was brief and alone could not account for the phytoplankton biomass concentrations exceeding 2 mg Chl a m^{-3} observed in our study. Ice algal sloughing from the sea ice to the water column contributes biomass to the phytoplankton community. However, this signal of ice-derived taxa is brief and non-ice derived taxa dominate phytoplankton blooms later in the spring and summer.

This is the peer reviewed version of the following article [Selz V, Laney S, Arnsten AE, Lewis KM, Lowry KE, Joy-Warren HL, Mills MM, van Dijken GL, Arrigo KR. 2017. Ice algal communities in the Chukchi and Beaufort Seas in spring and early summer: composition, distributions, and coupling with phytoplankton assemblages. *Limnology and Oceanography*] which has been published in final form at

doi:10.1002/lno.10757. This article may be used for non-commercial purposes in accordance with Wiley Terms and Conditions for Self-Archiving.

1.1 Introduction

Arctic shelves, the most productive regions of the Arctic Ocean, have experienced rapid changes in seasonal sea ice characteristics and melt progression over the last several decades (Serreze et al. 2007, Maslanik et al. 2007, Haas et al. 2008, Kwok and Rothrock 2009). Some of the most extreme changes have occurred in the Chukchi Sea, an inflow shelf in the western Arctic Ocean. Shifts in the timing of melt and freeze onset have altered the duration and extent of sea ice (Stroeve et al. 2014), a critical habitat for ice algal communities that support a diverse suite of upper trophic level organisms during the spring and early summer (Arrigo et al. 2009). Sea ice algae account for approximately 2 to 30% of total seasonal production (Legendre et al. 1992, Rysgaard et al. 2001, Arrigo 2013) and fuel both pelagic and benthic ecosystems following ice melt (Michel et al. 1996, Dunton et al. 2005, Grebmeier et al. 2006). Throughout the seasonal transition from ice cover to open water, ice algal communities serve as a rich and concentrated food source, which is especially important to consumers in early spring when phytoplankton concentrations are low (Michel et al. 1996, Durbin and Casas 2013).

The dynamics of the ice algal bloom, beginning in early March and peaking by mid to late May, are primarily dependent on the seasonal cycles of sea ice, light, and nutrient availability (Bergmann et al. 1991, Rózańska et al. 2009, Leu et al. 2015). In late fall and winter, phytoplankton are incorporated into sea ice during its initial formation and subsequent growth (Garrison et al. 1983, Booth 1984, Welch and Bergmann 1989, Gradinger and Ikävalko 1998, Rózańska et al. 2009, Niemi et al. 2011). Nutrient-rich seawater exchanges with the ice skeletal layer located at the ice-water interface and a network of brine channels allows for transport of nutrients within the full ice structure (Horner et al. 1992). Net algal growth occurs when light intensity increases in spring (Gosselin and Legendre 1990), provided that snow depth is sufficiently thin to allow adequate light transmission (Gosselin et al. 1986, Welch et al. 1987, Welch and Bergmann 1989, Bergmann et al. 1991, Cota et al. 1991). During this period, ice algal communities are acclimated to extremely low light and often exhibit high photosynthetic efficiencies (Bergmann et al. 1991) and photosynthetic and photoprotective pigment plasticity (Petrou et al. 2011, Alou-Font et al. 2013), enabling them to adjust to changes in the light environment on timescales of less than a week (Juhl and Krembs 2010, Alou-Font et al. 2013).

Whereas light controls ice algal bloom initiation, either surface water nutrient availability or melting processes set the upper limits on ice algal biomass (Cota et al. 1991, Rózańska et al.

2009). Snow and ice melt create stratified freshwater layers beneath the sea ice (Lavoie et al. 2005), inducing nutrient limitation by cutting off convective nutrient transport (Polashenski et al. 2015). Melting snow further alters the physical environment of the ice through local heating and brine flushing that lead to sloughing of algae from the bottom ice environment (Apollonio 1965, Fortier et al. 2002, Lavoie et al. 2005, Juhl and Krembs 2010). Rapid changes in snow thickness, and subsequently the light environment of ice algae, can also enhance photoinhibition, leading to lower growth rates (Juhl and Krembs 2010). After the remaining ice algae slough off or are flushed from their habitat in late spring and early summer (Lavoie et al. 2005), they either sink (Apollonio 1965, Tremblay et al. 1989), are consumed by zooplankton (Carey and Boudrias 1987, Tremblay et al. 1989, Michel et al. 1996), or seed phytoplankton communities (Horner and Schrader 1982, Hameedi 1978, Syvertsen 1991, Wiktor 1999, Mangoni et al. 2009). Since similar species are observed in the ice and water column (Booth 1984, Wiktor 1999, Schandelmeier and Alexander 1981, Syvertsen 1991, Szymanski and Gradinger 2016, Quillfeldt et al. 2003), the extent to which sea ice algae contribute to export to the benthic community versus seeding spring phytoplankton blooms remains of considerable interest.

Despite the essential roles ice algae play in seasonal production and export, few studies have assessed these communities in the pack ice of the Chukchi Sea. Because nutrient concentrations are high throughout the spring (Cota et al. 1991, Kirchman et al. 2009, Sukhanova et al. 2009, Arrigo et al. 2017), the Chukchi Sea has the potential to support higher ice algal production than lower nutrient regions such as the Canada Basin (Leu et al. 2015). Previous Chukchi Sea studies confirmed high and variable levels of spring ice algal production in pack ice (Meguro et al. 1966, Ambrose et al. 2005, Gradinger 2009), but were unable to identify the drivers of variability of the ice algal bloom.

Here we present results from three studies conducted in the Chukchi Sea, one in the spring of 2014 and two in the summers of 2010 and 2011 that assessed the environmental controls on ice algal community biomass distributions and physiological state. Observations of the coupled ice-pelagic community are rare and especially relevant in this region due to the recent changes in sea ice cover (Stroeve et al. 2014) and the discovery of massive phytoplankton blooms that develop beneath the ice in late spring and summer (Arrigo et al. 2014). The primary goal of the present study was to assess the dominant environmental factors influencing late spring and early summer ice algal community distributions and to quantitatively examine the maximum potential for ice algae to seed subsequent water column blooms of phytoplankton. Using field observations, we characterized microalgal community composition in both the sea ice and underlying water column. We then used statistical data analyses and a numerical simulation to quantitatively test

the hypothesis that sea ice algae can seed water column phytoplankton blooms in the Chukchi Sea.

1.2 Methods

The SUBICE and ICESCAPE field campaigns covered the spring to summer ice melt transition of the Chukchi Sea and western Beaufort Sea aboard the USCGC *Healy*. Sampling occurred from mid May through mid June 2014 (SUBICE) and mid June through late July 2010 (ICESCAPE I) and 2011 (ICESCAPE II). The summer ice stations from ICESCAPE I and II are analyzed and discussed as one summer season, since both were sampled at the same time of year, during the late stage of ice melt (melt-ponds present, no snow) when ice depth and depth-integrated ice algal biomass are similar (t-test, p = n.s). Summer sea ice (ICESCAPE) is compared to spring sea ice (SUBICE), which was sampled prior to advanced melt onset (ice-covered, no melt ponds, with snow) with significantly different ice depths and depth-integrated biomass. These three field studies accounted for 37 paired ice and water column stations (Figure 1.1).

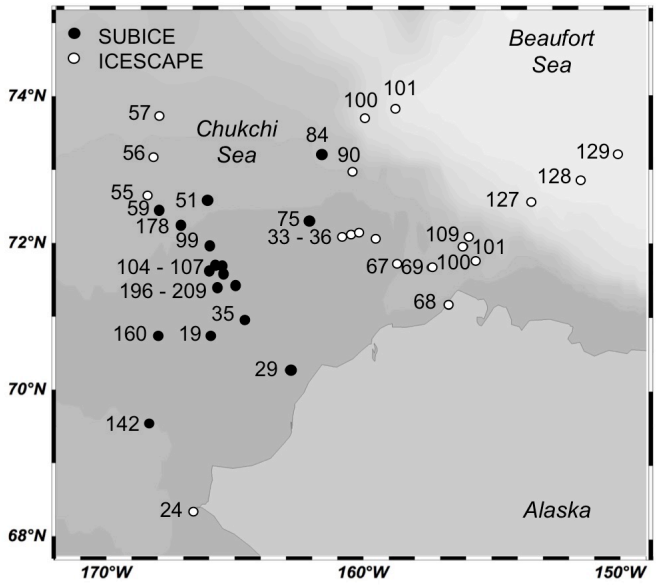

Figure 1.1 Ice stations occupied during the ICESCAPE (I and II; white circles) and SUBICE (black circles) cruises.

1.2.1 Characterizing the ice and water environment

Satellite Measurements of Sea Ice Cover. Special Sensor Microwave Imager (SSM/I, 25 km resolution) data obtained from the National Snow and Ice Data Center were used to quantify sea ice concentrations in our study area. For this study the timing of ice melt was defined as the

day at which sea ice concentration at a given station dropped below 50%. This threshold was used to calculate the number of days until ice melt after the day of sampling at each station. Images were also used to calculate the distance from the station to the ice edge, which was defined by the 50% ice concentration contour at the time of sampling. This 50% threshold for SSMI data best approximated the ice edge visible in the much higher resolution Moderate Resolution Imaging Spectroradiometer (MODIS) Aqua quasi-true color images and is consistent with methods used to detect the ice edge by Lowry et al. (2014) and Arrigo et al. (2012, 2014).

Ice and water column field sampling. Ice station sampling was conducted near solar noon at each ice station. Snow depth was measured directly with a meter stick and recorded at an array of 15 locations within a 5 m radius around ice core sampling sites. Sea ice cores were collected with a SIPRE ice corer (0.075 m interior diameter), measured for length, and cut into 0.1 m sections. Because ice coring can under sample tenuously attached bottom ice communities, we cored slowly and took care to disturb the bottom ice as little as possible. Our bottom biomass observations are within the range of others for this region (Ambrose et al. 2005, Gradinger 2009) and often higher than Arctic ice studies using other methods of ice algal collection, including SCUBA (Melnikov 1997) and a Slurp gun (Gosselin et al. 1997).

After collecting ice cores, 0.25 L of 0.2 µm filtered seawater (FSW) was added to bottom ice sections (0.1 m) to minimize osmotic shock due to melting, prior to transport to ship. Sea ice temperature profiles were measured in the field at 0.1 m intervals along one ice core following Polashenski et al. (2015). Ice core sections were stored in plastic containers for transfer to the ship in dark, thermally insulated coolers. Onboard, 2 L of FSW were added to maintain a salinity of >28 in melting sea ice samples and melted samples were analyzed within 6 to 8 hours of collection. Bulk salinity and nutrients were measured in melted core sections that did not receive FSW. Salinity was measured using either a hand-held refractometer (ICESCAPE I & II) or a Guildline 8400B salinometer (SUBICE). Water column samples were collected with a CTD rosette (~2, 5, 10, 25, 50 m) at or near corresponding ice stations. A subset of bottom sea ice (0.1 m) and surface water column samples was size-fractionated using 20 µm Nitex mesh. The >20 µm fraction was calculated by subtracting the <20µm fraction from the whole sample.

Nutrients. Inorganic nutrient samples from the water column and sea ice (bulk nutrients) cores that did not receive FSW were measured onboard the ship. Nitrate (NO_3^-), silicate ($Si(OH)_4$), phosphate (PO_4^{3-}), and ammonium (NH_4^+) concentrations were analyzed with a Seal Analytical continuous-flow AutoAnalyzer 3 (AA3) as described in Mills et al. (2015). Nutrients in bottom sea ice (0.1 m, (Ice_n), were calculated, assuming conservative mixing with seawater, from mean deepwater nutrient to salinity seawater ratios (SW_n:SW_s) and the bulk ice salinities

(Ice_s) where $SW_s:SW_n = Ice_s:Ice_n$

Irradiance. Incident surface irradiance was measured from 320 to 950 nm with 3 nm resolution using a RAMSES ACC-2 VIS TriOS hyperspectral radiometer system positioned just above the sea ice. Photosynthetically active radiation (PAR; 400 to 700 nm) available to the bottom ice algal layer was calculated using a two-layer light attenuation model including snow and ice

$$E_z = E_0 e^{(-k_s z)} + E_{ice} e^{(-k_{ice} z)} \quad (1)$$

where E_0 is the visible irradiance measured at the air-snow interface, E_{ice} is the visible irradiance modeled at the snow-ice interface, and k_s and k_{ice} are the attenuation coefficients for snow (16 m^{-1}; Grenfell and Maykut 1977) and for ice (1.4 m^{-1}; Ebert et al. 1995). Mean snow and ice depths (z) from each station were used to calculate light available to the upper surface of the bottom ice algal layer (E_z).

Spectral irradiance transmitted through the surface snow-ice layer was measured using a radiometer positioned immediately beneath the sea ice. The instrument had an articulating arm that extended the radiometer horizontally 2.5 m from the hole in which it was deployed. Approximately 15 irradiance measurements were made per station at solar noon. Mean daily under-ice surface water PAR was calculated from the measured light transmittance through the sea ice recorded at solar noon and the mean daily shipboard PAR. Mean daily under-ice surface water PAR was attenuated through the water column using the the Beer-Lambert law with a water column diffuse attenuation coefficient (k_w) of 0.1 m^{-1}, which was within the range measured during our study and others (Stambler et al. 1997). Mean daily PAR was calculated as the vertical integral of light in the mixed layer (ML) divided by the mixed layer depth (MLD).

1.2.2 Algal biomass, physiology, and taxonomic composition

Pigments, particulate organic carbon (POC), particulate organic nitrogen (PON) analysis. Samples (100-200 ml) for Chl *a* concentration were prepared by filtering either seawater or melted sea ice through 25 mm Whatman (GF/F). Chl *a* pigment concentrations were measured fluorometrically (Holm-Hansen et al. 1965) using a Turner 10-AU fluorometer (Turner Designs, Inc.) after extraction in 5 ml of 90% acetone in the dark at 3°C for 24 h. The fluorometer was calibrated using pure Chl *a* (Sigma). Samples (1000-2000 ml) for analysis of other pigments were measured using high performance liquid chromatography (Wright 1991), following Zapata et al. 2000. Pigment samples were flash frozen in liquid nitrogen and stored at -80°C until analysis. Samples for POC and PON were filtered onto pre-combusted (450°C for 4 h) 25 mm GF/Fs. Filters were dried at 60°C for approximately 24 h and then stored for later analysis

onshore where they were packed in tin capsules (Costech Analytical Technologies, Inc.) for elemental analysis on an Elementar Vario El Cube or Micro Cube elemental analyzer (Elementar Analysensysteme GmbH, Hanau Germany) interfaced to a PDZ Europa 20-20 isotope ratio mass spectrometer (Sercon Ltd, Cheshire, UK). The concentration of POC and PON in the sea ice was then calculated from the known volumes of melted sea ice and particle-free diluent seawater that was added to keep salinities >28.

Photosynthesis-irradiance relationships. P-E relationships were examined using a short term (2 h) ^{14}C-bicarbonate incorporation technique (Lewis and Smith 1983, as modified by Arrigo et al. 2010) on bottom ice sections (0.1 m, 1 section per station), in a photosynthetron using 14 light intensities ranging from 1 to 550 µmol photon m^{-2} s^{-1}. The carbon uptake rates were calculated using a nonlinear least-squares regression fit to the relationship of Platt et al. (1980), as modified by Arrigo et al. (2010)

$$P^* = P_S^* \left(1\text{-}e^{\frac{-\alpha^* E}{P_S^*}}\right) e^{\frac{-\beta^* E}{P_S^*}} \text{-} P_0^* \quad (2)$$

where P^* is the measured Chl *a*-specific photosynthetic rate (mg C mg^{-1} Chl *a* h^{-1}) at a given photosynthetron irradiance E (µmol photon m^{-2} s^{-1}), P^*_s is the light saturated photosynthetic rate in the absence of photoinhibition, α^* (mg C mg^{-1} Chl *a* h^{-1} (µmol photon m^{-2} s^{-1})$^{-1}$) is the initial slope of the P-E curve, b^* is the photoinhibition term (mg C mg^{-1} Chl *a* h^{-1} (µmol photon m^{-2} s^{-1})$^{-1}$), and P_0^* is the rate of DIC uptake in the dark. P-E parameters were only used when the fits were statistically significant (r^2 >0.70 and p <0.05). The maximum photosynthetic rate (P^*_m; mg C mg^{-1} Chl *a* h^{-1}) was then calculated as

$$P_m^* = P_s^* \left(\frac{\alpha^*}{\alpha^*+\beta^*}\right)\left(\frac{\beta^*}{\alpha^*+\beta^*}\right)^{\frac{\beta^*}{\alpha^*}}. \quad (3)$$

The photoacclimation parameter E_k (µmol photon m^{-2} s^{-1}) was calculated as $\frac{P^*m}{\alpha^*}$. Carbon-specific growth rate µ (d^{-1}) was then calculated from the measured photosynthetic parameter (α^*), the daily mean water column irradiance (E), and the POC:Chl a ratio as

$$\mu\ (d^{-1}) = \frac{\alpha^* E}{POC{:}Chl\ a}. \quad (4)$$

Maximum carbon-specific growth rates μ_{max} (d^{-1}) were calculated using P^*_m and POC:Chl *a* ratios. The accumulation rates of PON in the sea ice and therefore the uptake of N from the water column below (mmol N m^{-2} d^{-1}) was calculated from PON accumulation in the bottom 0.1 m of the ice, assuming a 60 d bloom period.

Variable fluorescence parameters. Melted diluted ice samples from the bottom core section (0.1 m) were dark acclimated in 60 ml HDPE bottles for 30 min at 0°C before measuring variable fluorescence parameters using a bench top fast repetition rate fluorometer (LIFT-FRR, Soliense; Kolber et al. 1998) at an excitation wavelength of 470 nm. Blanks were prepared by filtering the sample through a 0.2 μm polycarbonate syringe filter. Blank-corrected values (Cullen and Davis 2003) for initial fluorescence (F_o), maximum fluorescence (F_m), and the effective absorption cross section (σ_{PSII}, $Å^2$ $quanta^{-1}$) provide information on the photophysiological state of photosystem II (PSII). These data were used to calculate the maximum quantum efficiency of PSII (F_v/F_m; Maxwell and Johnson 2000).

Taxonomic composition. Samples from both the ice core bottom sections and the water column were examined for algal taxonomic composition. Digital micrographs of nano- and micro-size ice algae and phytoplankton were acquired with a custom-built Imaging FlowCytobot (IFCB; Olson and Sosik 2007) developed for shipboard use on icebreakers (Laney and Sosik 2014). Algae and phytoplankton in small volumes of seawater (1 to 5 ml) were injected through a cytometry flow cell (860 x 180 μm) and each Chl *a* containing particle (chain, colony, or cell) triggered the digital camera. To prevent large cells from clogging the flow cell samples were pre-filtered over 130 μm Nitex mesh. The combination of the size of the Nitex mesh, the size of the flow cell chamber, and the fluorescence trigger sensitivity limited the IFCB cell-size detection range to roughly 8 to 300 μm. All digital micrographs were classified manually and assisted by the supervised machine learning strategy discussed in Laney and Sosik (2014). Overall, 35 classes were identified in these samples, with 28 classes representing ice algae or phytoplankton identified to the genus level (Appendix A1).

1.2.3 Data analysis

Spring (SUBICE) and summer (ICESCAPE I & II) data were compared using Welch's *t*-test (*t* (adjusted degrees of freedom) = t-statistic, p value) and size-fractioned data from spring were compared using paired *t*-test analyses (R version 3.2.4). Relationships between biological and environmental variables were explored using Type I and II (OLS, MA) linear regression analyses (R, lmodel2, Legendre 2015). When high collinearity (condition number > 10) was detected, best subset regression and Bayesian Information Criterion (BIC) were used for model selection (R, LEAPS).

Taxonomic distributions and environmental variables were analyzed using both an ordination (Detrended Correspondence Analysis (DCA) and Canonical Correspondence Analysis (CCA)) and a clustering approach (Hierarchical Clustering Algorithm) to avoid biases in interpretation arising from using only a single nonparametric multivariate method (Ramette 2007).

Correspondence analyses (R, VEGAN, Oksanen et al. 2016) examine the variability in taxonomic composition across environmental gradients. This approach, frequently used in studies of terrestrial and freshwater ecology (reviewed in Ramette 2007), assumes that the taxonomic response is unimodal along an environmental gradient (Ter Braak 1985, Ter Braak and Prentice 1998). In our study region, seasonal succession cycles of ice algae and phytoplankton suggest that many of these taxa follow unimodal distribution patterns where specific taxa dominate in one of these environments: the spring sea ice algae peak bloom (summarized in Arrigo et al. 2009 and Leu et al. 2015), summer ice algae post-bloom (Rozanska et al. 2009), spring phytoplankton pre to early bloom (Suhkanova et al. 2009), summer phytoplankton peak bloom (Suhkanova et al. 2009, Laney et al. 2014), or summer phytoplankton post-bloom (Laney and Sosik 2014). The DCA provides a measure of unimodal response and supports the use of CCA if the dataset contains approximately 4 standard deviations or greater along the length of the DCA Axis 1, as seen in our study (Appendix A5) (Ramette 2007).

The CCA was used to test the hypothesis that taxonomic community composition is related to the seasonal ice melt cycle (Croft and Chow-Fraser 2007, Sharma and Jackson 2007, Ter Braak and Verdonoschot 1995, Ramette 2007). CCA constrains the ordination of the taxonomic matrix with standardized environmental variables and is appropriate with a clear *a priori* hypothesis (taxonomic community composition is related to the seasonal ice melt cycle). Matrices used in these analyses were comprised of bottom ice core and concurrent CTD water column samples. Environmental variables, which met the variance inflation factor criteria (VIF <10), including day of year (DOY), nutrient concentrations (NO_3^-, PO_4^{3-}, and $Si(OH)_4$), and salinity, were chosen as proxies for ice melt progression (Ter Braak & Verdonschot 1995). Environmental variables were log-transformed to reduce the effect of variable units within a site (McCune and Grace 2002, Ramette 2007).

We also utilized a hierarchical clustering method, using Bray-Curtis dissimilarity distances and complete-linkage, to visualize the structure of groups in the dataset. The resulting dendrogram depicts the varying levels of similarity or dissimilarity across communities. The cluster analysis used the same input matrix as the ordinations following additional processing. Data were transformed to relative abundance, a method often used to minimize variation resulting from total biomass numbers (McCune and Grace 2002). Additionally, rare taxa (defined as comprising <1% of the average community composition for all samples) and one outlier station (STN 178) were removed from the data matrix to decrease noise and increase signal detection while conserving information in the data set (McCune and Grace 2002). Based on the output dendrogram structure, the dendrogram tree was cut at dissimilarity ≈ 75% so that within cluster

similarity was 25% or greater.

1.2.4 Simulations: estimating the importance of sea ice seeding

Some of the taxa that comprise phytoplankton blooms are also found in sea ice as ice algae. As such, it is impossible to use field observations to determine the extent to which those sea ice algal taxa contribute to water column assemblages before or during an under-ice phytoplankton bloom. In order to quantify the potential accumulation and growth of ice-derived phytoplankton in the underlying water column (ice algae lost from the ice into the water column) compared to non-ice-derived phytoplankton throughout the seasonal sea ice cycle, we developed a model that simulated springtime ice algal-phytoplankton dynamics over the March to June period (Figure 1.2a and b). Seasonal progression in the model simulation was programmed to match our field observations using the date of observed peak ice algae biomass relative to the date of ice melt as a benchmark. For example, early spring (March to mid May) simulations corresponded to 118 to 42 days (peak ice algal biomass) before ice melt. The simulation tracked three separate pools of algal biomass: an ice algal component within the sea ice, an ice-derived phytoplankton component within the water column, and a non-ice-derived phytoplankton component within the water column (Figure 1.2b).

These biomass pools were further divided into broad taxonomic groups to understand the role ice algal communities play in seeding bloom-forming versus non-bloom-forming phytoplankton populations. The ice algal pool was divided into two groups based on our observations of sea ice algae and phytoplankton community composition and previous studies of spring and summer phytoplankton community composition in the Chukchi Sea (Sukhanova et al. 2009, Arrigo et al. 2014, Laney et al. 2014). Group A included taxa commonly found in ice algal blooms but not in phytoplankton blooms in the Chukchi Sea (genera *Nitzschia, Navicula, Melosira*, and unidentified pennate diatoms) and Group B included taxa found in sea ice in relatively small numbers but common in phytoplankton blooms in the Chukchi Sea (genera *Fragilariopsis, Thalassiosira, Chaetoceros,* and unidentified centric diatoms). A minor fraction of the ice algal biomass was comprised of unidentified taxa (<6%), dominated by small cells, and is not discussed due to its unidentifiable characteristics. During the simulation, the majority of ice algal biomass (Groups A and B) transitioned from the ice (A_i, B_i) to the water column (A_w, B_w). The non-ice-derived phytoplankton are taxonomically identical to the ice-derived Group B and are referred to as Group C (*Fragilariopsis, Thalassiosira, Chaetoceros*, and unidentified centric diatoms).

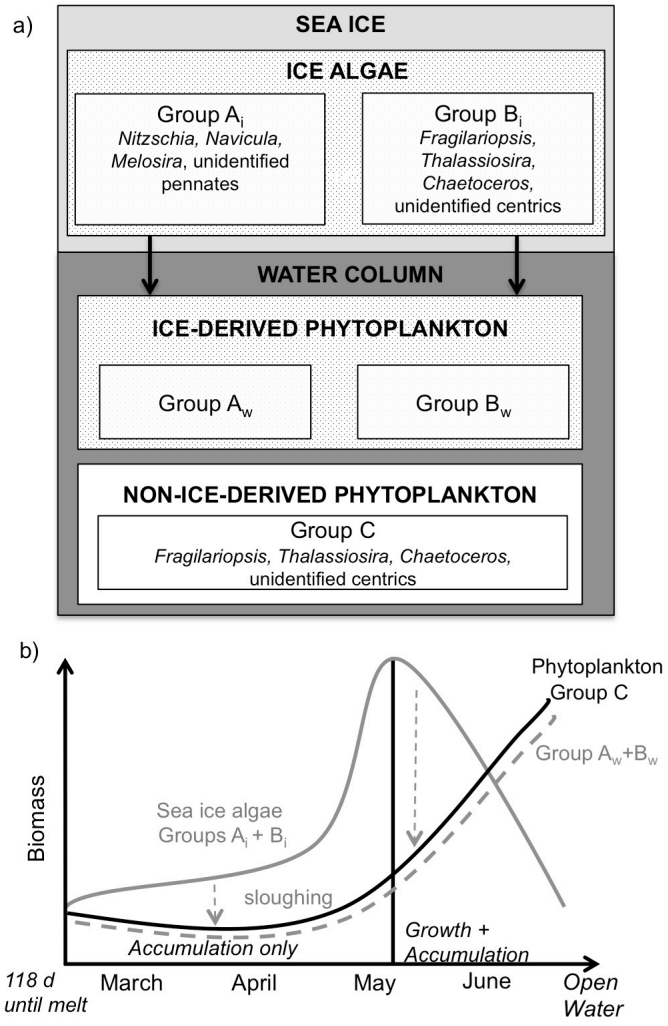

Figure 1.2 Diagram of conceptual model (a) coupling the ice algal (Groups A and B) and phytoplankton communities (Group C) (b) displaying simulations over time.

In using broad groupings based on genus (A, B, and C) rather than groupings further divided by species, modeling results represent the maximum potential for ice algae to seed bloom-forming (Group B) and non-bloom-forming phytoplankton taxa (Group A). Here we assume that 100% of the *Fragilariopsis, Chaetoceros,* and *Thalassiosira* in the sea ice and the water column are the same species, as has been observed by Szymanski and Gradinger (2016) for these genera in the Bering Sea. However, species of these genera are not always observed in both the sea ice and the water column (Quillfeldt et al. 2003). Therefore, we present an upper limit on the potential for ice algal seeding with broad community composition groups in the following model simulations.

Early spring community dynamics (March to mid May). To understand the maximum impact early spring ice algal sloughing has on phytoplankton community composition, we simulated the accumulation (μ_i) of ice algal biomass from March until mid May (when observed ice algal biomass peaked) in the bottom skeletal layer (0.03 m x 1 m x 1 m) of the sea ice. During this time, a constant daily fraction (0.01; Syzmanski and Gradinger 2016, Arrigo and Sullivan 1994, Saenz and Arrigo 2012, Saenz and Arrigo 2014) of the ice algae was assumed to slough off the ice into the water column, contributing to phytoplankton biomass. The taxonomic composition of these sloughed ice algae (ice-derived phytoplankton) was proportional to the ice community observed earliest in spring (STN 19 ice algae: 91% Group A_i, 3% Group B_i, and unidentified 6%). Groups A and B were programmed to slough off the ice (A_i, B_i) and accumulate in the water column (A_w, B_w) without subsequent growth (due to lack of light beneath the ice) until May. Group C was also maintained at a near zero concentration of 0.03 mg Chl *a* m^{-3} in the water column (Stabeno et al. 1998) until May due to low light levels. Starting in May, all phytoplankton (Groups A_w, B_w, and C) grew at the rate measured in our field study beneath the ice prior to loss of the ice algal layer (Groups A_w and B_w also continued to accumulate due to sloughing of A_i and B_i from the ice).

The rate at which ice algae accumulated in the sea ice from March to mid May was set so that ice algae would reach maximum biomass observed in our field study by the end of the early spring simulation (mid May). This accumulation rate includes the passive sloughing loss term set at 0.01 d^{-1}, estimated from measurements in the Bering Sea (Szymanski and Gradinger 2016) in early spring and used by other ice algal models (Arrigo and Sullivan 1994, Saenz and Arrigo 2012, Saenz and Arrigo 2014). Our calculated ice algal accumulation rate (0.14 d^{-1}) is lower than maximum growth rates observed in another ice algal study (0.29 d^{-1}, Zhang et al. 1999) and suggests a potential grazing rate of 0.14 d^{-1}, if we assume ice algal communities maximize growth rates over the early spring period. These grazing rates are within the range of those observed in early spring in the phytoplankton (Sherr 2009, Sherr 2013, Connell *in review*).

Phytoplankton (Groups A_w, B_w, and C) growth in the water column below the ice was generally limited by light. This growth rate (μ_w) was calculated from the average of the observed light-dependent photosynthetic rates of phytoplankton in our water column samples and the daily mean ML PAR prior to peak ice algal biomass (42 days before ice melt) (Equation 4). All groups in the phytoplankton (A_w, B_w, and C) are dominated by diatoms and assumed to grow at the same calculated growth rate, similar to other models that treat diatoms as one functional group (Tedesco et al. 2010, Tedesco et al. 2012). Throughout the early spring simulation, phytoplankton mortality from grazing losses were assumed to be negligible as phytoplankton concentrations

were low (<0.2 mg m^{-3}), since Sherr et al. (2013) observed negative or nonsignificant grazing rates at similarly low phytoplankton concentrations. Ice algae were assumed to slough off into a 40 m ML in March and April and a 20 m ML in May due to increased stratification over time. These MLDs are within the range of observations for our study region (~5 to 50 m MLD, mean 20±10 m).

Late spring community dynamics (mid May to mid June). After ice algae reached peak concentrations in mid May, they sloughed off the ice into the water column at a higher rate than in the early spring. The observed rate of decline in ice algal concentration between the time of maximum biomass (42 days before ice melt) and minimum biomass (2 days before ice melt) was used to calculate the sloughing rate for the duration of the late spring simulation. Assuming that sloughing was the only loss process impacting ice algal biomass during the late spring, this estimate represents the maximum potential of ice algae to seed the phytoplankton bloom.

To quantify the relative contributions of ice-derived biomass (Groups A_w and B_w) and non-ice-derived biomass (Group C) to the phytoplankton community later in the season as ice melts and the ML shoals, ice algae that sloughed off from the bottom ice layer were assumed to be dispersed into a 20 m ML from May 17 to May 31 and 10 m ML from June 1 to June 27, consistent with the range of MLDs observed in our study. All simulated community groups in the water column (ice-derived A_w and B_w, and non-ice-derived phytoplankton C) grew at rates calculated from the mean daily ML PAR and observed photosynthetic parameters (Equation 4) throughout May and June. Phytoplankton (ice derived: A_w and B_w, and non-ice-derived: C) were grazed in the water column at rates of 0.1 d^{-1} and 0.25 d^{-1} for the entire simulation, which are within the range of grazing rates measured in the Bering Sea (Sherr 2009) and Chukchi Sea (Connell in review, Sherr 2013) in early spring.

1.3 Results

1.3.1 Environmental ice characteristics

Snow and ice thickness. Snow thickness in spring varied from 0.01 to 0.26 m, averaging 0.07 ± 0.05 m throughout the SUBICE study region (Table 1.1), but had melted prior to the two summer ICESCAPE cruises (Table 1.2), leading to extensive melt pond formation. Mean ice thickness decreased from 1.23 ± 0.22 m in spring to 1.02 ± 0.20 m in summer (*t*-test $t(31) = 3.1$, $p = 0.004$). There was no relationship between ice thickness and snow thickness ($r^2 = 0.08$, p = n.s.). All stations were dominated by first year sea ice (FYI), with the exception of one multiyear

ice (MYI) station (STN 84). STN 84 also exhibited the coldest bottom ice temperature (-2.2 °C), compared to the mean bottom temperature at FYI stations (-1.2 °C).

In spring, surface melt was minimal in May and this pattern persisted through early June due to variable temperatures and a snowfall event (Arntsen unpubl.). Freezing air temperatures and the absence of melt ponds, which are generally present in this region in early June (Stroeve et al. 2014), suggested delayed melt progression relative to previous years. Advanced surface melt in spring was only observed at the southernmost station near the receding ice edge (STN 142) and stations in mid June (STN 196 and 209), where melt ponds were beginning to form. Conversely, at summer stations, the ice was decaying rapidly as snow had melted and melt pond coverage ranged from 5 to 65% of total surface area (Polashenski et al. 2015).

Table 1.1 Physical properties of sea ice during the spring SUBICE (05/18/14 to 06/17/14) cruise. - No data available.

Station	Date	Latitude	Longitude	Snow Depth m	Ice Thickness m	Bottom Ice Temperature °C
19	05/18/14	70.710	-166.280	-	-	-1.6
29	05/20/14	70.240	-163.246	0.05	1.05	-1.6
35	05/22/14	70.910	-164.990	0.15	1.08	-1.4
51	05/24/14	72.556	-166.394	0.10	1.50	-1.7
59	05/26/14	72.437	-168.313	0.08	1.41	-1.7
75	05/28/14	72.274	-162.448	0.06	0.97	-1.7
84	05/30/14	73.200	-161.960	0.26	1.34	-2.2
99	06/02/14	71.940	-166.330	0.05	1.39	-1.1
104	06/03/14	71.591	-166.377	0.13	1.65	-0.7
105	06/04/14	71.670	-166.110	0.08	1.15	-1.2
106	06/05/14	71.660	-165.890	0.05	1.17	-1.3
107	06/06/14	71.580	-165.820	0.03	1.49	-1.1
142	06/09/14	69.510	-168.707	0.03	0.88	-0.6
160	06/11/14	70.710	-168.310	0.09	1.18	-0.9
178	06/13/14	72.210	-167.480	0.04	1.40	-0.9
196	06/15/14	71.360	-166.042	0.02	1.07	-0.9
209	06/17/14	71.390	-165.340	0.03	1.10	-0.9

Table 1.2 Physical properties of sea ice during the summer ICESCAPE I and II (06/22/10 to 07/19/11) cruises. - No data available.

Station	Date	Latitude	Longitude	Snow Depth m	Ice Thickness m	Bottom Ice Temperature °C
24	06/22/10	68.303	-166.981	0	1.10	-
33	06/24/10	72.030	-159.877	0	0.90	-
34	06/25/10	72.091	-160.814	0	1.04	-
35	06/26/10	72.115	-160.538	0	1.30	-
36	06/27/10	72.061	-161.199	0	1.10	-
67	07/02/10	71.692	-159.040	0	1.10	-
68	07/03/10	71.119	-157.026	0	0.83	-
69	07/04/10	71.645	-157.746	0	1.07	-
100	07/09/10	71.732	-156.007	0	0.65	-
101	07/10/10	72.062	-156.281	0	1.08	-
109	07/11/10	71.934	-156.428	0	0.70	-
55	07/04/11	72.632	-168.726	0	0.92	-
56	07/05/11	73.165	-168.493	0	1.00	-
57	07/06/11	73.717	-168.268	0	1.35	-
90	07/07/11	72.958	-160.771	0	0.92	-
100	07/12/11	73.702	-160.290	0	1.10	-
101	07/13/11	73.834	-159.076	0	0.82	-
127	07/17/11	72.543	-153.835	0	0.80	-
128	07/18/11	72.834	-151.891	0	1.30	-
129	07/19/11	73.185	-150.438	0	1.30	-

Inorganic nutrients. Nutrient concentrations within bottom ice (0.1 m) at the ice-ocean interface (Table 1.3) ranged from 0 to 21.1 μM NO_3^-, 0.27 to 5.61 μM PO_4^{3-}, and 0.7 to 26.1 μM $Si(OH)_4$ throughout spring. Nutrient concentrations in bottom ice were low in summer and ranged from 0 to 1.30 μM NO_3^-, 0.07 to 0.26 μM PO_4^{3-}, and 0.2 to 0.7 μM $Si(OH)_4$. Assuming conservative mixing with seawater to calculate nutrients available to sea ice algae, it appears $Si(OH)_4$ and NO_3^- were most limiting in both spring and summer. In spring, bottom ice NO_3^- and $Si(OH)_4$ concentrations were below conservative mixing estimates at approximately 50% of the stations and in summer bottom ice NO_3^- and $Si(OH)_4$ were below conservative mixing estimates at 67% and 100% of the stations, respectively, indicating biological drawdown. In both seasons, PO_4^{3-} exceeded conservative mixing estimates at the majority of stations (90% in spring, 67% in summer). Interestingly, NH_4^+ concentrations were often above conservative mixing estimates in spring (78% of stations) and summer (100% of stations), indicating increased remineralization within the sea ice.

Table 1.3 The bulk salinities, observed nutrient concentrations (μM), and ratios of observed to estimated nutrient concentrations from the bottom ice cores (0.01 m): estimated nutrient concentrations are derived from conservative mixing with seawater. Si represents $Si(OH)_4$.

Station	Salinity	Bottom Ice Concentrations				Observed:Estimated Concentrations			
		NO_3^-	PO_4^{3-}	Si	NH_4^+	NO_3^-	PO_4^{3-}	Si	NH_4^+
Spring									
29	5.05	0.45	1.37	6.6	0.25	0.24	4.92	0.93	1.10
35	7.67	21.08	3.15	19.0	1.09	7.38	7.45	1.76	3.15
51	11.43	6.96	1.97	15.7	0.81	1.64	3.13	0.97	1.57
59	8.86	16.61	3.61	26.1	1.25	5.04	7.39	2.09	3.13
75	8.55	2.56	3.39	17.4	0.65	0.80	7.20	1.44	1.69
84	8.85	0.05	0.41	0.7	0.49	0.02	0.84	0.06	1.23
99	7.30	16.13	2.73	5.5	1.09	5.94	6.79	0.53	3.31
104	4.18	0.00	0.27	1.6	0.11	0.00	1.17	0.27	0.58
105	8.40	1.96	0.49	15.0	0.27	0.63	1.06	1.27	0.71
106	7.09	5.53	2.49	10.9	0.69	2.10	6.37	1.09	2.16
107	5.57	4.76	2.14	7.7	9.28	2.30	6.97	0.98	36.94
142	5.30	0.02	0.47	1.9	0.10	0.01	1.61	0.25	0.42
160	4.26	0.02	0.95	3.0	0.36	0.01	4.05	0.50	1.87
196	7.81	5.23	5.61	22.5	0.91	1.80	13.04	2.04	2.58
Summer									
33	3.00	0.03	0.19	0.4	1.06	0.03	1.28	0.15	8.22
34	2.00	0.08	0.26	0.4	1.08	0.13	2.64	0.23	12.56
35	3.00	0.02	0.08	0.3	0.12	0.02	0.54	0.11	0.93
36	2.00	0.00	0.07	0.2	0.31	0.00	0.71	0.11	3.60
68	1.50	0.48	0.17	0.5	1.07	1.04	2.30	0.38	16.59
69	1.00	1.30	0.09	0.2	0.50	4.24	1.83	0.23	11.63
100	0.50	0.30	0.05	0.4	0.10	1.96	2.03	0.92	4.65
101	4.00	0.85	0.16	0.7	0.57	0.69	0.81	0.20	3.31
109	2.00	0.31	0.10	0.5	0.21	0.51	1.01	0.29	2.44

Sea ice can be a nutrient source or sink to the water column depending on the relative concentrations within the two habitats. In our study most mean bulk spring ice to surface water (I:SW) nutrient ratios were less than unity (Table 1.4), implying that sea ice would dilute SW nutrient concentrations once it melted. In contrast, most summer I:SW NO_3^- ratios and one $Si(OH)_4$ ratio were greater than unity. In these instances, SW nutrients were generally low (<0.05 μM NO_3^- and <0.39 μM $Si(OH)_4$, Appendix A2) and sea ice was a nutrient source.

Table 1.4 Ratios of the Ice:Surface Water (I:SW) nutrient concentrations (mol:mol). Sea ice nutrients represent the weighted mean bulk nutrient concentrations. - No Data Available.

Station	Ice:Surface Water			
	NO_3^-	PO_4^{3-}	$Si(OH)_4$	NH_4^+
Spring				
29	0.36	0.68	0.07	0.98
35	0.13	0.41	0.06	0.40
51	0.03	0.25	0.03	0.27
59	0.14	0.47	0.07	0.17
75	0.04	0.53	0.06	0.58
84	0.09	0.45	0.07	3.16
99	0.05	0.37	0.02	0.37
104	0.01	0.34	0.06	0.14
105	0.01	0.19	0.03	0.23
106	0.04	0.25	0.04	0.25
107	0.03	0.29	0.06	1.75
142	6.52	0.44	0.14	-
160	0.01	0.21	0.02	0.83
178	0.02	0.17	0.07	0.32
196	0.04	0.35	0.06	0.40
209	0.01	0.14	0.04	0.83
Summer				
33	3.66	0.18	0.57	-
68	0.00	0.23	1.02	6.19
55	0.53	0.12	0.03	1.07
69	16.01	0.13	0.14	-
56	0.00	0.09	0.02	6.38
57	1.00	0.11	0.08	-
90	-	0.10	0.15	-
100	6.51	0.10	0.04	1.55
101	44.73	0.14	0.13	3.21
109	-	0.11	0.16	2.53
100	-	0.12	0.07	-

1.3.2 Ice algal biomass variability

Over the three cruises, depth-integrated ice algal Chl *a* decreased from a spring maximum of 110 mg m^{-2} to a summer minimum of <0.1 mg m^{-2}. Mean concentrations in spring (40 $\pm$ 28 mg Chl *a* m^{-2}) were significantly higher than summer (0.5 $\pm$ 1.5 mg Chl *a* m^{-2}) (Table 1.5; $t(16) = 5.6$, $p < 0.001$). The magnitude of depth-integrated POC and PON followed a pattern similar to

Chl *a* over the spring (2575 ± 931 and 195 ± 109 mg m^{-2}, respectively) to summer (696 ± 756 and 46 ± 24 mg m^{-2}, respectively) melt transition (Figure 1.3b and c; $t(28, 16) = 6.6, 5.5$, $p < 0.001, 0.001$). POC was positively correlated to PON in spring and summer, and POC:PON ratios were lower in spring (m=8.9) than summer (m=40.5) (Figure 1.3a). Similarly, POC was positively correlated to Chl *a* and the POC:Chl *a* ratios increased two to three orders of magnitude from spring to summer (Figure 1.3b), indicative of increasing detritus and decreasing algal biomass through summer.

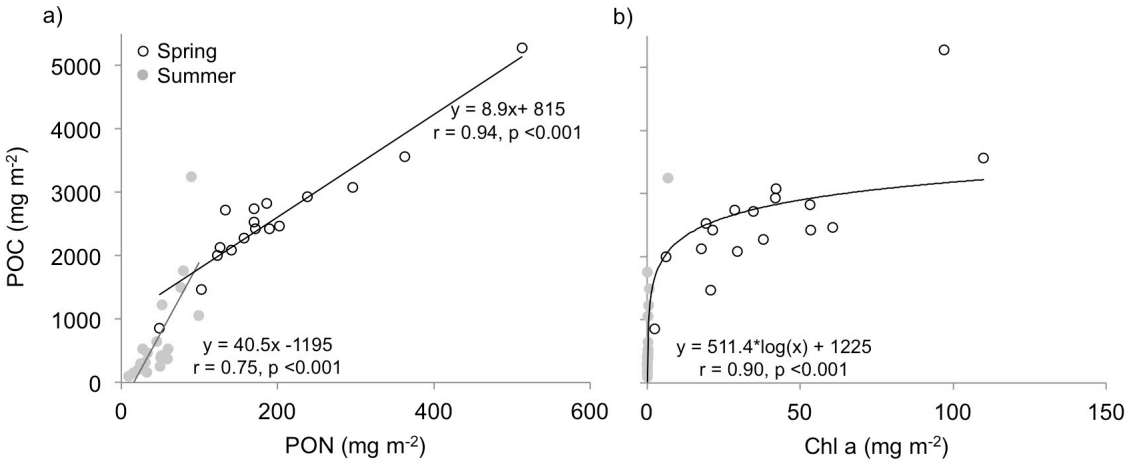

Figure 1.3 Spring (SUBICE, white circles) and summer (ICESCAPE I & II, gray circles) (a) depth-integrated particulate organic carbon (POC) vs. particulate organic nitrogen (PON; mg m^{-2}) and (b) Depth-integrated POC vs. Chlorophyll *a* (mg m^{-2}) at ice stations.

Table 1.5 Integrated ice algal biomass and bottom ice algal photosynthetic parameters.

Station	Date	Chl *a*	POC	PON	P^*_m	α	Ek
Spring							
19	5/18/14	41.59	-	-	-	-	-
29	5/20/14	31.64	2730	151	0.39	0.014	28
35	5/22/14	109.88	3564	362	0.25	0.014	19
51	5/24/14	42.11	3082	296	0.06	0.009	7
59	5/26/14	60.72	2469	203	-	-	-
75	5/28/14	38.03	2274	157	0.07	0.007	9
84	5/30/14	2.53	853	49	0.08	0.008	11
99	6/2/14	20.80	1470	103	0.27	0.025	11
104	6/3/14	17.63	2128	126	0.15	0.013	12
105	6/4/14	19.26	2529	169	0.04	0.003	18
106	6/5/14	53.49	2427	189	0.13	0.011	13
107	6/6/14	21.37	2423	172	0.16	0.013	12
142	6/9/14	6.19	1999	123	0.06	0.004	11
160	6/11/14	53.14	2821	186	-	-	-
178	6/13/14	41.99	2926	238	0.10	0.005	19
196	6/15/14	96.92	5280	512	0.15	0.012	19
209	6/17/14	29.46	2083	141	0.07	0.006	11
Summer							
24	6/22/10	7.32	3246	90	-	-	-
33	6/24/10	0.46	1224	52	-	-	-
34	6/25/10	0.40	1757	79	-	-	-
35	6/26/10	0.41	1054	99	-	-	-
36	6/27/10	0.29	641	45	0.28	0.005	54
67	7/2/10	0.36	528	60	-	-	-
68	7/3/10	0.16	291	28	-	-	-
69	7/4/10	0.31	471	34	0.34	0.003	112
100	7/9/10	0.26	533	27	0.29	0.004	72
101	7/10/10	0.83	1493	76	-	-	-
109	7/11/10	0.23	321	31	-	-	-
55	7/4/11	0.15	422	51	0.11	0.007	16
56	7/5/11	0.24	388	51	-	-	-
57	7/6/11	0.18	373	59	-	-	-
90	7/7/11	0.06	206	21	-	-	-
100	7/12/11	0.07	304	24	-	-	-
101	7/13/11	0.04	98	9	-	-	-
127	7/17/11	0.07	150	15	-	-	-
128	7/18/11	0.04	261	49	-	-	-
129	7/19/11	0.09	161	33	-	-	-

Spring ice algal communities. Algal biomass was concentrated near the bottom of the ice (0.1 m) during spring, accounting for 60 ± 20% of depth-integrated Chl *a* (excluding MYI and internal layer STN 142 and 160) (Figure 1.4a). Bottom ice concentrations ranged from 12 to 2760 mg Chl *a* m^{-3} and averaged 395 ± 263 mg m^{-3} (Table 1.6, Figure 1.4a). Vertical distributions of POC and PON were similar to Chl *a* in spring, with biomass concentrated in bottom ice (Figure 1.4b and c**)**. Most bottom ice nutrients (NO_3^-, PO_4^{3-}, $Si(OH)_4$, but not NH_4^+), were positively correlated with bottom ice algal biomass (r = 0.80, 0.62, 0.79, respectively, p <0.05) (Tables 1.3 and 1.6). In contrast, surface water nutrient concentrations available to the ice algal community were not correlated with bottom ice algae, with the exception of a positive correlation between surface water NH_4^+ and bottom ice Chl *a* (r = 0.77, p <0.001). While most surface water nutrients were not correlated with ice algal biomass, the lowest nutrient concentrations were associated with the lowest bottom ice algal biomass (STN 84 and 142; Table 1.6 and Appendix A2).

Spring bottom ice algal communities varied on small spatial scales across a single ice floe, with standard deviations spanning three orders of magnitude (Table 1.6). Despite this variability, a linear regression analysis demonstrated that biomass at the bottom of FYI cores was positively correlated with days until ice melt (r^2 = 0.68, p<0.05, Appendix A6) and distance from the edge of the ice pack (r^2 = 0.45, p <0.05).

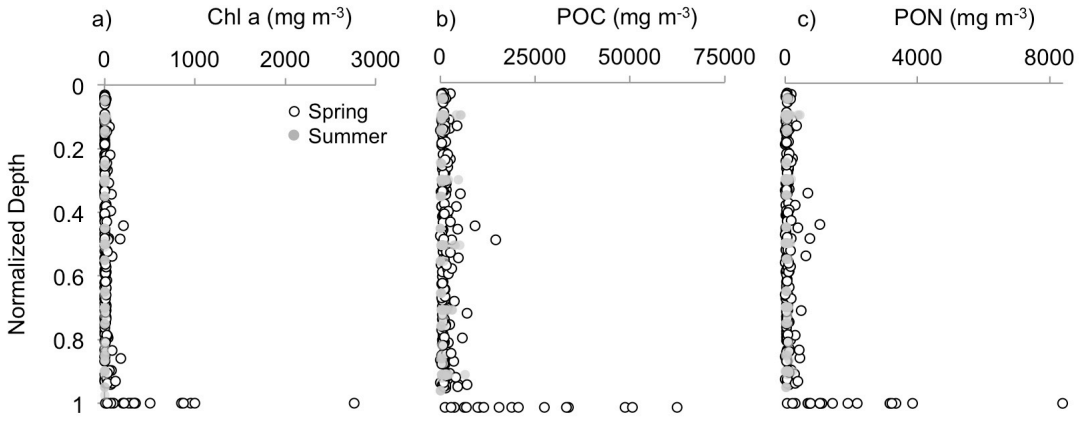

Figure 1.4 Spring (SUBICE, white circles) and summer (ICESCAPE I & II, gray circles) vertical distribution of (a) Chlorophyll *a,* (b) Particulate organic carbon (POC), and (c) Particulate organic nitrogen (PON) biomass (mg m^{-3}). Core depths are normalized where 0 is the ice-atmosphere interface and 1 is the ice-water interface.

Within the late spring ice algal community the fraction of large (>20 μm) ice algal cells was positively correlated with ice algal biomass and often dominated the bottom ice, representing 47

to 89% of the total bottom ice biomass (Table 1.6). Smaller ice algae (<20 μm) were rarely dominant and were limited to stations with the lowest Chl *a* concentrations (STN 84 and 142) and/or with depleted nutrients (STN 142 and 160). Similar to Chl *a*, large ice algae (>20 μm) accounted for the largest fraction of POC and PON in the bottom community, with the exception of MYI (STN 84) and low nutrient stations (STN 142 and 160) (Table 1.6).

Summer ice algal communities. In contrast to spring, bottom ice algal communities in the summer only contributed 25 ± 18% of total depth-integrated biomass. Summer ice cores had a median Chl *a* concentration of 0.21 mg m^{-3} (range: 0.04 to 23.5 mg Chl *a* m^{-3}), which indicated that the high biomass associated with the bottom ice communities in spring had been lost from the sea ice by summer. Mean POC and PON concentrations in summer were no higher in bottom ice sections than they were in the rest of the core.

Table 1.6 Characteristics of bottom ice (0.1 m) algal communities in spring (SUBICE).

Station	Mean Biomass		μ_{max}	N accumulation[x]	>20 μm:Total Biomass		
	Chl *a* mg m^{-3}	± sd	d^{-1}	mmol N m^{-2} d^{-1}	Chl *a**	POC	PON
29	228	168	0.12	0.05	0.70	0.39	0.26
35	962	1016	0.02	0.36	-	-	-
51	743	218	-	0.19	0.91	0.79	0.78
59	771	232	0.06	0.16	0.91	0.79	0.73
75	427	61	0.03	0.10	0.87	0.82	0.76
84	18	11	0.09	0.005	0.47	0.26	0.22
99	407	72	0.14	0.07	0.88	0.83	0.79
104	285	103	0.04	0.05	0.87	0.74	0.71
105	329	76	0.02	0.13	0.79	0.95	0.85
106B	536	294	0.06	0.15	-	-	-
107B	273	409	0.06	0.04	0.87	-	-
142	12	8	-	0.02	0.57	-	-
160	108	53	0.03	0.04	0.63	0.45	0.44
178	344	181	0.11	0.07	0.88	0.81	0.68
196	482	276	0.02	0.18	0.83	0.82	0.68
209	395	60	0.07	0.07	0.84	0.84	0.78

* >20 um Chl *a* v. Total Chl *a:* $y = -1.02*\log(x) + 7.66$, $r^2 = 0.85$, $p < 0.001$,
[x]calculated from PON concentrations in bottom sea ice (Cota et al. 1987).

1.3.3 Ice algal physiology

Variable fluorescence parameters. Over both spring and summer, sea ice algal F_v/F_m decreased with DOY (Figure 1.5a). In addition, the effective absorption cross section (σ_{PSII}) was

slightly lower in spring (525 ± 75 Å^2 quanta^{-1}) than in summer (647 ± 104 Å^2 quanta^{-1}) (t(7.4)= 2.6, p <0.05). During the spring season, multiple linear regression analysis showed that the combined effect of under-ice surface seawater temperature (Figure 1.5b) and near bottom (0.05 m) ice temperature explained 73% of the decline in F_v/F_m ($F_{2,11}$ = 14.53, r^2 = 0.73, p <0.001). Surface water temperatures were also positively correlated with both transmitted irradiance (r = 0.78, p <0.05) and percent transmitted irradiance (r = 0.79, p <0.05), indicating that as temperature and light increased, the photophysiological state of the ice communities declined. In contrast to spring, F_v/F_m was low in summer and was not significantly correlated to any environmental variables.

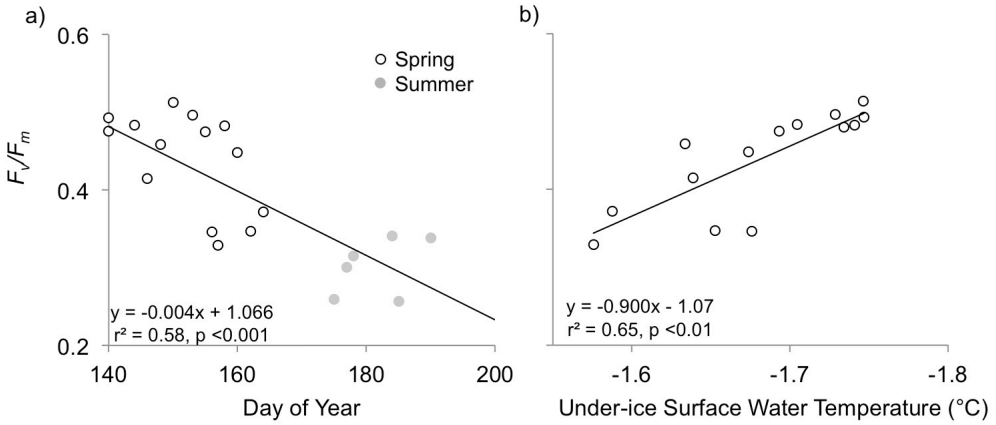

Figure 1.5 (a) Spring (SUBICE, white circles) and summer (ICESCAPE I & II, gray circles) photosynthetic efficiency of photosystem II (F_v/F_m) versus day of year and (b) spring (SUBICE, white circles) F_v/F_m versus the sub-ice surface water temperature.

Photosynthetic parameters and growth rates. Spring ice algal communities were characterized by lower P^*_m (0.14 ± 0.10 mg C mg^{-1} Chl *a* h^{-1}) and higher α^* (0.02 ± 0.04 mg C mg^{-1} Chl *a* h^{-1} (µmol photon m^{-2} s^{-1})$^{-1}$) relative to summer (P^*_m = 0.30 ± 0.03 mg C mg^{-1} Chl *a* h^{-1}, α^* = 0.009 ± 0.008 mg C mg^{-1} Chl *a* h^{-1} (µmol photon m^{-2} s^{-1})$^{-1}$))(Table 1.5). Photosynthetic parameters were not correlated with any environmental factors. The photoacclimation parameter (E_k) further suggested that spring bottom ice communities were acclimated to lower light levels, sometimes as low as 7 µmol photon m^{-2} s^{-1}, compared to summer communities, which had a maximum E_k value of 112 µmol photon m^{-2} s^{-1} (Table 1.5). Estimates of daily mean PAR reaching the spring bottom ice algal layer (17 to 289 µmol photon m^{-2} s^{-1}, Figure 1.6) were approximately seven times higher than the mean E_k (14 ± 6 µmol photon m^{-2} s^{-1}) and often 1 to 2 orders of magnitude higher than daily PAR at 1 m water depth beneath the sea ice (Figure 1.6).

Throughout the spring sampling period (SUBICE), maximum biomass-specific growth rates (μ_{max}) derived from the maximum rates of photosynthesis (P^*_m) and POC:Chl *a* ratios were low, with a mean of 0.06 ± 0.04 d^{-1} and range of 0.02 to 0.14 d^{-1}. PON accumulation rates (based on a 60 day bloom period) in the bottom 0.1 m ice sections ranged from 0.005 to 0.36 mmol N m^{-2} d^{-1} and averaged 0.11 ± 0.09 mmol N m^{-2} d^{-1} (Table 1.6).

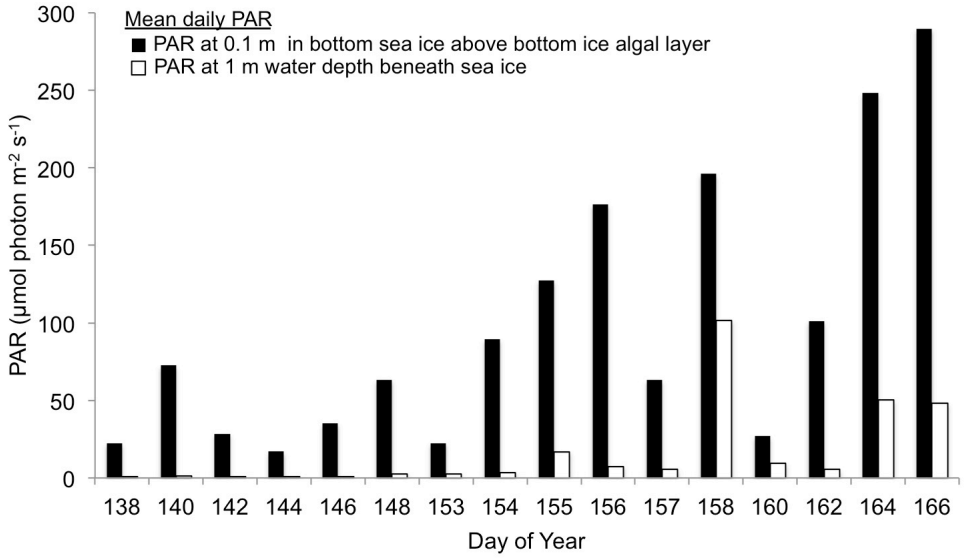

Figure 1.6 Mean daily photosynthetically active radiation (PAR) (µmol photon m^{-2} s^{-1}) over time (DOY) for the under-ice surface water (1 m; observed, white bar) and the 0.1 m bottom ice environment (above bottom ice algal layer; estimated, black bar) in spring at first year ice stations (SUBICE).

Algal pigment distributions. Photosynthetic accessory carotenoid pigments (PSC: fucoxanthin, peridinin, neoxanthin, and alloxanthin) normalized to Chl *a* were 2-fold higher in spring (0.69 ± 0.08 g:g) than in summer (0.25 ± 0.10 g:g) ($t(25) = 12.6$, $p < 0.001$, Table 1.7). In contrast, photoprotective carotenoid pigments (PPC: diadinoxanthin, diatoxanthin, violaxanthin, zeaxanthin, lutein, and b-carotene) normalized to Chl *a* were nearly 3-fold lower in spring (0.16 ± 0.24 g:g) than in summer (0.54 ± 0.17 g:g) ($t(18) = -4.7$, $p < 0.001$, Table 1.7). While pigment ratios varied, the most common PSC and PPC pigments remained dominant in both seasons. Fucoxanthin made up an average of 99 ± 2% and 76 ± 19% of PSC pigments in spring and summer, respectively, with few exceptions (STN 56 and 101). The photoprotective xanthophyll cycle pigments, diadinoxanthin and diatoxanthin, dominated PPC ratios (by weight), except at a few stations (STN 67, 56 and 100).

Table 1.7 Photosynthetic accessory (PSC), photoprotective pigments (PPC), and examples of dominant PPC pigments expressed as ratios to chlorophyll *a* (g:g)

Station	Photosynthetic Accessory Pigments	Photoprotective Pigments	Fucoxanthin	Diadinoxanthin + Diatoxanthin
Spring				
19	0.76	0.08	0.76	0.07
35	0.72	0.07	0.72	0.06
51	0.76	0.14	0.75	0.12
59	0.69	0.06	0.68	0.05
75	0.69	0.13	0.68	0.13
99	0.71	0.06	0.71	0.05
104	0.60	0.07	0.60	0.05
106	0.58	0.08	0.58	0.08
160	0.72	0.14	0.72	0.12
178	0.72	0.09	0.71	0.09
196	0.82	0.92	0.77	0.87
209	0.52	0.09	0.52	0.09
Summer				
24	0.44	0.3	0.44	0.25
33	0.28	0.46	0.25	0.29
35	0.2	0.39	0.13	0.14
36	0.15	0.61	0.12	0.22
67	0.11	0.61	0.09	0.06
68	0.18	0.62	0.15	0.3
69	0.24	0.61	0.22	0.34
55	0.42	0.17	0.39	0.12
56	0.13	0.32	0.06	0.06
57	0.16	0.62	0.12	0.14
90	0.21	0.56	0.17	0.23
100	0.19	0.73	0.13	0.17
101	0.33	0.75	0.08	0.33
127	0.32	0.6	0.25	0.35
128	0.25	0.71	0.19	0.31
129	0.35	0.56	0.31	0.24

1.3.4 Coupling between ice algal and phytoplankton communities.

Ice algal, phytoplankton, and mixed community clusters. Hierarchical clustering structure revealed major types of communities in spring (SP) and summer (SU) that were dominated by either taxa common to ice algal (I) or phytoplankton (P) blooms (Appendix A3, Figure 1.7a).

Mixed phytoplankton communities (MIX) highlighted the degree of overlap between ice algae and phytoplankton communities, where neither taxon common to ice algae nor phytoplankton blooms were dominant (Appendix A3, Figure 1.7a). Spring ice algal communities (SP-I; clusters I and II in Figure 1.7b) were dominated by varying proportions of *Nitzschia, Navicula,* and unidentified pennate diatoms, and are referred to as SP-I. Spring phytoplankton communities grouped into three clusters (III, IV, VIII in Figure 1.7a). Cluster III was dominated by *Thalassiosira, Fragilariopsis,* and unidentified centric diatoms and is referred to as the spring bloom-forming phytoplankton community (SP-P III). Cluster IV was comprised of *Thalassiosira, Fragilariopsis*, small and large unidentifiable cells, and a broader mix of pennate diatoms common to sea ice. Cluster VIII had higher proportions of common ice algal taxa relative to *Thalassiosira* and *Fragilariopsis*, as well as a high proportion of unidentifiable cells. Together, clusters IV and VIII are defined as a spring mixture of ice algae and phytoplankton (SP-MIX IV and VIII). Summer ice community groupings (SU-I; clusters VI and IX in 1. 7a) were driven by variations in the relative abundance of *Pyramimonas*, dinoflagellates, and small cells and were defined as those typical of summer ice. Summer phytoplankton groupings (SU-P; clusters V and VII in Figure 1.7a) were controlled by varying proportions of *Chaetoceros* and small cells and defined as those typical of the summer water column.

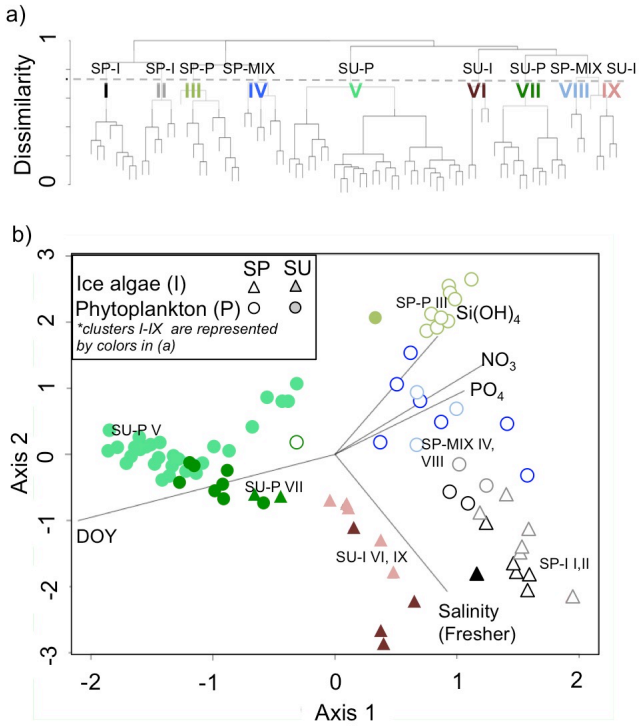

Figure 1.7 Cluster and correspondence analysis results (CCA): (a) Dendrogram displaying clusters (I-IX) of hierarchical clustering analysis divided into clusters dominated by spring (SP-) and summer (SU-) ice algal (I), phytoplankton (P), and mixed (MIX) communities. MIX communities were defined as those phytoplankton communities where neither taxa common to ice algae or taxa common to phytoplankton blooms were dominant, rather they were a mix of both groups of taxa. (b) CCA of spring (open symbol) and summer (closed symbol) ice algal (triangles) and phytoplankton (circle) communities. Vectors represent surface nutrients ($Si(OH)_4$, NO_3^-, PO_4^{-3}), salinity, and day of year (DOY). Results from the hierarchical clustering analysis (a) (Clusters I to IX) are overlaid on the CCA plot and are represented by color.

Seasonal ice algal and phytoplankton community succession. The degree of coupling between ice algal and phytoplankton communities varied over the spring to summer transition (Appendix A3). At the start of the sampling period in mid May, phytoplankton community composition (STN 19, SP-P III) was distinct from the ice algal communities. However, bottom ice temperatures abruptly increased from an average of -1.68 $\pm$ 0.25 °C in late May (May 19 to 30) to -0.96 $\pm$ 0.22 °C in June (June 2 to June 19) (Table 1.1) in concert with increases in air temperatures. Consequently by the first week of June, phytoplankton communities were dominated by ice-derived taxa and either classified as SP-MIX VIII or SP-I II (STN 99 and 106) depending on depth due to their high proportions of common ice algal taxa such as *Nitzschia* and *Navicula*. By the second week of June (June 9 to 15) at stations further along in the melt cycle (STN 142 and 160, as indicated by days until ice melt), *Fragilariopsis* and *Thalassiosira* were

again the dominant phytoplankton taxa (SP-P III, SP-MIX IV). The phytoplankton community in the Central North region resampled in mid June (STN 196, previously STN 106) still resembled ice algal communities, but to a lesser extent (SP-MIX IV), as water-blooming taxa, including *Thalassiosira, Fragilariopsis*, and *Chaetoceros*, had increased in relative abundance. These observations show that the dominance of common ice algal taxa in the water column was short-lived.

Seasonal community succession suggested by cluster analysis was further reflected in the CCA eigenvalues for Axis 1 and 2 (Figure 1.7b). Seasonal melt progression (time): DOY, salinity, and inorganic nutrient concentrations explained 76% of the constrained variance in community composition (Figure 1.7b). The strong seasonal signal persisted within the phytoplankton, with spring (SP-P III) and summer (SU-P V and VII) phytoplankton clusters correlating with the DOY and nutrient gradient. The CCA highlighted the contrast between the spring pre-bloom phytoplankton community (SP-P III) dominated by centric diatoms and the pennate diatom *Fragilariopsis*, which coincided with high nutrient concentrations, and the summer bloom phytoplankton community (SU-P V and VII) dominated by *Chaetoceros* and small cells, which coincided with depleted nutrients. The spring MIX communities (SP-MIX IV and VIII) followed a transition from ice algae (SP-I I and II) dominated by *Nitzschia*, *Navicula*, and unidentified pennates to phytoplankton (SP-P III) in spring.

1.3.5 Ice algal seeding event simulations

Model simulations were motivated by the above analysis of our field observations that suggest that prior to melt-induced ice algal loss from the sea ice, mean water column Chl *a* concentrations were low (<0.5 mg m^{-3}, Figure 1.8d open circles) and included both SP-P III (dominated by taxa common to phytoplankton blooms, similar to modeled groups B (ice-derived) and C (non-ice-derived)) and SP-MIX IV and VIII communities (dominated by a mix of taxa common either to ice algal or phytoplankton blooms) (Figure 1.8a, Appendix A3). The presence of SP-MIX indicated the early footprint of ice algae in the water column. The sloughing of the bottom layer marked the temporary increase in the co-occurrence of SP-MIX IV and VIII and SP-I I and II communities (dominated by taxa common to ice algal blooms and similar to modeled Group A) in the phytoplankton. Thus, we explored the potential for ice algal communities in early and late spring to contribute to water column phytoplankton blooms. We used observed ice algal and phytoplankton biomass, physiology, grazing rates, and taxonomic composition to initialize and constrain the model. Using model simulations and field data, we assessed the potential for spring ice algal communities to seed under-ice phytoplankton blooms in both early and late spring.

Early spring. In this simulation, we assessed the potential for ice algae to seed the water column during March to May, prior to rapid ice melt (Figure 1.8a-c). Water column biomass increased through a combination of slowly sloughing off ice algae (March to May) and phytoplankton growth in the water column (May) (Figure 1.8a-c) at a rate of 0.02±0.02 d^{-1} (μ_w), the mean rate we measured 42 to 60 days before sea ice melt. Based on a value for μ_i of 0.14 d^{-1} and an assumed constant sloughing rate of 0.01 d^{-1} (Szymanski and Gradinger 2016), the ice algal bloom within the sea ice reached its peak biomass of ~974 mg Chl *a* m^{-3} by mid May (day 42 in Figure 1.8), similar to the maximum observed in our study. From March to mid May, Group C (non-ice-derived phytoplankton) biomass exceeded that of Groups A_w and B_w (ice-derived) biomass in the water column (Figure 1.8a). By mid May, Group A_w (ice-derived) composed the majority of the phytoplankton for the rest of the simulation (Figure 1.8a and b) due to the combination of continued sloughing, growth in the water column, and the shoaling of the ML. At the end of the early spring simulation, prior to the higher rates of sloughing of the bottom ice algal layer, total phytoplankton concentrations ($A_w + B_w + C$) remained low (<0.2 mg Chl *a* m^{-3}). The majority of phytoplankton biomass was comprised of Group A_w (0.11 mg Chl *a* m^{-3}, Figure 8b), while Group C (0.037 mg Chl *a* m^{-3}) and Group B_w (0.004 mg Chl *a* m^{-3}) were 1 to 2 orders of magnitude lower, respectively (Figure 1.8c).

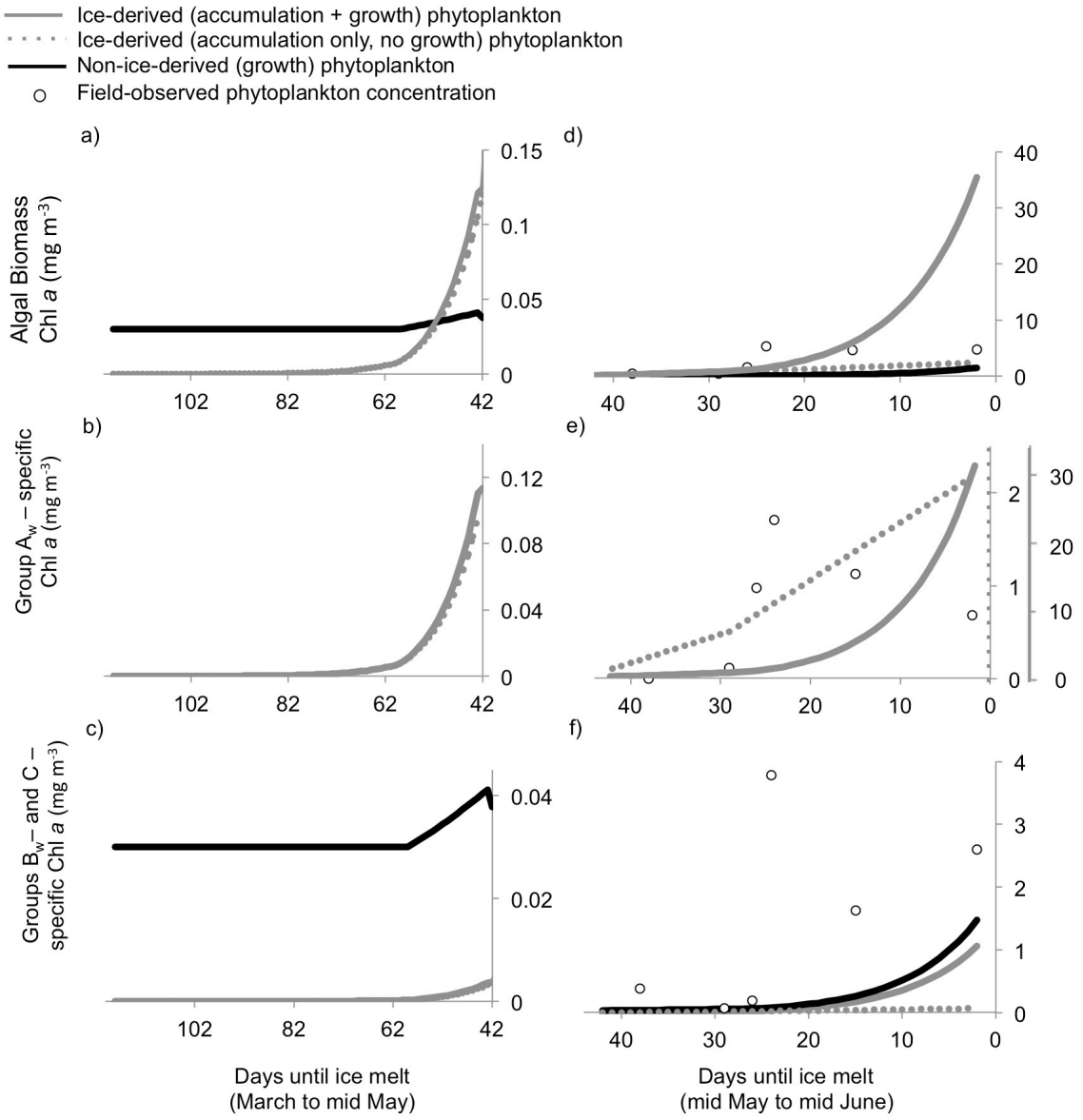

Figure 1.8 Simulated ice-derived (growth and accumulation, solid gray line; accumulation only of Group A and B, dotted gray line) and non ice-derived phytoplankton (Group C, black line) from (a-c) March to mid May (118 to 42 days until ice melt) and from (d-f) mid May to mid June (42 to 2 days until ice melt) in the mixed layer below the sea ice. Simulated taxa-specific Chl *a* include (b,e) those taxa common to ice algal blooms (Group A) and (c,f) taxa common to phytoplankton blooms (Group B and C). Simulations from mid May to mid June are overlaid with observed concentrations (open circle) of (d) total phytoplankton Chl *a*, (e) Group A, (f) Group B and C. (e) Observed concentrations and Group A - accumulation only are represented on the dotted y-axis (0-2 mg m^{-3}) and Group A accumulation and growth is represented on the solid gray y-axis (0 – 30 mg m^{-3}).

Bloom-forming phytoplankton taxa originating in the water column (Group C) greatly exceeded the ice-derived equivalent (Group B_w) in the model simulation (Figure 1.8c). In order for Group B_w (0.004 mg Chl *a* m^{-3}) to reach the concentration of Group C (0.037 mg Chl *a* m^{-3}) in early spring, ice algae melting out from the sea ice would either need to more than double their loss rate or would need to grow at a rate of 0.14 to 0.30 d^{-1} over a one to two week period in the water column, respectively, assuming exponential growth once in the water column. These hypothetical growth rates are unrealistic, since they are 5 to 10 times higher than observed phytoplankton growth rates ($\mu_w = 0.02 \pm 0.02$ d^{-1}). These results suggest that observed light levels beneath the ice do not support the growth required for ice algae (Group B_w) to seed or significantly contribute to bloom-forming phytoplankton taxa populations (Group C) in early spring.

Late spring. To quantify the combined effect that higher rates of sloughing and increased stratification have on ice algal-phytoplankton coupling, we simulated bottom ice algae (974 mg Chl *a* m^{-3}) sloughing off into a 20 m ML in mid to late May and a 10 m ML in June (2 to 42 days before ice melt) at a rate of ~23 mg Chl *a* m^{-3} d^{-1} (Figure 1.8d-f). Simulated phytoplankton concentrations at the start of the simulation in mid May were composed of Group A_w (0.11 mg Chl *a* m^{-3}), Group B_w (<0.01 mg Chl *a* m^{-3}), and Group C (0.037 mg Chl *a* m^{-3}). Observed growth rates (0.01 to 0.92 d^{-1}) were light-limited and highly variable over the late spring sea ice cycle (2 to 42 days until ice melt). Therefore, we used mean light-dependent growth rates observed for low phytoplankton biomass (42 to 25 days until sea ice melt, $u_w = 0.15 \pm 0.15$ d^{-1}) and high phytoplankton biomass (24 days or fewer until ice melt, $u_w = 0.52 \pm 0.39$ d^{-1}) in the first and second halves of the simulation, respectively (Figure 1.8d).

Throughout the simulation, the ice-derived taxa common to ice algal blooms (Group A_w) exceeded non-ice-derived taxa common to phytoplankton blooms (Group C) in the phytoplankton due to accumulation via sloughing, growth in the water column, and the continued shoaling of the ML from May to June (Figure 1.8d-f). At the end of the simulation (mid June), simulated ice-derived algae (Group A_w, common ice algal taxa) comprised the majority of the total biomass (32.25 mg Chl *a* m^{-3}) (solid gray line, Figure 1.8d). Groups B_w and C (ice-derived and non-ice-derived taxa common to phytoplankton blooms, respectively) composed 2.54 mg Chl *a* m^{-3} of the phytoplankton biomass, the majority of which (~60%) originated in the water column (Group C, black solid line, Figure 1.8f), rather than being seeded from the sea ice (Group B_w, solid gray line, Figure 1.8f). These results, similar to the early spring simulation, show that the majority of bloom-forming phytoplankton taxa in the phytoplankton originate in the water column (Group C), not the sea ice (Group B). However, Group B (ice-derived taxa common to phytoplankton

blooms) has the potential to contribute a maximum of ~40% to the bloom-forming phytoplankton population, through both accumulation from the sea ice and growth in the water column.

In contrast to simulated biomass, observed phytoplankton concentrations increased from an initial value of 0.47 mg Chl *a* m^{-3} to 1.57 mg Chl *a* m^{-3} approximately 26 days before ice melt (open circles, Figure 1.8d). This initial increase in field observations was driven by taxa common to ice algal blooms (equivalent to taxa simulated in Group A_w: 0.98 mg Chl *a* m^{-3}) rather than taxa common to phytoplankton blooms (equivalent to Group B_w and C: 0.20 mg Chl *a* m^{-3}). Taxa equivalent to Group A_w accounted for the majority of the observed phytoplankton biomass, similar to simulated estimates (open circles, Figure 1.8e). However, observed phytoplankton biomass then abruptly increased by 3-fold and persisted throughout the latter half of the ice melt period (open circles, Figure 1.8d). This large increase was driven by taxa in Group B_w and C (common phytoplankton blooming taxa) that eventually composed 35 to 70% of the observed phytoplankton biomass (open circles, Figure 1.8e and f).

Modeled concentrations of Group B_w and C (black and gray solid lines, Figure 1.8f) were similar to observations of equivalent taxa (open circles, Figure 1.8f) under the condition that Group B_w accumulated from sloughing and growth and Group C accumulated from growth. In contrast, modeled concentrations of Group A_w, under the condition of accumulation and growth (solid gray line, Figure 1.8e), did not agree with observations of equivalent taxa (open circles, Figure 1.8e). Modeled concentrations of Group A_w were similar to field observations (open circles, Figure 1.8e) only if Group A_w accumulated via sloughing (dotted gray line, Figure 1.8e) and did not grow in the water column. Under these conditions (accumulation only, no growth; dotted gray line, Figure 1.8e), the model results of Group A_w were close to observed concentrations of common ice algal taxa in the phytoplankton (equivalent to Group A_w, open circles, Figure 1.8e). Thus, comparison of field observations and simulations suggests that Group A_w taxa (common to ice algal blooms) accumulate in the water column from sloughing events, but not growth, while Group B_w (ice-derived but common to phytoplankton blooms) taxa accumulate from both growth and sloughing events in late spring.

1.4 Discussion

1.4.1 Spring controls on ice algal communities

Spring ice algal biomass during our study is comparable to other studies in the Western Arctic. Our mean spring depth-integrated ice algal biomass (39.9 $\pm$ 28 mg Chl *a* m^{-2}) was similar to that of the Shelf-Basin Interaction (SBI) cruises (37.9 $\pm$ 81.4 mg Chl *a* and phaeopigments m^{-2}, Gradinger 2009) and our maximum value (110 mg Chl *a* m^{-2}) was similar to that in Resolute

Passage (100 mg Chl *a* m^{-2}, Welch and Bergmann 1989). However, our spring depth-integrated POC and PON estimates were 2-fold higher than those reported by Gradinger (2009) from a 2002 study. These differences are likely attributable to interannual and spatial variability. Our spring cruise sampled more of the shelf than the off-shelf region and sampling continued later into the spring as irradiance increased, relative to the Gradinger (2009). The mean spring Chl *a* concentration in bottom ice during our study (395 mg m^{-3}) was 3-fold higher than the few previous measurements of spring ice algal biomass in the Chukchi Sea (123 mg m^{-3}, Ambrose et al. 2005; 120.3 mg m^{-3}, Meguro et al. 1966). Furthermore, the range of bottom Chl *a* concentrations in our study (12 to 961 mg m^{-3}) encompassed other Arctic values such as in the Canadian Arctic Archipelago (704 mg m^{-3}) and the Beaufort Sea (427-711 mg m^{-3}) (reviewed in Arrigo et al. 2009). Our estimates of bottom ice biomass are on the upper end of ice algal biomass for the Western Arctic, but both our study and others may underestimate biomass, as ice sampling methods can miss ice algal matt and strand communities previously observed in the Chukchi Sea (Ambrose et al. 2005, Gosselin et al. 1997).

While ice algal biomass distributions in early spring are tightly linked to light availability (Gosselin et al. 1986, Welch and Bergmann 1989, Cota and Smith 1991, Cota et al. 1991), this relationship can become decoupled in late spring (reviewed in Leu et al. 2015). Our observations were comparable to other late spring studies where proxies for light availability, such as snow or ice depth, were not correlated to ice algal biomass (Gosselin et al. 1985, Cota and Horne 1989). Ice algal communities in our study were acclimated to low light levels, exhibited by their low photoacclimation parameter (E_k <20 μmol photon m^{-2} s^{-1}). Additionally, the estimated light available to ice algae generally exceeded both photoacclimation levels and the minimum irradiance needed for ice algal growth (2 to 9 μmol $photon^{-1}$ m^{-2} s^{-1}, Horner and Schrader 1982; Gosselin et al. 1986), suggesting that light was not the dominant factor controlling ice algal biomass in late spring. The major control on horizontal light variability, snow depth, also remained low (<0.1 m) with few exceptions throughout the spring, in agreement with depth categories from a multi-year analysis (Mundy et al. 2007, Leu et al. 2015). The combination of higher irradiance relative to photoacclimation and the lack of large-scale snow variability suggests that ice algae were not light limited and explains the absence of a relationship between snow depth and algal biomass in mid to late spring. In contrast, a prior study conducted earlier in the melt season and on larger scales showed the percent ice algal coverage (ratio of area of bottom ice occupied by ice algae to total bottom ice area) did correlate with proxies for light availability (snow depth; Ambrose et al. 2005). Differences in scale, methodology (autonomous

vehicles vs. ice core samples), and interannual ice and snow variability may have contributed to differences in the importance of light between the two Chukchi Sea studies.

Late stage ice algal blooms are more typically controlled by nutrient limitation (Leu et al. 2015). Nutrient availability in ice is largely controlled by seawater-ice exchange and, to a lesser extent, desalination and regenerative supply (Cota et al. 1987). $Si(OH)_4$ is often reported to be the main limiting (Cota et al. 1990, Gosselin et al. 1990) or co-limiting nutrient (Smith et al. 1997) in Arctic sea ice. However, in our study, $Si(OH)_4$ (as well as NO_3^- and PO_4^{3-}) in bottom ice was much higher than predicted by conservative mixing at half of the spring ice stations. Because of the reduced internal cellular storage potential for $Si(OH)_4$ relative to NO_3^- and PO_4^{3-} (Nelson and Gordon 1982, Wheeler 1983, Cota et al. 1987), its availability throughout spring suggests that there was ample ice-seawater exchange during most of our spring survey. Without this enhanced nutrient supply from seawater exchange, the ice algal bloom may have reached nutrient limitation within several days or weeks depending on growth rate and initial ice nutrient concentrations (Cota et al. 1987, Cota et al. 1990, Cota et al. 1991, Gradinger 2009). Ignoring desalination and regenerative supply, we estimate that an input of ~1 m^3 of water (2% of the NO_3^- water column inventory for a uniformly mixed 50 m water column) through skeletal layer convection (Wakatsuchi and Ono 1983) and turbulent mixing (Cota et al. 1987, Cota et al. 1991) is needed per m^2 of sea ice to support the observed spring biomass, similar to previous Chukchi Sea surveys that estimated N demand from biomass accumulation (0.27 - 0.62 mmol N m^{-2} d^{-1} summarized in Cota et al. 1987).

Previous modeling studies suggest that during late bloom stages, moderate biomass losses are driven by snow melt-induced brine flushing, channel enlargement, and channel interconnection (Gradinger et al. 1991, Fortier et al. 2002, Lavoie et al. 2005), and to a lesser extent, biologically-mediated ice melt due to radiative absorption by algae (Zeebe et al. 1996, Lavoie et al. 2005). During our study ice degradation processes were largely responsible for driving biomass and physiological variability of the spring bloom despite sampling during mid to late spring, prior to widespread surface melt and melt pond formation. For instance, declines in ice algal biomass and physiology over the spring season were significantly related to proxies for ice melt progression on scales ranging from tens of meters to tens of kilometers. Despite the high biomass variability within an ice floe, melt impacts were detected across many ice floes. Spring bottom ice algal concentrations were positively correlated with days until ice melt using our metric of 50% ice cover loss, suggesting that ice melt on the scale of kilometers can serve as an indicator of the seasonal decline in ice algal biomass in spring. Similarly, seasonal declines in ice F_v/F_m could be largely explained by warming surface water and bottom ice temperatures.

Both direct and indirect processes involved in ice melt likely contributed to the decline of the ice algal bloom observed in our study. Local bottom ice processes during melting, including heating and flushing, may reduce ice algal attachment, spur the sloughing of ice algal layers, and potentially allow larger grazers to access a larger fraction of the ice algal habitat (Krembs et al. 2000). Warming sea ice also decreases nutrient supply to the ice algal habitat by reducing convective exchange with under-ice surface waters (Polashenski et al. 2015), as indicated by the different salinity and nutrient concentrations in the sea ice relative to the underlying surface waters. Additionally, while ice and surface ocean temperatures best explained F_v/F_m variability, these predictors were also positively correlated with irradiance, suggesting that warmer temperatures were associated with higher light levels. Despite the potential mechanisms for light stress, ice algal communities had relatively low photoprotective pigment ratios (stress defined as >0.4 by Alou-Font et al. 2013) that suggested light was not a primary stressor. The ice algal biomass decline was primarily driven by loss from melting ice, but reduced growth due to decreased nutrients and/or photoinhibition, as suggested by Juhl and Krembs (2010), may help explain the strong significant inverse relationships between ice algal biomass and ice melt and environmental temperatures.

1.4.2 Biological coupling of ice-ocean algal communities

Over the course of the seasonal cycle, observations of shared species between the ice and water column (Taniguchi et al. 1976, Hameedi 1978, Horner and Schrader 1982, Zhou et al. 2015) are expected because the water column phytoplankton are incorporated into the ice during freeze-up (Garrison et al. 1983; Niemi et al. 2011). Phytoplankton and ice algal communities begin to diverge as taxa employ strategies to overwinter in the sea ice (Horner and Alexander 1972, Zhang et al. 1998, Krembs et al. 2011, Leu et al. 2015). As the ice algal bloom takes off in spring, the ice environment further selects the most well adapted ice algal taxa in spring. Multiple studies over the last several decades in the Chukchi Sea have observed that the spring bottom-ice algal communities are predominantly composed of pennate diatoms (Meguro et al. 1966, Ambrose et al. 2005, Quillfeldt et al. 2003, this study) and the centric ice diatom *Melosira arctica* (Ambrose et al. 2005, this study), similar to ice algal community composition throughout the Arctic (reviewed in Leu et al. 2015). The two dominant ice pennate diatom genera in our study (*Nitzschia* and *Navicula*) are also prevalent in ice communities of the Canadian Archipelago (Galindo et al. 2014) and the Beaufort Sea (Horner and Schrader 1982).

Coupled observations of sea ice and pelagic communities from our study and in other systems suggest that community composition and the timing of ice algal release play a large part in determining the degree to which ice algae seed the subsequent phytoplankton blooms that

develop once ice cover diminishes (Legendre 1981). Our observations and modeling results suggest that the loss of the bottom ice algal layer in late May and early June temporarily elevated phytoplankton concentrations and affected phytoplankton community composition in the upper 10 to 20 m of the water column. Field results (this study) show that ice-derived taxa briefly dominated the phytoplankton community and elevated phytoplankton Chl *a* by 1 to 2 mg m^{-3} approximately 20 to 30 days before ice melt. These enhanced concentrations of ice-derived taxa observed in the phytoplankton (open circles, Figure 1.8e) are explained in the model by sloughing of ice algae into the water column (gray dotted line, Figure 1.8e), without subsequent growth (gray solid line, Figure 1.8e). The comparison between modeled and measured concentrations of common ice algal taxa (*Nitzschia, Navicula*, unidentified pennates) in the water column suggests that these taxa are temporary residents of the water column and are either exported to the benthos or are grazed upon by zooplankton and do not grow and seed phytoplankton. Coupled ice-ocean studies from Hudson Bay have also found that ice-derived taxa (similar to Group A) elevate under-ice Chl *a* concentration, but do not explain continued increases in phytoplankton abundance (comprised of taxa similar to Group B_w and C) beneath the sea ice throughout the melt cycle (Legendre 1981).

Field observations suggest that phytoplankton concentrations exceeding 1-2 mg Chl *a* m^{-3} are due to the growth of taxa common to phytoplankton blooms, such as *Fragilariopsis*, *Thalassiosira*, and other centric diatoms. While these taxa also are found in the ice, our model suggests that concentrations of these ice-derived taxa were insufficient to yield the concentrations observed throughout spring and alone, did not explain biomass of bloom-forming phytoplankton taxa in the water column. However, through both accumulation and growth in the water column, these ice-derived bloom-forming phytoplankton taxa (Group B_w) can represent up to 40% of the total bloom-forming phytoplankton population by the time of ice melt.

Past phytoplankton surveys of ice-edge and open water blooms in the Chukchi Sea have shown both the presence and absence of ice-derived taxa (Hameedi 1978, Alexander 1980, Horner and Schrader 1982, Quillfeldt et al. 2003, Sukhanova et al. 2009). Alexander (1980) hypothesized that inconsistencies in algal community composition were due to the transitory nature of ice algae in the water column. Recent studies across Arctic polar and subpolar regions have presented similarly varied conclusions of the ice algal impact on the phytoplankton in the water column. In an open water bloom in the North Water Polynya, Tremblay et al. (2006) found no ice-derived effect on phytoplankton bloom development. Conversely, Galindo et al. (2014) observed under-ice blooms in the Canadian Archipelago that were associated with rapid ice melt, stratification, and ice-derived phytoplankton in near-surface waters. Blooms associated with ice-

derived taxa were shorter in duration and lower in magnitude than blooms dominated by non-ice-derived taxa, which were observed in less stratified conditions where melt was delayed (Galindo et al. 2014). Previous Bering Sea studies have suggested that sea ice algae make substantial contributions to phytoplankton (Taniguchi et al. 1976, Saito and Taniguchi 1978, Alexander and Chapman 1981, Schandelmeier and Alexander 1981, Horner 1982, Zhou et al. 2015) and a recent coupled ice algae-phytoplankton survey (Szymanski and Gradinger 2016) suggested that the loss of the bottom algal layer has the potential to dominate the phytoplankton bloom in this region. Bering Sea community composition data from Syzmanski and Gradinger (2016) suggest that the ice-derived bloom-forming taxa in the phytoplankton (*Chaetoceros, Fragilariopsis*) would be 1 to 14-fold higher than the non-ice-derived component, with complete sloughing of the bottom ice algal layer into a 50 m ML. However in their study, despite the influx of seed populations, they suggested the bloom was delayed due to lack of light availability (Szymanski and Gradinger 2016).

Beyond directly seeding phytoplankton, our data suggest that ice algal communities have the potential to impact the light and nutrient availability of the water column below. For instance we observed that spring ice melt served as a source of NH_4^+, which persisted through summer. Other polar studies have observed sporadic spikes in water column NH_4^+ and urea in June and attributed these to the onset of seasonal ice melt (Brandini and Baumann 1997, Conover et al. 1999) or to the grazing of ice algal cells that are melting into the water column (Conover et al. 1999). The sloughing of the ice algal layer in spring will also increase light transmission through the ice, thereby alleviating light limitation and increasing phytoplankton growth. Multiple studies have suggested that sea ice algae shade phytoplankton communities (Horner and Schrader 1982) and the loss of the sea ice algae increases light transmission (Campbell et al. 2015) and phytoplankton production (Grainger 1977).

1.5 Concluding remarks

Coupled ice-ocean studies across the Arctic polar and subpolar regions highlight the impact that changing ice duration and extent may have on linkages between ice algal and phytoplankton communities. Communities are rarely clearly separated “floristically, temporally, and spatially” (Horner 1996) making teasing apart community linkages challenging, if not impossible. Shifts in the timing of ice melt relative to phytoplankton bloom onset may weaken or enhance ice-ocean coupling across the Arctic. As evidenced by the study on community composition in the Bering Sea (Syzmanski and Gradinger 2016), delays in phytoplankton bloom development relative to ice melt suggest that ice algae can have pronounced impacts on seeding of the water column and

potentially "prime" the system for a bloom. In these instances, the continued addition of bloom-forming phytoplankton taxa from the sea ice outpaces the slow growth or maintenance of the non-ice-derived phytoplankton. While accumulation of sloughed ice algae in the water column may slightly elevate biomass levels, processes delaying stratification postpones the phytoplankton bloom.

Conversely, under current conditions in the Chukchi Sea in late spring (this study), the resurgence of observed dominant bloom-forming phytoplankton taxa over taxa common to ice algal blooms in the water column suggests that ice communities have a minor impact on seeding early season phytoplankton blooms, but rather briefly elevate phytoplankton concentrations. Observed light-dependent phytoplankton growth rates were sufficient to support observed concentrations of bloom-forming phytoplankton. The influx of ice-derived bloom-forming phytoplankton taxa played a lesser (relative to the Bering Sea study), but still supporting role in bloom development. Under conditions where the phytoplankton bloom occurs before or corresponds with ice melt onset the growth of non-ice-derived bloom-forming phytoplankton outpaces the addition of these taxa from the sea ice.

Interannual variability in melting conditions of snow and sea ice may further influence the connection between the ice algal and phytoplankton communities. For instance field observations in the Chukchi Sea (this study) and the Canadian Archipelago (Galindo et al. 2014) showed that under melt conditions where the ice algal bottom layer gradually sloughs off of the sea ice from mid May to mid June, the under-ice phytoplankton community is dominated by taxa common to phytoplankton blooms in the Canadian Arctic Archipelago and the Chukchi Sea. However, for another study year in the same region of the Canadian Arctic Archipelago, rapid ice melt conditions, where the entire ice algal biomass layer sloughed into the water column over the course of a week (rather than a month), resulted in a phytoplankton bloom dominated by pennate diatoms common to ice algae that drew down surface NO_3^- in a few days (Galindo et a. 2014). A comparison of this study with our own further suggests that both the timing and rate of ice algal release relative to environmental and biological controls on phytoplankton growth impacts phytoplankton bloom dynamics in late spring and early summer.

Limited observations of the superposition of ice-derived biomass on under-ice phytoplankton communities across different regions makes it difficult to assess its impact on early season under-ice bloom dynamics to the broader Arctic. Our study, and others (Galindo et al. 2014, Syzmanski and Gradinger 2016), highlight how the timing and rate of ice algal release to the water column, relative to processes controlling phytoplankton growth (i.e. water column stratification/light availability), impact the coupling between the ice algal and phytoplankton communities. These

processes can vary on an annual basis for a given region and should be considered when assessing the impact of ice algal seeding on phytoplankton blooms. Understanding the full range of mechanistic processes coupling ice and ocean communities will advance our knowledge of their impacts on primary production across rapidly evolving sea ice conditions.

Chapter 2

Drivers of Ice Algal Bloom Variability from 1980 – 2015 in the Chukchi Sea

SELZ VS, SAENZ BT, VAN DIJKEN GL, ARRIGO KR

Sea ice provides an important habitat for the ice algae that fuel upper trophic levels in early spring, prior to phytoplankton bloom development. In the Chukchi Sea, the ice environment has experienced large-scale changes in snow cover, ice thickness and extent, and timing of ice advance (freeze up) and retreat (melt). Using a 1-D coupled physical biological ice ecosystem model and observed distributions of sea ice, we investigated how changing ice conditions may have impacted ice algal bloom dynamics for the central Chukchi Sea between 1980 and 2015. Model results suggest that over this 35-year time period, annual ice algal net primary production (NPP) decreased by 22%. Modeled snow and ice melt, as well as satellite-derived ice retreat, occurred progressively earlier in the spring from 1980 to 2015, even though modeled ice and snow thicknesses showed no temporal trends. Variable snow and ice thicknesses cause highly variable light available to ice algae in early spring. Therefore, there was no interannual trend in the timing of the start of the ice algal bloom. Rather, over time, ice algal blooms ended earlier in spring due to earlier onset of ice melt and ice retreat. Results suggest that the length of the ice season sets the upper bound on annual ice algal NPP, with early melt years corresponding to lower NPP compared to more productive, later melt years. Linear regression results suggest that within early versus late melt year groupings, snow plays a secondary, yet important role in determining annual ice algal NPP. As sea ice thins and melts earlier in spring, future snow dynamics will be an important factor determining the onset of the ice algal bloom, and thus the duration of the bloom in an early melt, shortened ice season scenario.

2.1 Introduction

Sea ice is an important component of the western Arctic ecosystem that provides habitat and critical food sources to upper trophic levels in spring and early summer (Michel 1996). Algae living within the sea ice fuel ice-associated food webs, are significant contributors to biogeochemical cycles (Hayashida et al. 2017), and export carbon to the benthic community on shallow continental shelves (Michel et al. 2006, Kedra et al. 2015). Additionally, ice algal communities impact phytoplankton by altering the light (Arntsen in prep) and nutrient environment (Mortensen et al. 2017) of the water column. In some cases, ice algae directly seed phytoplankton blooms (Jin et al. 2007, Galindo et al. 2014), although seeding may be variable and transient (Selz et al. 2017), depending on ice algal and phytoplankton communities and environmental conditions (Tedesco et al. 2012). Given the importance of ice algae to pelagic and benthic ecosystems, they are especially relevant to the shallow Chukchi Sea, which harbors some of the most productive waters in the world and supports culturally relevant upper trophic level organisms (Kedra 2015).

Ice algae in the Chukchi Sea are highly productive in spring and reach a maximum biomass of ~1000 mg Chl *a* m^{-3} in bottom sea ice, with depth-integrated values of >100 mg m^{-2} (Ambrose et al. 2005, Gradinger 2009, Selz et al. 2017). Observations suggest that Arctic sea ice communities are most active in the bottom skeletal layer (1 – 4 cm) of the sea ice (Maykut 1985). These high ice algal biomass levels are likely attributable to the high nutrient concentrations observed in the water column that extend across the Chukchi shelf in spring, replenished annually by winter mixing (Arrigo et al. 2017). Multiple observations suggest that nutrient availability in the ice sets the upper limit for ice algal production (Michel et al. 2006*,* Kirst and Wiencke 1995) and drives regional scale changes in sea ice algal production (Smith et al. 1990, Gradinger 1999, 2008). Furthermore, Deal et al. (2011) suggested that even in waters with low surface nutrient concentrations, high ice growth rates would enhance nutrient exchange and supply sufficient nutrients to the ice algal community.

Since the Chukchi Sea has higher spring nutrient concentrations (Arrigo et al. 2017) than other western Arctic regions, such as the Beaufort Sea (Watanabe et al. 2015) and the Canadian Archipelago (Mortensen et al. 2017), it has the potential to support higher ice algal biomass in spring (Jin et al. 2012). Because most existing sea ice ecosystem models predict that ice algal biomass increases proportionally to nutrient addition (Jin et al. 2006, Pogson et al. 2011, Tedesco and Vichi 2014, Mortensen et al. 2017), the Bering and Chukchi seas are thought to have among the highest rates of sea ice algal production in the Arctic (Deal et al. 2011, Jin et al. 2012, Watanabe et al. 2015).

Models also confirm that while nutrient availability sets the maximum algal biomass that can accumulate within the ice, it does not control the timing or duration of ice algal blooms (Pogson et al. 2011, Tedesco and Vichi 2014, Mortensen et al. 2017). Rather bloom timing is determined by snow and ice thickness (Lavoie et al. 2005, Pogson et al. 2011, Tedesco and Vichi 2014), which control the amount of light that is transmitted through the sea ice (Arrigo et al. 1991). In addition, as light penetrating the snow and sea ice is absorbed and converted to heat, it accelerates the decline of ice algal blooms by melting the high biomass bottom-most layers of the sea ice (Lavoie et al. 2005, 2009, Pogson et al. 2011). At the start of the spring, ice algal growth rates are limited by light (reviewed in Leu et al. 2015) and 1-D modeling studies at different sites throughout the Arctic show that this light limitation persists until the bloom peaks (Jin et al. 2006, Lavoie et al. 2005, 2009, Mortensen et al. 2017). After peak biomass has been reached, blooms may be limited by nutrient depletion (Mortensen et al. 2017), oscillate between light and nutrient limitation, or be terminated by sea ice melt (Lavoie et al. 2005, 2009, Jin et al. 2006, Pogson et al. 2011).

The physical characteristics of sea ice during melt can further exacerbate both light and nutrient limitation of ice algal blooms. The fresh melt water lens that develops beneath melting sea ice reduces the nutrient flux to the skeletal layer (Lavoie et al. 2005, Lavoie et al. 2009), while higher damaging levels of irradiance may penetrate the thinner sea ice and reduce algal growth rates (Juhl and Krembs 2010). Combined, the increased nutrient-limitation and photodamage associated with melting ice prevents ice algae from maintaining their position in the sea ice (Juhl and Krembs 2010). In the Chukchi Sea, ice melt appears to be the dominant process, more so than nutrient limitation or photodamage alone, controlling late season ice algal biomass variability and bloom decline (Selz et al. 2017).

The physical factors that control ice algal bloom dynamics in the Chukchi Sea have undergone drastic changes over the last 35 years (Stroeve et al. 2007). This shallow inflow shelf has experienced later freeze onset and earlier retreat of local sea ice, shortening the length of the sea ice season (Stroeve et al. 2007, Stroeve et al. 2014). The ice pack itself has become thinner over the past 50 years (Kwok and Rothrock 2009, Horvat et al. 2017), with a 56% decrease in snow depth (Webster et al. 2014). Given these changes and their relevance to sea ice algal production over the spring season in the Chukchi Sea, the goal of our study was to understand how changing sea ice conditions affect annual ice algal bloom dynamics, phenology, and production, over the 1980 to 2015 period. To achieve this goal, we modified an existing 1-D coupled physical-biological sea ice model (Saenz and Arrigo 2012, 2014) for use in the Chukchi

Sea, forced with satellite-derived sea ice concentrations, atmospheric reanalysis data and modeled surface irradiance.

2.2 Methods

Model Description. We used a modified version of the one-dimensional heat-, and mass-conserving Sea Ice Ecosystem State Model (SIESTA) model of Saenz and Arrigo (2012, 2014) to simulate vertical ice pack physics in the Chukchi Sea. Sea ice is represented in a maximum of 42 layers within the vertical 1-D sea ice column (Saenz and Arrigo 2012, 2014). Sea ice physics including thermodynamics, hydrodynamics, snow dynamics, and atmosphere-ocean boundaries and their computation are described in detail in Saenz and Arrigo (2012, 2014).

The sea ice ecosystem model is based on that of Arrigo and Sullivan (1994) and modified by Saenz and Arrigo (2012, 2014). Briefly, state variables in the model include ice algae, organic detrital material (ODM), and four different nutrients, including nitrate (NO_3^-), ammonium (NH_4), phosphate (PO_4^{3-}), and silicate ($Si(OH)_4$). Ice algal growth rate is modeled as a function of light, macronutrients, salinity, and temperature. The temperature-dependent specific growth rate is multiplied by the limitation index, the single most limiting light or nutrient resource, and a sub-optimal salinity term further detailed in Arrigo et al. (1993). Modeled ice algal nutrient stoichiometry is fixed. Ice algae may be transformed into ODM through senescence or zooplankton grazing via a daily loss rate, or lost from the sea ice model domain through sea ice melting. The bottom skeletal layer of the sea ice (the growing layer of ice at ice-water interface) contains the majority of algal biomass and is allowed to reach a maximum thickness of 0.05 m in model simulations based on field observations of elevated concentrations in bottom sections from the Chukchi Sea, similar to other arctic skeletal layer thickness observations (0.03 m: Maykut et al. 1985) used in ice ecosystem models (0.02 - 0.05 m: Lavoie et al. 2005, Jin et al. 2012, Dupont 2012, Mortensen et al. 2017).

Light within the sea ice is calculated using a two-stream spectral radiative transfer model that simulates thin-layer scattering (Briglieb and Light 2007, as detailed in Saenz and Arrigo 2012). Briefly, five scattering classes: cold snow, warm snow, warm sea ice, cold mirabilite-containing sea ice, and eutectic ice are used to calculate spectral irradiance and heat absorption in the photosynthetically active radiation (PAR) range. Shortwave radiation outside the PAR range, calculated as a fraction of PAR, is attenuated as a single band with a spectrally-weighted absorption coefficient (Saenz and Arrigo 2012).

Forcing Data. The model is forced with atmospheric European Center for Medium-Range Weather Forecasts (ECMWF) reanalysis data and daily surface spectral irradiance modeled from

Greg and Carder (1990) for a 1.5 x 1.5 degree latitude and longitude grid centered in the central Chukchi Sea (71.4°N and 166.9 °W). ECMWF reanalysis variables including air temperatures, wind speed, and humidity were used to calculate the surface heat flux as further detailed in Saenz and Arrigo (2012). ECWMF 2 m air temperatures were in good agreement with values recorded from the mast of the USCGC *Healy* ($y = 0.84x + 1.05$, $r^2 = 0.92$, p value <0.05) during the spring SUBICE 2014 expedition to the Chukchi Sea. ECWMF reanalysis variables, including total precipitation, were used to model snow accumulation for dry and wet snow (100 and 330 kg m^{-3}; Pomeroy et al. 2001). Snow thickness may change based on sublimation, melting and percolation, and brine drainage-related processes, which are detailed in Saenz and Arrigo (2014).

Special Sensor Microwave Imager (SSM/I) and Advanced Microwave Scanning Radiometer for EOS (AMSR-E) data were used to determine start and end dates for the annual sea ice cycle. The start of the sea ice season each year was defined as the day when the running seven-day mean of ice concentration exceeded 50%. The end of the sea ice season was defined as the day when the running seven-day mean sea ice concentration fell below 50%. The 50% threshold was chosen based on observations of Selz et al. (2017) that showed that this metric corresponded with the decline of the ice algal bloom in the Chukchi Sea. Snow and ice temperatures were initialized following Arrigo et al. (1993).

Model Runs. Model parameters, including the fraction of snow lost from the modeled domain per precipitation event and the ocean heat flux, were tuned so that the modeled maximum snow and sea ice thicknesses for the standard 2014 run agreed with the mean observed during the 2014 SUBICE cruise (0.13 ± 0.07 and 1.3 ± 0.19, respectively , 26 May – 15 June; Figure 2.1a,b). The resulting modeled PAR beneath the sea ice and the depth-integrated biomass peak and bloom decline fell within the range of 2014 SUBICE cruise observations (Figure 2.1c,d). Snow lost from the domain per precipitation event was tuned in thick/thin snow 2014 runs to match the minimum and maximum 2014 snow observations (i.e. more/less snow accumulated per precipitation event) and to explore intraseasonal variability.

All model runs were initialized with thin ice (0.2 m) and snow (0.01 m) on the ice advance date determined for that particular ice season. Initial seawater nutrient concentrations (Table 2.1) were taken from May 2014 field observations, recorded prior to biological drawdown, and assumed to represent maximum nutrient concentrations in winter and early spring (Arrigo et al. 2017). Initial nutrient, algal, and detrital concentrations in each sea ice layer were proportional to concentrations in the seawater, based on the initial brine fraction of each sea ice layer (Table 2.1).

Subsequently, we ran the model for 35 years (1980 – 2015) to simulate interannual variation in ice algal bloom characteristics within the spring and early summer season. The ice algal bloom

period is defined as the time over which depth-integrated biomass remained >5 mg Chl *a* m^{-2} when ice concentrations (derived from satellite data) were > 50%.

Table 2.1 Model parameters and initial values.

Model Parameter	Value	Unit
Maximum algal growth rate at 0	0.81	per day
Algal temperature-dependent growth rate constant	0.631	per °C
POC remineralization rate	0.03	per day
Remineralization efficiency	1	fraction
Maximum spectral photoadaptation parameter	18	μEin m^{-2} s^{-1}
Algal/Detritus C:Chl a ratio	35	g/g
Algal detritus C:N ratio	7	mol/mol
Algal/detritus C:P ratio	106	mol/mol
Algal/detritus C:Si ratio	4	mol/mol
Half-saturation algal rate constant for NO3 uptake	1	uM
Half-saturation algal rate constant for NH4 uptake	1	uM
Half-saturation algal rate constant for PO4 uptake	0.1	uM
Half-saturation algal rate constant for SiO4 uptake	4	uM
Seawater detrital concentration	0	uM
Seawater Nitrate concentration	20	uM
Seawater Ammonium concentration	1	uM
Seawater Phosphate concentration	2.8	uM
Seawater Silicate concentration	50	uM
Seawater Algal concentration	1	mg m3
Seawater Detrital concentration	0	mg m3

Data Analyses. We performed sensitivity analyses to assess within year and interannual variability in ice algal bloom dynamics driven by changes in snow and ice thickness. Early winter ice thickness and the snow lost per precipitation event parameter for year 2014 were adjusted so that maximum snow and ice thicknesses in the sensitivity analyses matched the full range of maximum ice and snow thicknesses from the resulting 1980 to 2015 modeled record. Correlation and linear regression analysis were used to identify how the characteristics of the sea ice environment and the ice algal bloom changed over time and a p value of <0.05 denotes significance.

2.3 Results

2.3.1 The Standard Run

Snow and Sea Ice. In all three 2014 model runs (standard, thin snow, thick snow), snow accumulated from the date of ice advance in late fall (Nov 21, date not shown on Figure 2.1) and reached a maximum in the first week of June before starting to melt. In the standard model run, snow thickness reached a maximum of 0.17 m on 4 Jun (Figure 2.1a). These modeled maximum values were similar to the observed mean snow thicknesses (0.13 ± 0.07; Figure 2.1a). Snow decreased in thickness from 5 June to 25 June and this timing corresponded with observed declines in snow thickness (Figure 2.1a). The thick snow model run peaked on the same date as the standard model run and matched the maximum observed snow depth (Figure 2.1a), but did not fully melt before the date of ice retreat (<50% ice concentration derived from satellite imagery). The thin snow run reached a maximum thickness a couple days earlier on 2 June and melted between 3 and 21 June, falling within the lower range of observations (Figure 2.1a).

In all three 2014 model runs, sea ice concentrations exceeded 50% on 21 November, 2013 marking the date of sea ice advance (data not shown). In the standard run, sea ice increased from the initialized thickness of 0.2 m to a maximum thickness of 1.29 m on 19 May before the bottom skeletal layers started to thin (Figure 2.1b). By the time of ice retreat as determined by satellite, sea ice had thinned by ~ 0.06 m. In the thick snow run, sea ice characteristics were almost identical to the standard run (Figure 2.1b). In the thin snow run, sea ice thicknesses reached a maximum of 1.39 m on 15 May. Ice in the thin snow run had thinned by ~0.08 m by the time of ice retreat.

Ice Algal Biomass. When simulating the mean ice and snow thicknesses of the observational data (Figure 2.1a,b) in the standard run, ice algal biomass increased slowly from <1 mg Chl *a* m^{-2} on 22 February (data not shown) to the bloom threshold of >5 mg Chl *a* m^{-2} on 4 May (35 – 175 mg C m^{-2}) . Biomass increased much more rapidly over the next 24 days, peaking at 50 mg Chl *a* m^{-2} (1.75 g C m^{-2}) on 28 May. Modeled seasonal maximum biomass values fell within the top half of the observed maximum values (41 – 97 mg Chl *a* m^{-2} (1.44 – 3.40 g C m^{-2}); Figure 2.1c). At the peak of the bloom, > 85% of the biomass was located in the bottom ~0.05 m of the sea ice. The decline in modeled biomass agreed with the range of values observed from 26 May to 15 June during SUBICE (Figure 2.1c). Over a 30-day period, biomass declined to 9 mg Chl *a* m^{-2} (45 g C m^{-2}) at ice retreat, with 40% of the total biomass remaining in the bottom 0.05 m of the sea ice, marking the end of the ice algal bloom (Figure 2.1c). Modeled vertical biomass distributions in the bottom of the sea ice (40-85%) agree with observed distributions (60 ± 20%) (Selz et al. 2017).

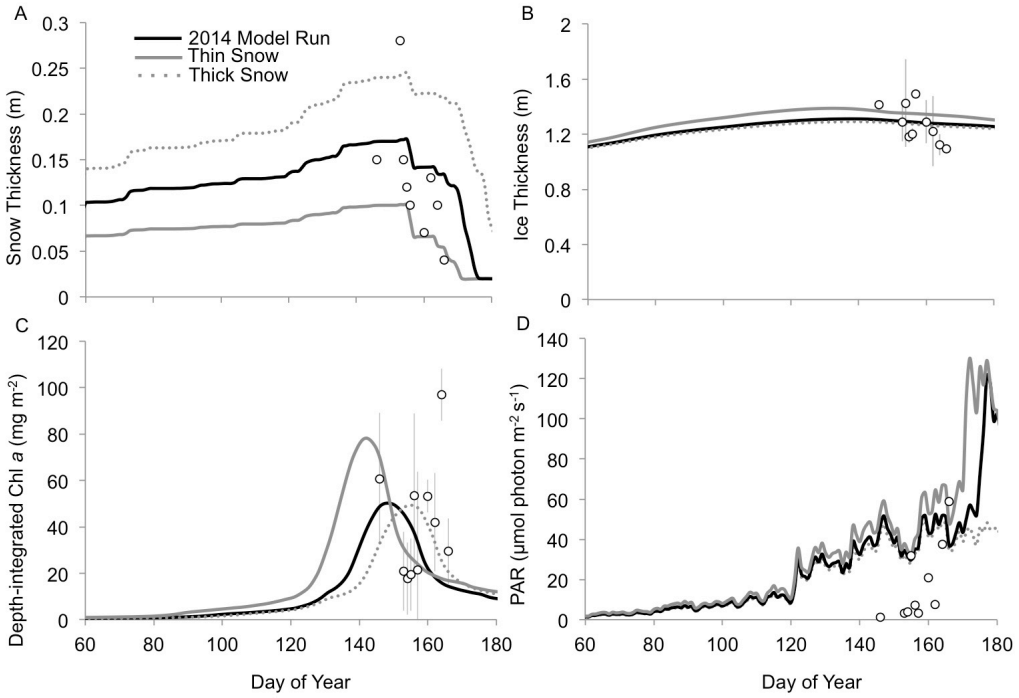

Figure 2.1 Comparison of modeled physical (a) snow (m) and (b) ice thickness (m) and biological variables (c) depth-integrated biomass (Chl a mg m^{-2}) and (d) photosynthetically active radiation (µmol photon m^{-2} s^{-1}) (line) to field observations ((mean ± sd; open symbols) for year 2014. Thin snow (solid gray line) and thick snow (dotted gray line) model runs represent the upper and lower (± sd) snow thicknesses of 2014 field data.

In the thick snow run, biomass was initially similar to the standard run, with the same dates of growth onset and bloom onset (> 5 mg m^{-2}, gray dotted line; Figure 2.1c). After bloom onset, the period of rapid increases in biomass between 5 May and 4 June lasted a week longer, but reached a similar maximum peak in biomass (49 mg Chl *a* m^{-2}) compared to the standard run. Peak biomass under thick snow matched the later biomass peak and timing of decline observed in field samples. Biomass declined over a 23-day period to a minimum of 12 mg Chl *a* m^{-2} at ice retreat (Figure 2.1c).

In the thin snow run, biomass increased slowly from <1 mg Chl *a* m^{-2} on 12 February to > 5 mg Chl *a* m^{-2} on 14 April (solid gray line, Figure 2.1c). After bloom onset, biomass rapidly increased to a peak of 78 mg Chl *a* m^{-2} on 22 May over a period of 38 days, growing longer and reaching higher biomasses earlier than that of the standard or thick snow run. Peak biomass in the thin snow run matched the earlier peak and higher biomass values observed during SUBICE. Over a 36-day period, peak biomass declined to 12 mg Chl *a* m^{-2} at ice retreat (Figure 2.1c).

Light. PAR beneath the bottom layer of sea ice algae (bottom PAR) increased from 0 in January to approximately 1 μmol photon m^{-2} s^{-1} on 22 February, the date when ice algae started to slowly accumulate in the standard run. Bottom PAR reached ~ 21 μmol photon m^{-2} s^{-1} at the date of bloom onset and ~ 45 μmol photon m^{-2} s^{-1} during the peak of the bloom (Figure 2.1d). Modeled bottom PAR agreed with the upper end of measurements made in the seawater beneath the sea ice in early – mid June (32 – 58 μmol photon m^{-2} s^{-1}; Figure 2.1d). PAR, rather than nutrients, was the main limiting resource from the initial stages through the peak (28 May) and subsequent decline of the bloom with the limitation index ranging from 0 to 0.40. On 19 June the main limiting resource switched from light to $Si(OH)_4$ for 11 days until ice retreat (0.40 – 0.45).

Modeled bottom PAR for the thick snow run was similar to the standard run in early winter when biomass started to slowly accumulate to above the bloom threshold. Bottom PAR for the thin snow run reached 1 μmol photon m^{-2} s^{-1} a week earlier than the mean (standard) and thick snow runs. Bottom PAR was often ~ 10 and 25 μmol photon m^{-2} s^{-1} higher under thin snow than mean snow (black line) or thick snow (dotted gray line) conditions in early and late spring, respectively (Figure 2.1d). PAR remained the main limiting resource (limitation index = 0 – 0.40) for thick and thin snow scenarios until well into the bloom decline when it switched to $Si(OH)_4$ on 25 June and 5 June, respectively. Model sensitivities to snow and sea ice are presented in detail in Results section Sensitivity Analyses.

2.3.2 Snow, Ice, and Algal Bloom Dynamics: 1980 to 2015

For all model runs from 1980 to 2015, maximum seasonal snow depths averaged 0.15 ± 0.04 m and ranged from 0.08 to 0.30 m on late spring sea ice (Figure 2.2a). The dates of snow melt onset ranged from 19 May to 21 June, averaging 9 June ± 9 days (Figure 2.2b) for all modeled years. For our domain, there was no discernable interannual trend in maximum snow depth or date of snow melt onset between 1980 and 2015.

The date of ice advance (freeze up) exhibited marked interannual variability (Figure 2.2c), ranging from as early as 26 August to as late as late as 13 December. The date of ice retreat was much less variable, ranging from 11 June to 9 August between 1985 and 2015 (Figure 2.2d). Over time between 1980 and 2015, sea ice advanced later in autumn ($y = 1.21x - 2107$, $r^2=0.29$, $p<0.05$) and retreated earlier in the spring ($y=-0.76x + 1692$, $r^2=0.38$, $p<0.05$).

Modeled sea ice thickness averaged 1.62 ± 0.18 m and reached a maximum that ranged from 1.14 to 1.89 m (Figure 2.2e) for all years studied. There was no statistically significant relationship between modeled maximum ice thickness and year, date of ice retreat, or date of advance. Over the 35-year study period, modeled sea ice reached maximum thickness on dates that ranged from 13 May to 10 June. Shortly after the date of maximum thickness, sea ice started

to thin (i.e. melt; Figure 2.2f), which began progressively earlier each year, melting approximately a month earlier in 2015 than in 1980 (r = -0.37, p = 0.027; Figure 2.2f). The date of sea ice melt onset was not related to the timing of snow melt onset. Modeled sea ice for all years between 1980 and 2015 started to thin when satellite ice concentrations were still as high as 77%, and in most years >90% (except for 1990, 1993, 1999, 2003, and 2015). The number of days between the start of ice melt and the timing of ice retreat decreased with time between 1980 and 2015 (r = -0.47, p< 0.01), suggesting that large scale melting rates had increased with time.

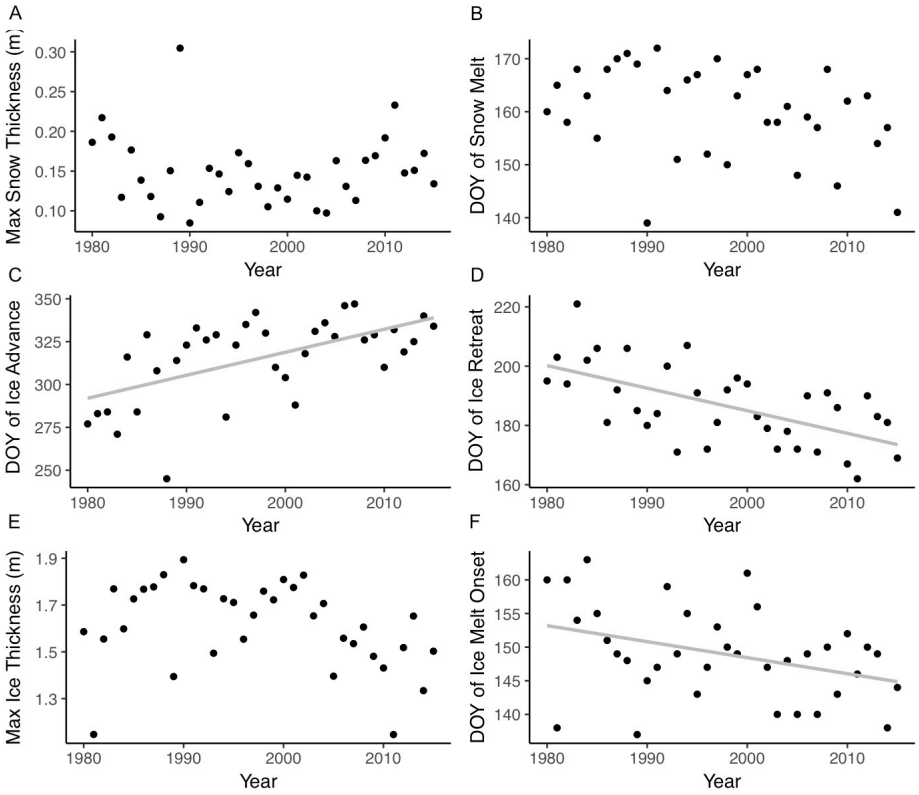

Figure 2.2 Trends in physical ice parameters over 1980 to 2015. Gray line denotes significant correlation ($p < 0.05$).

Modeled total ice algal net primary production (NPP) over the 1980 to 2015 period ranged from 2.69 to 6.52 g C m^2 y^{-1} (mean = 4.58 ± 0.74) and decreased significantly with time (r = -0.41, p = 0.01; Figure 2.3a). Within the seasonal ice algal bloom, the peak of depth-integrated biomass ranged from 1.4 to 2.4 g C m^{-2} and blooms peaked sometime between 28 May and 19 June. The day the bloom reached peak depth-integrated biomass was highly correlated with the day the ice started to melt (r=0.97, p<0.01). Light was the primary factor limiting ice algal biomass from winter to late spring during the initial stage and peak bloom for all years from 1980

to 2015. Light limitation switched to $Si(OH)_4$ limitation during the bloom decline period with a mean of 14±7 days after peak bloom for the entire 35 year period.

The duration of the modeled ice algal blooms (defined as number of days that depth-integrated Chl *a* remained ≥5 mg m^{-2}) ranged from 34 to 96 days, averaged 58 ± 12 days, and decreased with time (r = -0.49, p> 0.01; Figure 2.3b). In a given year, ice algal biomass first exceeded the bloom threshold sometime between 18 April and 23 May (Figure 2.3c). There was no significant temporal trend in the timing of the start of the ice algal bloom (Figure 2.3c). Open water often appeared before modeled depth-integrated biomass fell below 5 mg m^{-2}; therefore the retreat of sea ice marked the end of the bloom. Given the lack of a temporal trend in bloom onset, bloom duration was controlled by the earlier ice melt over the 1980 to 2015 period.

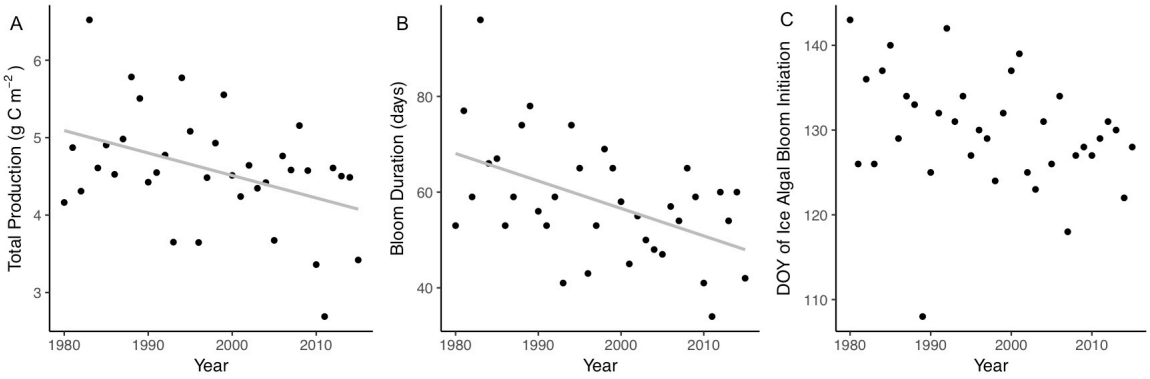

Figure 2.3 Trends in ice algal dynamics over 1980 to 2015. Gray line denotes significant correlation (p<0.05).

2.3.3 Sensitivity Analyses

We tested the sensitivity of the model to changes in snow and sea ice thickness to explore the relative importance of these variables in controlling the interannual variability in ice algal bloom dynamics using the extremes in modeled maximum snow and ice depths for 1980 to 2015 and atmospheric forcing from 2014 (the year for which we have observational data for comparison). Atmospheric forcing, such as spring time air temperature warming (>0° C), was within 1 standard deviation of the 35 year mean. In simulations where we tested the model sensitivity to different snow cover, we used the ice thickness from the 2014 simulation (Figure 2.4); in simulations where we tested the model sensitivity to different ice thickness, we used the snow depths from the 2014 simulation (Figure 2.5). In each case we only change a single parameter from the standard run.

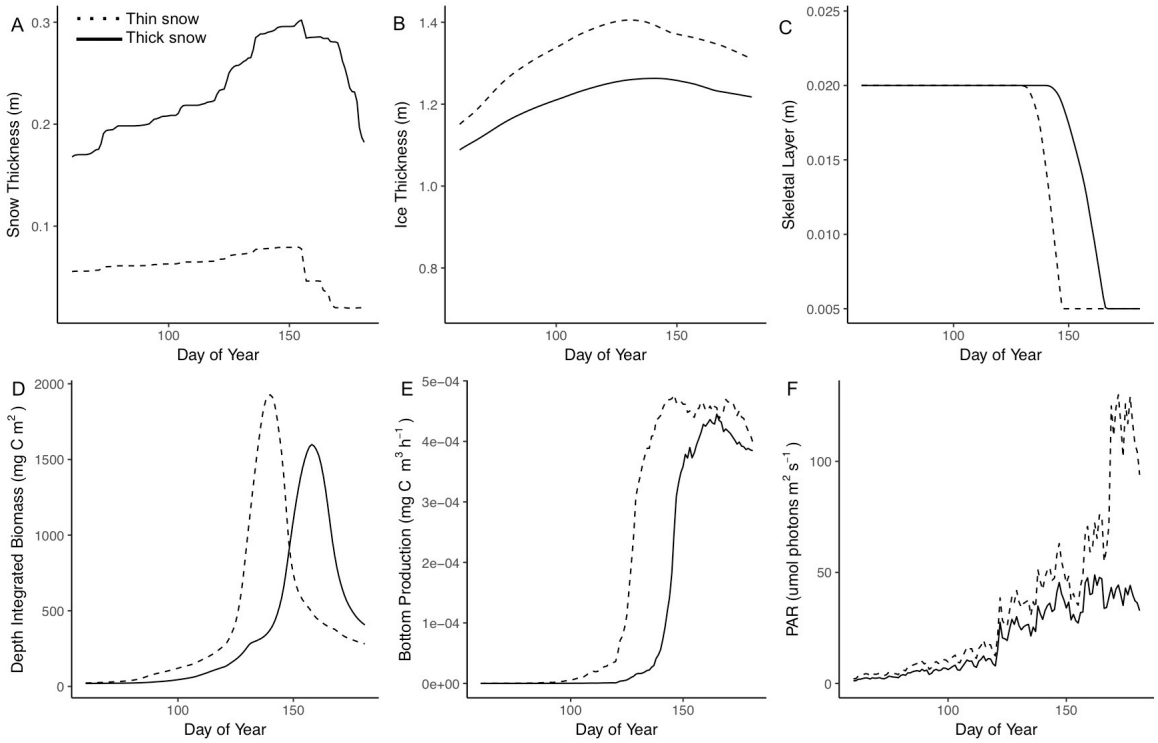

Figure 2.4 Sensitivity of modeled variables to maximum and minimum snow thicknesses observed over the 1980 to 2015 period for the 2014 sea ice season. (a) Snow thickness (m), (b) Ice thickness (m), (c) Skeletal layer thickness (m), (d) Depth-integrated biomass (mg C m^{-2}), (e) Bottom production (mg C m^{-3} h^{-1}), and (f) Photosynthetically Active Radiation (PAR) (µmol photon m^{-2} s^{-1}).

Physical Sea Ice Processes. Sensitivity analyses revealed that thicker snow cover slowed ice growth and resulted in a thinner sea ice pack (Figure 2.4 a,b). Sea ice cover simulated under maximum snow thicknesses (solid gray line: maximum range for 1980 to 2015, Figure 2.4) reached a maximum depth of 1.26 m, which was 0.14 m thinner than sea ice grown under the minimum snow thickness (gray dotted line, Figure 2.4a,b). The skeletal ice layer beneath thin snow melted 10 days earlier and at a faster rate than under thick snow (Figure 2.4c).

Conversely, sea ice thickness had a minimal effect on snow depth, with snow melting a few days earlier on thinner versus thicker sea ice (Figure 2.5a,b). Similar to snow, sea ice thickness affected the timing of the loss of the productive bottom skeletal ice layer. The skeletal layer under the thinnest sea ice conditions melted 12 days earlier than under the thickest sea ice conditions (Figure 2.4-5b,c). Unlike snow, sea ice thickness did not alter the rate of ice melt, but instead

influenced the total thickness of the skeletal layer, being 5 mm thicker in thicker ice (Figure 2.5c).

Light was the primary factor limiting ice algal NPP and biomass for both ice and snow sensitivity analyses. Not surprisingly, changes in snow thickness rather than changes in ice thickness had the greatest influence on bottom PAR (Figure 2.4-5f). Mean seasonal bottom PAR under thin snow (55 µmol photon m^{-2} s^{-1}) was 62% higher than that under thin snow (34 µmol photon m^{-2} s^{-1}), while mean seasonal bottom PAR under thick and thin ice were similar (44 and 46 µmol photon m^{-2} s^{-1}, respectively).

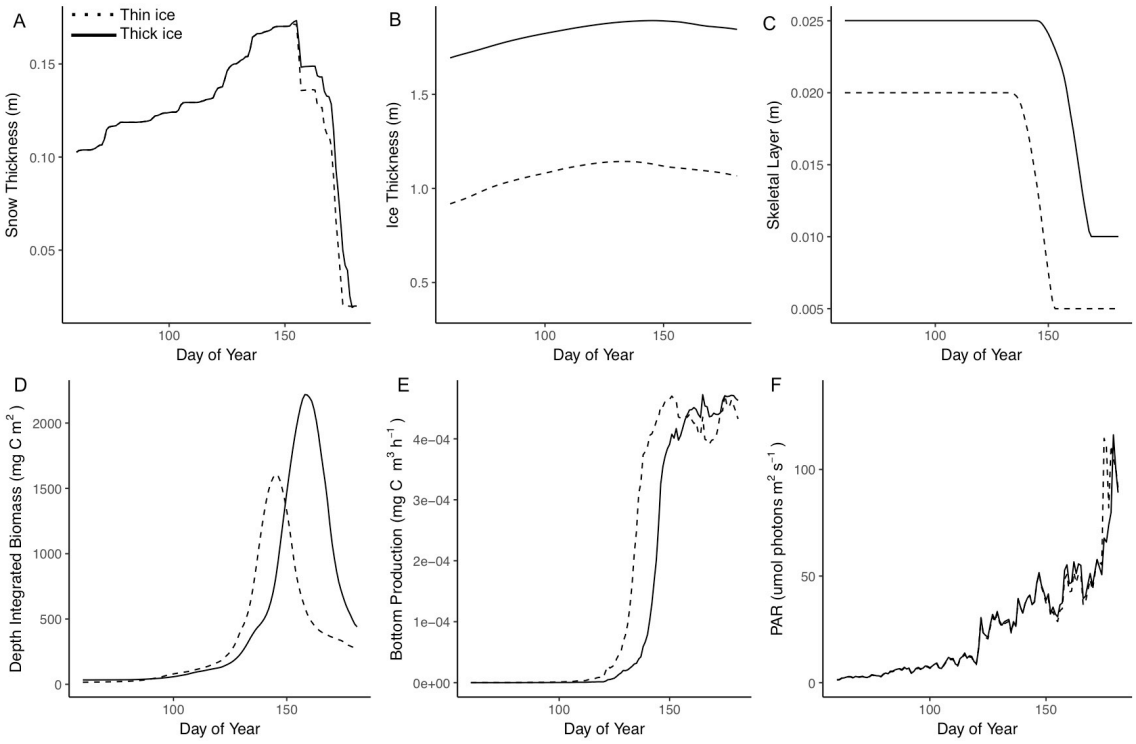

Figure 2.5 Sensitivity of modeled variables to maximum and minimum sea ice observed over the 1980 to 2015 period for the 2014 sea ice season. (a) Snow thickness (m), (b) Ice thickness (m), (c) Skeletal layer thickness (m), (d) Depth-integrated biomass (mg C m^{-2}), (e) Bottom production (mg C m^{-3} h^{-1}), and (f) Photosynthetically Active Radiation (PAR) (µmol photon m^{-2} s^{-1}).

Ice Algal Bloom Dynamics. Depth-integrated NPP was highest under thin snow cover (5.22 g C y^{-1}) and lowest under thick snow (3.70 g C y^{-1}; Figure 2.4d). Under standard snow conditions (i.e. in 2014), total annual NPP for simulated thick (4.69 g C y^{-1}) and thin (4.39 g C y^{-1}) sea ice were similar (Figure 2.5d) and lower than that of NPP under thin snow. Peak depth-integrated carbon biomass was highest under the thickest sea ice (2.22 g C m^{-2}) and thinnest snow cover (1.93 g C m^{-2}) than under the thickest snow (1.60 g C m^{-2}) and thinnest sea ice (1.61 g C m^{-2}) (Figure 2.4-5d). Under the thinnest snow cover, ice algal blooms started two weeks earlier (21 April) and therefore lasted two weeks longer than blooms growing under the thickest snow. There were smaller differences between blooms in thick and thin ice; thin ice blooms started six days earlier than those in thick ice (1 May and 7 May, respectively). Ice algal blooms in the high biomass bottom ice layer under the thinnest snow had higher mean rates of NPP (0.029 mg C m^{-3} d^{-1}) than blooms under the thickest snow (0.020 mg C m^{-3} d^{-1}) (Figure 2.4e). Mean NPP rates of ice algae in thin and thick bottom sea ice, where the majority of biomass was located, were similar (0.024 and 0.026, respectively) (Figure 2.5e).

We also simulated the combined effects of differences in both sea ice and snow thickness (Figure 2.6a,b). Depth integrated annual NPP was highest under thin snow cover regardless of ice thickness; annual NPP under both thick ice/thin snow (5.27 g C y^{-1}) and thin ice/thin snow (5.11 g C y^{-1}) was greater than NPP under thick ice/thick snow and thin ice/thick snow (3.98 and 3.40 g C y^{-1}, respectively; Figure 2.6d). Mean daily NPP was also higher under thin snow in both thick and thin ice (0.029 and 0.028 mg C m^{-3} d^{-1}, respectively) than under thick snow in both thick and thin ice (0.022 and 0.018 mg C m^{-3} d^{-1}, respectively; Figure 2.6e).

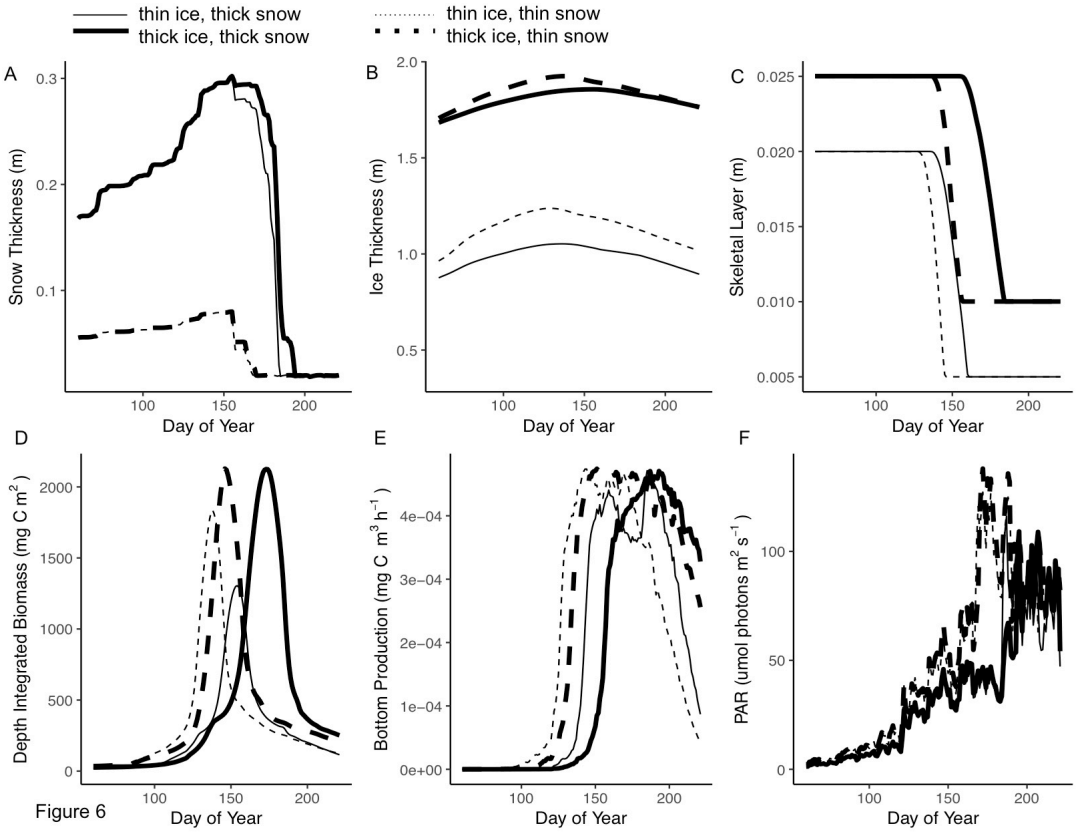

Figure 2.6 Sensitivity of modeled variables to maximum and minimum sea ice and snow thickness combinations observed over the 1980 to 2015 period for the 2014 sea ice season. (a) Snow thickness (m), (b) Ice thickness (m), (c) Skeletal layer thickness (m), (d) Depth-integrated biomass (mg C m^{-2}), (e) Bottom production (mg C m^{-3} h^{-1}), and (f) Photosynthetically Active Radiation (PAR) (µmol photon m^{-2} s^{-1}).

Ice algal blooms under thin snow started earlier in both thick and thin ice (27 April and 19 April, respectively) and lasted longer (65 and 73 days) than blooms growing under thick snow, which started later in the season (22 June and 4 June in thick and thin ice, respectively) and persisted for a shorter length of time (52 and 58 days in thick and thin ice, respectively; Figure 2.6d). Depth-integrated Chl *a* did not drop below the bloom threshold of 5 mg m^{-2} before sea ice retreat (defined by 50% satellite ice concentration; Figure 2.6d), suggesting that the bloom could have continued longer in all conditions. Light was the primary factor limiting ice algal NPP and biomass in the extreme sensitivity analyses (Figure 2.6f). Light had lower limitation index values (<0.40) than $Si(OH)_4$ until after the peak and subsequent decline of the bloom and the loss of the productive bottom layer (Figure 2.6f). Mean seasonal PAR for ice algal growth was approximately two times higher under thin snow than thick snow for both thick and thin ice.

To further understand the interaction between the impact of snow and ice melt timing on ice algal communities over the 1980 to 2015 period, sea ice seasons were grouped into periods where ice retreated early (9 – 29 June), moderate (30 June – 19 July), and late (20 July – 8 August). These groupings revealed that the timing of ice retreat set approximate bounds on annual NPP (Figure 2.7). Ice retreating later in the season had consistently higher annual NPP than ice retreating earlier. Within the early and late retreat periods, linear regression analysis showed that snow thickness explained 71% and 44% of the variability in annual NPP, respectively. There was no relationship between snow and NPP within the typical moderate retreat period.

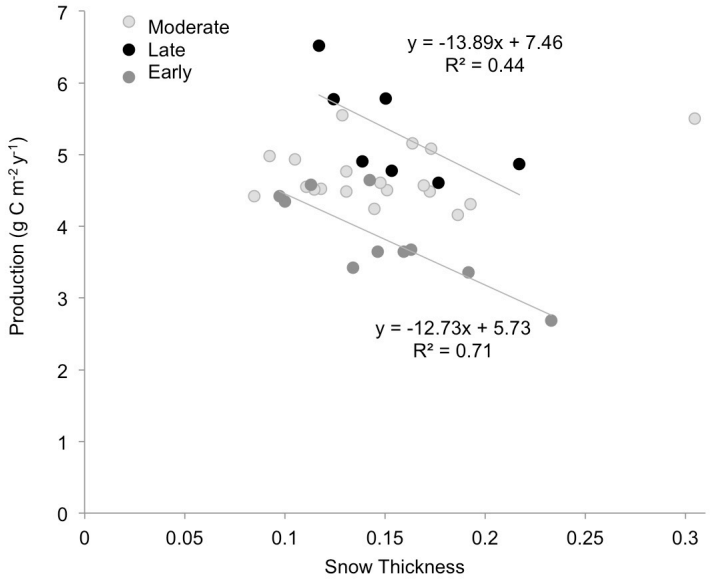

Figure 2.7 Snow Thickness (m) versus Production (g C m^{-2} y^{-1}) for early (June 9-29 (doy 160-180)), moderate (June 30-July 19 (doy 181-200)), and late (July 20-August 08 (doy 201-220)) sea ice retreat groupings. The gray line denotes a significant correlation.

2.4 Discussion

Arctic sea ice or coupled ice-ocean models have been applied to the landfast ice of Barrow, Alaska (Jin et al. 2006), the Canadian Archipelago (Lavoie et al. 2005, Pogson et al. 2011, Mortensen et al. 2017), and the pack ice of the Beaufort Sea (Lavoie et al. 2009), Baltic Sea (Tedesco et al. 2009, 2010), and Nansen Basin (Duarte et al. 2017). Several studies have incorporated 1-D models (Jin et al. 2006, Mortensen et al. 2017) into 3-D coupled ice-ocean models and examined the spatial distribution of primary production and ice-associated biogeochemical cycles across the broader Arctic (Deal et al. 2011, Jin et al. 2012, Ji et al. 2013, Watanabe et al. 2014, Hayashida et al 2017). Our 1-D arctic modeling study focuses on how the ice ecosystem has changed over time and examines the potential for data-constrained interannual variability in physical sea ice processes to impact ice biology over the 1980 to 2015 period in the Chukchi Sea. Here, we discern between what controls interannual variability and drives secular trends in sea ice algal NPP.

2.4.1 Controls on interannual variability in ice algal NPP from 1980 to 2015.

Modeled annual ice algal NPP is within the range of values estimated by other 1-D and 3-D ice algal models for the western Arctic (0.7 – 5 g C m^{-2}, Jin et al. 2012, Deal et al. 2011, Mortensen et al. 2017). Interannual variability in ice algal NPP is impacted by the physical snow and sea ice characteristics that influence bloom duration, and bloom production rates over the spring season. Sensitivity analyses showed that changes in snow thickness were the primary control, as changes in sea ice thickness had less of an influence on annual ice algal NPP. The full range of modeled ice and snow thicknesses accounted for approximately 30% and 50% of the range of values for bloom duration and annual ice algal NPP over the 1980 to 2015 period.

In addition to controlling bloom onset and growth rates of the spring ice algal bloom, snow, and to a lesser extent sea ice thickness, in concert with atmospheric conditions, impact the timing of ice melt, the loss of the productive bottom layer of ice algae from the sea ice, and thus the decline of the ice algal bloom from its peak concentration (Lavoie et al. 2005, Pogson et al. 2011, Tedesco et al. 2014, this study). Our results and others (Duarte et al. 2017) suggest that ice algal blooms persist in the presence of some basal melting, depending on the definition of a "bloom period". Using our threshold value of >5 mg C m^{-2} to define a bloom, sensitivity analyses showed that productive bottom ice layers disappeared approximately a week to a month earlier under thin snow than under thick snow, regardless of ice thickness. While depth-integrated biomass sharply decreased during this period of bottom melt, values remained above the bloom threshold until ice retreat. Therefore, sensitivity analyses showed that despite the ice starting to melt earlier, ice algal

blooms under thin snow had higher light-driven growth rates for a longer period of time, and therefore higher annual ice algal NPP, than blooms under thick snow.

Our results are similar to those of a conceptual 1D ice algal ecosystem model (Tedesco et al. 2014) that showed higher algal biomass accumulates under thin snow than under thick snow. Tedesco et al. (2014) employed a relative threshold value, set by the amplitude and the standard deviation of ice algal biomass where positive values (biomass value – standard deviation) represent the bloom period. If we examine our results using the bloom definition of Tedesco et al. (2014), we still see higher peak biomass and higher annual ice algal NPP under thin (1.4 g C m^{-2} and 3.29 g C m^{-2} y^{-1}, respectively) than under thick (1.1 g C m^{-2} and 2.97 g C m^{-2} y^{-1} respectively) snow conditions, but the difference between the two conditions is relatively small (Figure 2.8).

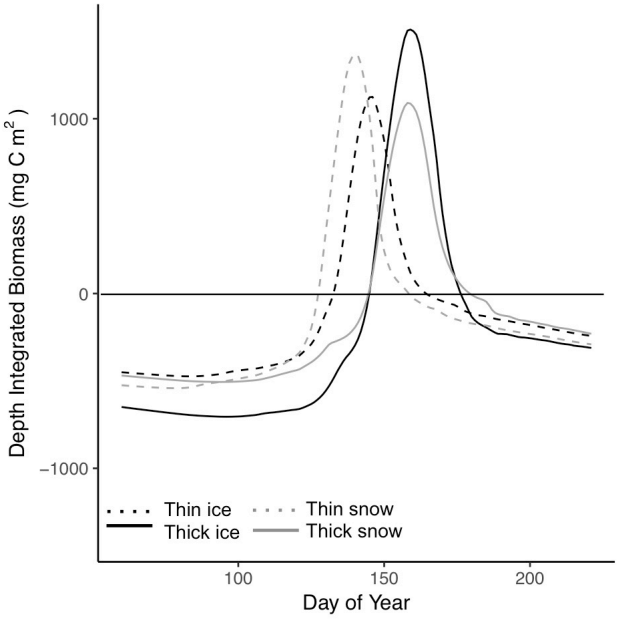

Figure 2.8 Depth-integrated biomass (mg C m^{-2}) from snow and sea ice sensitivity analyses (shown in figure 2.4) using a relative threshold metric (from Tedesco et al. 2014).

2.4.2 Drivers of secular declines in ice algal NPP from 1980 to 2015.

Our modeling results suggest that annual ice algal NPP has decreased 22% over the 1980 to 2015 period. While snow and ice thickness could account for 50% of the range of modeled ice algal NPP, they did not exhibit a discernable trend over time and therefore could not explain the temporal decline of the ice algal bloom. Since these features also control bloom onset, after incoming solar surface irradiance increases above a growth-supporting threshold, the start and overall growth of the spring ice algal bloom did not drive the temporal decline in ice algal NPP

between 1980 and 2015. In contrast to thickness characteristics, snow and ice melted earlier and ice retreated earlier in spring from 1980 to 2015. Earlier retreat of the sea ice in late spring and early summer significantly shortened ice algal bloom duration by 30% over time during our study. In comparing the annual ice algal NPP of early-ice retreat and late-ice retreat years, the timing of ice retreat and its effect on bloom duration ultimately determines the maximum for annual ice algal NPP. In our modeling results, the timing of ice retreat overrode the effects of ice and snow thickness on annual ice algal NPP. Therefore, earlier sea ice retreat shortened bloom duration and drove secular changes in annual ice algal NPP and this signal persisted despite snow-driven interannual variability.

The retreat of sea ice (observed from satellite) prior to complete melt in our model agrees with other studies showing that wind dynamics and fraction of open water impacting albedo feedbacks (not included in our model) play significant roles in sea ice retreat (Belchansky et al. 2004, Screen et al. 2011, Stammerjohn 2012). Therefore, large-scale wind-driven advection and the fraction of open water (represented as satellite-observed ice concentrations) played key roles in driving earlier ice retreat in spring, earlier termination of the ice algal bloom, and a decline in annual ice algal NPP from 1980 to 2015.

2.4.3 Implications for Future Climate

The combined effects of snow depth controlling ice algal NPP rates and atmospheric conditions setting the timing of ice retreat, impacted ice algal NPP over the 1980 to 2015 period. Our model results suggest that thinner snow packs have the potential to partially offset melt-driven declines in annual ice algal NPP. While it is probable that the length of the sea ice season that sets the upper bound on ice algal NPP will continue to shorten in the future as the Arctic warms, how the snow pack is likely to respond remains uncertain. A thinner snowpack would be conducive to the early onset of ice algal blooms and compensate for shorter bloom periods caused by earlier ice retreat. Alternatively, a thicker snowpack would delay the start of the ice algal bloom, shorten the duration of ice algal blooms, and lead to even lower lower annual ice algal NPP.

Even though our results based on precipitation patterns showed no trends in snow depth over time, models and observations for the Chukchi Sea, as well as the broader Arctic, showed that precipitation has increased over the recent past (1950 to 1999, Min et al. 2008). However, despite this precipitation increase, snow depths decreased by 56% over this period, with later advance (freeze up) of sea ice in fall and winter reducing the amount of snow accumulation (Webster et al. 2014). Arctic precipitation is projected to continue to strengthen over the 21st century (Bengtsson et al. 2011, Bintanja and Selton 2014), but it is uncertain how this will affect future snow pack

conditions. While one modeling study suggested that snow depths will continue to decrease due to both later advance of sea ice in fall and winter and increased rainfall (Hezel et al. 2012), another study suggested that precipitation will increase by 50% in the Arctic (~30% in the Chukchi Sea region) and will predominantly fall as snow in winter (Bintanja and Selton 2014). While the direction of change remains uncertain, changes to future snow thickness will play an important role in either amplifying or compensating for the effects of the shortening sea ice season on annual ice algal NPP.

2.5 Conclusions

Our results agree with other field and modeling studies that show that the duration of the ice season is important in controlling annual ice algal NPP (Tedesco et al. 2014, this study) and that snow thickness, and related light availability, determines the onset of the ice algal bloom (Leu et al. 2015, this study). However, snow and ice thickness can only explain 50% of the modeled range in ice algal NPP over our 35 year study period. Instead, the timing of both ice melt and ice retreat exerts a primary role in terminating the ice algal bloom by constraining the length of the algal growing season, and ultimately limiting annual NPP (Lavoie et al. 2005, Pogson et al. 2011, Tedesco et al. 2014, Selz et al. 2017, this study). Trends over the 1980 to 2015 period suggest that annual ice algal NPP will continue to decrease as ice melts and open water appears earlier in the spring season, unless thinner snow and ice enhances NPP and lengthens the duration of the ice algal bloom.

Chapter 3

Distribution of *Phaeocystis antarctica*-dominated sea ice algal communities and their potential to seed phytoplankton across the west Antarctic Peninsula in spring

SELZ VS, LOWRY KE, LEWIS KM, JOY-WARREN HL, VAN DE POLL W, NIRMEL S, TONG A, ARRIGO KR

The western Antarctic Peninsula has experienced extreme changes in the timing of sea ice melt and freeze up, shortening the duration of the seasonal sea ice cycle. While previous research demonstrated connections between multiple pelagic trophic levels and the physics of the sea ice, few studies have assessed the sea ice ecosystem or its linkage to the ocean ecosystem in this region. Through a field survey and ship-board experiments, our study focused on characterizing the spring ice algal bloom and elucidating its role in seeding phytoplankton communities post-ice melt in high and low light conditions. Field data revealed that algal communities in slush layers, often formed from the flooding of seawater (infiltration layers), dominated biomass distributions in the sea ice throughout the region and showed distinct photophysiological characteristics from interior or bottom ice communities. Sea ice algal biomass reached 120 mg Chl a m^{-2} and was often dominated by Phaeocystis antarctica. Shipboard growth experiments showed that prior light history (ice or water column), rather than community composition (phytoplankton and ice algae were comprised of similar taxa), primarily drove physiological responses to high and low light. P. antarctica generally dominated the community in growth experiments at the end of the six-day incubation period. Settling column experiments suggested that P. antarctica's higher sinking rates relative to other taxa may explain its minor contributions to the summer phytoplankton community in single cell form and its absence in colonial form, observed in the long term ecological record of this region.

This chapter was originally published in Selz V, Lowry KE, Lewis KM, Joy-Warren HL and others (2018) Distribution of *Phaeocystis antarctica*-dominated sea ice algal communities and their potential to seed phytoplankton across the western Antarctic Peninsula in spring. Mar Ecol Prog Ser 586:91-112. https://doi.org/10.3354/meps12367.

Ian Stewart <ian.stewart@int-res.com> Mon, Apr 9, 2018 at 12:21 AM
To: Virginia Selz <virginiaselz@gmail.com>

Dear Virginia

Asserting that inter-Research is the copyright holder, you are hereby licensed to include an author-generated typescript of the accepted version of your article Selz et al. 82018) Mar Ecol Prog Ser 586:91–112 https://doi.org/10.3354/meps12367 in your PhD thesis to be submitted to Stanford University, under the following conditions:

(1) Since it was published first, the MEPS article must be clearly cited, and preferably all the original authors acknowledged.
(2) The chapter should be integrated into the body of the thesis proper, i.e. not issued as a separate electronic file or printed fascicule.

With best wishes

Ian Stewart
Permissions
Inter-Research

[Quoted text hidden]
Ian Stewart
Production Manager – Marine Ecology Progress Series
Inter-Research Science Center
Nordbünte 23
21385 Oldendorf/Luhe
Germany
Tel: (+49) (4132) 93269-(155)
Email: ian.stewart@int-res.com
Fax: (+49) (4132) 8883 www.int-res.com

3.1 Introduction

Sea ice harbors a rich microbial community comprised of bacteria, algae, and zooplankton that is critical in fueling upper trophic levels in early spring (Ackley and Sullivan 1994), yet there is a paucity of field data on ice algal blooms in Antarctic sea ice (Meiners 2012). Even less is understood about the fate of ice algae following ice melt and their potential role in seeding the water column and impacting phytoplankton bloom development. Ice algal blooms contribute approximately 10 to 28% of annual primary production in ice-covered regions across the Southern Ocean (Arrigo and Thomas 2004) and sea ice often contains bloom-forming phytoplankton taxa such as diatoms and *P. antarctica* (Garrison et al. 1987, Mangoni et. al 2009, Lannuzel et al. 2013). Beyond the role ice algae play in initiating spring production in the ice and potentially in the water column (Ackley and Sullivan 1994), they also contribute to biogeochemical cycling of carbon and sulfur through their production of organic carbon and dimethylsulfoniopropionate (DMSP), respectively (Vancoppenolle et al. 2013, Tison et al. 2010). Understanding the coupling between the ice and ocean ecosystem is thus critical, especially in regions with rapidly changing ice conditions, such as the western Antarctic Peninsula (WAP).

The WAP and surrounding seas have experienced rapid and intense warming over the last 50 years (Marshall et al. 2002, Vaughan et al. 2003, Turner et al. 2005, Meredith and King 2005). Increasing spring and winter surface temperatures have been accompanied by declines in sea ice concentration and duration (Stammerjohn et al. 2008). The changing properties of sea ice, including thinning and greater lead fractions (Liu et al. 2004, Stammerjohn et al. 2008), and increasingly warm northerly winds (Massom et al. 2006) promote earlier spring melt. Warm northerly winds also contribute to delayed freeze up and limit the northward advance of sea ice (Stammerjohn et al. 2008). These ice-atmosphere interactions modify ice dynamics along the WAP and are sensitive to large-scale atmospheric variability, including the Southern Annular Mode (SAM) and the El Niño Southern Oscillation (ENSO) (Stammerjohn et al. 2008, Massom et al. 2006).

Changes in WAP sea ice dynamics have impacted primary producers on regional scales. Across the WAP, both satellite records spanning three decades (Montes-Hugo et al. 2009) and long-term field studies suggest that phytoplankton bloom magnitude (Vernet et al. 2008, Annett et al. 2010, Venables et al. 2013, Rozema et al. 2017), size structure, and community composition (Montes-Hugo et al. 2008) are driven by ice-influenced resource availability (light and nutrients). Large-scale atmosphere-ice-ocean interactions affect the stratification of the water column (Massom and Stammerjohn 2010) and the intrusion and upwelling of nutrient-rich upper Circumpolar Deep Water (UCDW) into the surface ocean (Martinson et al. 2008). These

atmosphere-ice-ocean dynamics impact the availability of light and nutrients to phytoplankton and have been linked to large-scale changes in primary productivity along a north-south gradient (Montes-Hugo et al. 2009, Venables et al. 2013). Between 1979 and 2004, the northern section of the WAP (as defined by Montes-Hugo et al. 2009) transitioned from a seasonally ice-covered to a nearly ice-free region. This decreased ice cover led to enhanced wind-driven mixing and reduced light availability (Montes-Hugo et al. 2009, Ducklow et al. 2013, Steinberg et al. 2015). These physical changes corresponded to an 89% reduction in surface summer phytoplankton chlorophyll *a* (Chl *a*) over a 30-year period (Montes-Hugo et al. 2009) and a predominance of small phytoplankton, such as cryptophytes (Montes-Hugo et al. 2008). In contrast, in the southern WAP, shifts from perennial to seasonal ice have maintained ice-melt induced stratification in spring, increasing light availability in recent years (Montes-Hugo et al. 2009). These favorable growth conditions in the southern WAP have been linked to a 66% increase in surface Chl *a* over a 30-year period (Montes-Hugo et al. 2009) and a predominance of large diatoms (Montes-Hugo et al. 2008).

In addition to the phytoplankton community, decadal surveys have linked the abundance of secondary producers to ice conditions, with the two dominant grazers—krill and salps—following opposing trends (Ross et al. 2008, Ross et al. 2014, Steinberg et al. 2015). While the abundance of some krill species corresponded to high ice conditions, increased salp abundance coincided with low ice conditions (Steinberg et al. 2015, Ross et al. 2008, Ross et al. 2014). Other studies have observed shifts from krill to salp dominance with decreasing sea ice on shorter timescales (Ducklow et al. 2007, Loeb et al. 1997), particularly in the northern WAP (Bernard et al. 2012). The strong linkage of krill populations to sea ice dynamics is likely driven by the necessary role that sea ice plays as a refuge (Daly and Macaulay 1988) and food source for juvenile krill (Kottmeier and Sullivan 1987, Marschall 1988, Daly 1990).

The Antarctic ice pack acts as a habitat for multiple trophic levels that are supported by ice algal communities found at the surface, interior, or bottom of the ice (Arrigo and Thomas 2004), depending on its physical structure. During late winter and early spring, snow loading often depresses the surface of the ice below sea level, resulting in surface flooding, melting snow, and seawater percolating through the ice (Perovich et al. 2004). Variations in salinity and temperature lead to freezing point differentials throughout the vertical profile of the sea ice, creating a "honeycomb-like ice matrix filled with sea water below a surface layer of snow and ice" (Ackley et al. 2008, Ackley and Sullivan 1994), or slush layers. These slush layers, also known as gap (Ackley and Sullivan 1994, Jeffries 1997) or infiltration layers, can support high concentrations of algal biomass (172 to 370 mg Chl *a* m^{-3}, Kattner et al. 2004, Fritsen et al. 1998, Fritsen et al.

2001), potentially due to their porous nature and enhanced seawater exchange (Massom et al. 2006). Flooding occurs over approximately 15-30% of the ice pack in Antarctica (Wadhams et al. 1987) and up to 50% of the ice area along the WAP (Saenz and Arrigo 2014), especially in late winter and early spring (Perovich et al. 2004). Because of this enhanced flooding, Perovich et al (2004) suggested that sea ice in the WAP experiences an extended spring from August to December and further indicated that these widespread porous layers may be more accessible to juvenile krill along the WAP than elsewhere in the Antarctic sea ice.

Along the WAP, physical mechanisms, such as flushing of melt water through brine channels or infiltration of surface waves (Thomas et al. 1998) and the mechanical break up of ice expel the slush and ice algae into the water column and create an ice slurry at the surface (Massom et al. 2006). During this early spring period, ice-derived phytoplankton can potentially serve as a seed population in the water column (Massom et al. 2006). However, despite the potential ecological significance of ice algae in early spring (Ackley and Sullivan 1994) to both upper trophic levels (Perovich 2004) and primary production (Massom 2006), to date there have been few field studies of ice biology and its potential linkages to the water column along the WAP. Using field survey data, our study characterizes the spring sea ice algal bloom along the WAP, significantly advancing our knowledge of the biomass, physiology, and species composition of sea ice communities in mid to late spring. In addition, we use controlled experiments to focus on the potential for ice algal communities to seed phytoplankton communities under different light conditions in the water column. Together these results show whether sea ice algal communities contribute to pelagic primary production after melting out of the sea ice along the WAP. To our knowledge, this is the first dataset of these measurements taken along the Long Term Ecological Research grid (LTER) in spring (November).

3.2 Methods

Samples were collected from the R/VIB *Nathaniel B. Palmer* along an extended LTER grid of the WAP (Figure 3.1, Table 3.1) during the *Phaeocystis antarctica* Adaptive Responses in the Antarctic Ecosystem (Phantastic II) cruise (NBP14-09). Sea ice stations were conducted at or near main water column stations when the following were present 1) sea ice and 2) suitable weather conditions. Sea ice and water column samples were collected between 3 and 21 November 2014.

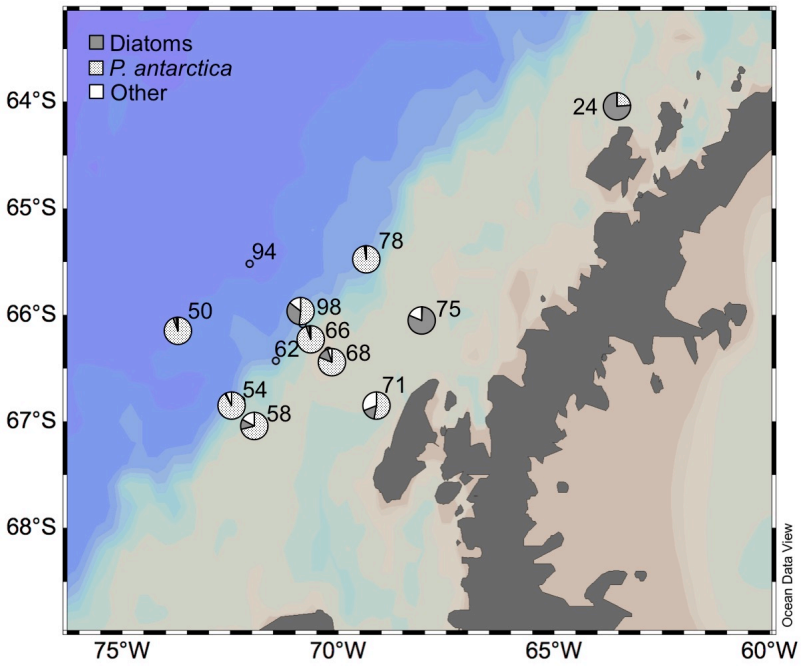

Figure 3.1. Sea ice algal community composition in slush layers at ice stations.

Table 3.1a Geographic location and physical description of ice stations (STN) (nd represents no data)

STN	Date	Lat	Lon	Mean Core Depth (m)	± SD	Mean Snow Depth (m)	± SD
24	11/3	-64.027	-63.584	0.45	0.07	0.11	0.02
50	11/9	-66.129	-73.570	0.50	0.14	0.06	0.05
54	11/10	-66.798	-72.240	0.69	0.26	0.13	0.04
58	11/11	-66.976	-71.914	1.06	0.10	0.08	0.06
62	11/12	-66.429	-71.438	0.60	0.02	0.19	0.07
66	11/13	-66.086	-70.831	0.88	0.42	0.11	0.05
68	11/14	-66.334	-70.231	0.66	0.01	0.13	0.09
71	11/15	-66.838	-69.088	1.18	0.05	0.25	0.13
75	11/16	-65.995	-68.068	1.15	0.57	0.35	0.09
78	11/17	-65.403	-69.394	0.39	0.01	0.09	0.06
94	11/20	-65.517	-72.049	0.42	0.03	0.24	0.06
98	11/21	-66.051	-70.899	0.80	0.02	0.14	0.04

Table 3.1b Geographic location and physical description of ice stations (STN) (nd represents no data)

STN	Ice Temp (°C)	Mean Salinity Nonslush Layer	± SD	Mean Salinity Slush Layer	± SD	Free-board (m)
24	nd	10	1	15	4	0.01
50	-1.30	5	1	9	1	0.03
54	nd	5	1	11	2	0.02
58	-1.00	5	1	10	-	0.08
62	-0.10	9	3	14	2	-0.01
66	-0.80	7	2	12	1	0.05
68	-2.70	10	3	14	1	0.02
71	-6.60	8	2	13	2	0.03
75	-1.80	9	3	11	6	-0.01
78	-1.10	7	3	10	0	0.01
94	-0.50	7	2	-	-	-0.05
98	-1.30	6	2	10	0	0.03

3.2.1 Field Data Collection

Sea Ice and Water Column Sampling. On ice floes, snow thickness was measured using a meter stick at 15 randomly selected locations around the core site. Sea ice surface temperature was measured using a temperature probe at the snow-ice surface. Once ice cores were drilled, ice thickness was measured using a meter stick. Cores were cut into 0.1 m sections using a stainless steel ice saw and the sections were placed in separate plastic containers to melt. Slush layers were sampled by scooping ice slush directly from the floe into plastic containers. All ice samples were stored in coolers until onboard processing for nutrients, biomass, and physiology. Immediately after returning to the ship, 0.2 μm filtered seawater (FSW) was added to ice samples (except ice cores analyzed for nutrients and salinity) to minimize osmotic shock to the ice algae during melt by maintaining salinity > 28. Freeboard (f_b), the height of the sea ice above sea level, was calculated as $\rho_s h_s + \rho_i h_i = \rho_w (h_i - f_b)$ (Timco and Frederking 1996**)** using the density of seawater (ρ_w: *1029 kg* m^{-3}), snow (ρ_s: 390 kg m^{-3}; Massom et al. 2001), and sea ice (ρ_i: 920 kg m^{-3}: Ackley et al. 2008) as well as the mean ice (h_i) and snow thicknesses (h_s) measured at ice stations.

Water column samples for growth and settling column experiments were collected from the CTD rosette at a depth of approximately 10 m at ice station locations. Both water column and ice samples underwent the same analyses: particulate organic carbon (POC), particulate organic nitrogen (PON), Chl *a* and other algal pigments, taxonomic composition (using CHEMTAX-HPLC and FlowCam), photophysiological parameters (quantified using photosynthesis vs.

irradiance curves (PvE) and Fast Rate Repetition Fluorometry (FRRF)), and salinity and nutrients (silicate ($Si(OH)_4$), nitrate (NO_3^-), and phosphate (PO_4^{3-})).

3.2.2 Growth Experiments (Shipboard Incubations)

To determine the viability of ice algae that melted out of the slush layer relative to water column phytoplankton under sustained high and low light levels, we conducted six-day shipboard incubation experiments in a temperature (0ºC) and light controlled incubator. Experiments were conducted on 3, 10, and 17 November 2014 using ice algae (from the slush layer) and seawater (from 10 to 20 m) collected at stations (STNs) 24, 54, and 78 (Figure 3.1). Slush samples collected at ice stations for experiments were melted in 4 L of FSW to maintain salinities >32. Samples from the ice and water column were incubated in 4 L Whirl-Pak bags (Nasco). Because of the large biomass concentration differences between ice and seawater, we further diluted slush ice samples with ~3.7 L of 0.2 µm filtered seawater (FSW ~34 salinity) collected near ice stations to match biomass concentrations in seawater samples. Dilutions were calculated from *in vivo* fluorescence of ice and seawater to achieve the same biomass concentrations in ice and seawater samples. Triplicate samples were incubated under either high (200 ± 31 µmol photon m^{-2} s^{-1}) or low (91 ± 25 µmol photon m^{-2} s^{-1}) light. The high light level was similar to the mean light in a shallow mixed layer (ML) (250 µmol photon m^{-2} s^{-1}, Mills et al. 2010) and summer MLs in the Ross Sea (180±110 µmol photon m^{-2} s^{-1}, Smith and van Hilst 2003). The low light level was similar to the mean light in a deep ML (65 µmol photon m^{-2} s^{-1}, Mills et al. 2010) and mid to late spring MLs in the Ross Sea (96±58 µmol photon m^{-2} s^{-1}). Experiment 1 (Exp 1) was conducted under a 12 h light:12 h dark (12:12 h) cycle. Maintaining a 12:12 h light cycle was not possible after Exp 1. Exp 2 and 3 were conducted under 24 h light. Treatments were subsampled on day zero (T0), four (T4), and six (T6) for $Si(OH)_4$, NO_3^-, PO_4^{3-}, POC, PON, Chl *a*, other algal pigments, taxonomic composition, and photophysiological parameters. To ensure that treatments remained in nutrient-replete conditions over the six-day experiment, we replaced the water removed for sampling at T4 with 2 L of FSW. Growth rates (r) were calculated, assuming exponential growth ($P_F = P_0 * e^{(rt)}$) over two days (t), where P_0 and P_F are the initial and final biomass, respectively

Statistical differences among treatments in the growth experiment were analyzed using a two-way analysis of variance (two-way ANOVA, R). Main effects included light level (high versus low) and community type (ice algae versus phytoplankton). When the two-way ANOVA interaction term (light × community type) was significant ($p < 0.05$), differences among treatments were analyzed using the Tukey Honest Significant Difference (HSD) test. Statistical differences between T0 and T6 measurements were analyzed using a paired *t*-test.

3.2.3 Settling Column Experiments

To determine the export potential of ice algae and phytoplankton, we conducted settling column experiments in duplicate or triplicate (n=2,3) using samples collected from the sea ice slush layer (STNs 50, 58, 62, 66, 68, 71, 78) and near surface waters (STNs 2, 15, 38, 40, 44, 48). Conducting simultaneous ice algal and phytoplankton settling experiments was not possible due to the limited number of settling columns. Settling columns were constructed out of capped polycarbonate tubes (d = 0.07, l = 0.46 m) with three sampling ports positioned to collect buoyant, neutral, and settled particles, following Johnson and Smith (1986) and Bienfang (1981). Experiments were conducted in a temperature (0ºC) and light (~60 µmol photon m^{-2} s^{-1}) controlled incubator. Samples from the water column and sea ice were added to the settling columns in duplicate or triplicate and then sampled for Chl *a* at each port after ~24 h. For a limited number of stations, settling column experiments were sampled after 2 h (STNs 2 and 40), 4 h (STNs 15, 38, 40, and 58), 8 (STNs 15), and 15 h (STNs 44 and 50) to assess how well sinking rates were estimated after 24 h. A subset of samples was also analyzed for taxonomic composition. Sinking rate (ψ, m d^{-1}) was calculated from the equation of Bienfang (1981), modified by Johnson and Smith (1986):

$$\psi = f_s * l/t \quad (1)$$

where f_s is the fraction of Chl *a* that sank over the length of the column (l, m) during the settling period (t, d).

3.2.4 Sample Analyses

Nutrients. Inorganic nutrient samples were filtered with a 0.2 µm syringe filter and stored at -20˚C (NO_3, PO_4^{3-}) or 4˚C ($Si(OH)_4$) for later analysis upon return. NO_3^- and $Si(OH)_4$ concentrations were analyzed at the Royal Netherlands Institute for Sea Research (NIOZ) on a WestCo SmartChem 200 discrete autoanalyzer,

Pigments, POC, and PON. Samples were collected by filtering seawater or melted sea ice through 25 mm Whatman glass-fiber filters (GF/F, nominal pore size 0.7 µm). Chl *a* was measured in triplicate using a Turner 10-AU fluorometer (Turner Designs, Inc.) after extraction in 5 ml of 90% acetone in the dark at 3°C for 24 h (Holm-Hansen et al. 1965). The fluorometer was calibrated using a pure Chl *a* standard (Sigma).

Samples were analyzed for phytoplankton pigments by High Performance Liquid Chromatography (HPLC), as described below. Filters were freeze-dried for 48 h and pigments were extracted using 90% acetone (v/v) for 48 h (4˚C, darkness). Pigments were separated by HPLC (Waters 2695) with a Zorbax Eclipse XDB-C8 column (3.5 µm particle size), using the method of Van Heukelem and Thomas (2001). Detection was based on retention time and diode

array spectroscopy (Waters 996) at 436 nm. Pigments were manually quantified using standards (DHI lab products). Analyzed pigments include Chlorophylls: *a,* b, c_2, c_3, photoprotective index pigments (PPC: Diadinoxanthin (DD), Diatoxanthin (DT), Violaxanthin (Viola), Zeaxanthin (Zea), Lutein, and Beta-carotene), and taxonomic marker pigments (Peridinin (Per), 19-Butanoyloxyfucoxanthin (19-But), 19-Hexanoyloxyfucoxanthin (19-Hex), Fucoxanthin (Fuco), and Alloxanthin (Allo)). Community composition was estimated from pigments (HPLC) using the CHEMTAX analysis package (version 1.95) (Mackey et al. 1996) (Appendix A4). Taxonomic composition of CHEMTAX-HPLC is compared to FlowCam analyses in results and presented in the results and discussion from FlowCam analysis.

POC samples were filtered onto pre-combusted (450°C for 4 h) GF/Fs. Filters were dried at 60°C for approximately 24 h and then stored for later elemental analysis on a Elementar Vario El Cube or Micro Cube elemental analyzer (Elementar Analysensysteme GmbH, Hanau Germany) interfaced to a PDZ Europa 20-20 isotope ratio mass spectrometer (Sercon Ltd, Cheshire, UK). The concentration of POC and PON in the sea ice was then calculated from the known volumes of melted sea ice and the FSW diluent water additions.

Photosynthesis versus Irradiance Curves. PvE measurements were made using a short-term (2 h) ^{14}C-bicarbonate uptake technique (following Lewis and Smith (1983), modified by Arrigo et al. 2010) on samples collected from the sea ice and the water column. PvE measurements were made (n=1: one measurement per sample due to time constrains and space limitations) on high biomass layers of the sea ice and growth experiments treatments.

Samples spiked with ^{14}C-bicarbonate were incubated under 14 light intensities ranging from 0 to 700 µmol photon m^{-2} s^{-1}. Carbon uptake rates were calculated using a nonlinear least-squares regression fit to the relationship of Platt et al. (1980), as modified by Arrigo et al. (2010):

$$P^* = P_s^* \left(1 - e^{\frac{-\alpha^* E}{P_s^*}} \right) e^{\frac{-\beta^* E}{P_s^*}} - P_0^* \qquad (2)$$

where P^* is the Chl *a*-specific photosynthetic rate (mg C mg^{-1} Chl *a* h^{-1}) at a given irradiance E (µmol photon m^{-2} s^{-1}), P_s^* is the light saturated photosynthetic rate (mg C mg^{-1} Chl *a* h^{-1}) in the absence of photoinhibition, α^* is the initial slope of the PvE curve (mg C mg^{-1} Chl *a* h^{-1} (µmol photon m^{-2} $s^{-1})^{-1}$), P_0^* is the rate of DIC uptake in the dark, and b^* is the photoinhibition term at high light (mg C mg^{-1} Chl *a* h^{-1} (µmol photon m^{-2} $s^{-1})^{-1}$). The maximum photosynthetic rate in the absence of photoinhibition (P_m^*) was then calculated from:

$$P^*_m = P^*_s\left(\frac{\alpha^*}{\alpha^*+\beta^*}\right)\left(\frac{\beta^*}{\alpha^*+\beta^*}\right)^{\frac{\beta^*}{\alpha^*}} \quad (3)$$

PvE parameters were only used when fits were significant ($r^2 > 0.7$ and $p < 0.05$). The photoacclimation parameter (E_k; µmol photon m^{-2} s^{-1}), was calculated as P^*_m/a^*.

FRRF Measurements. Melted and diluted ice samples (as described above) from 0.1 m core sections, water column samples, and growth experiment treatment samples were dark acclimated for 30 min at 0°C before measuring fluorescence. Blanks were prepared by filtering the sample through a 0.2 µm polycarbonate syringe filter. Variable flourecence parameters of blanks and samples were measured using a bench top fast repetition rate flourometer (LIFT-FRR, Soliense, Kolber 1998) at an excitation wavelength of 470 nm. Blank-corrected values (Cullen and Davis 2003) for initial fluorescence (F_o), maximum fluorescence (F_m), and the effective absorption cross section (σ, Å^2 quanta^{-1}) give information on the photophysiology of photosystem II (PSII). Fluorescence measurements were used to calculate the maximum quantum efficiency of PSII (F_v/F_m; Maxwell and Johnson 2000).

FlowCam Analyses. Samples were collected and analyzed from slush and non-slush ice core sections, settling column experiments, and growth experiment treatments (T0 and T6). Nano- and micro-size phytoplankton and ice algae were imaged with a FlowCam (VS IVc, Fluid Imaging Technologies) under 40x magnification. To prevent large cells from clogging the flow cell chamber, samples were pre-filtered with 300 µm Nitex mesh. Particles in seawater or melted ice core (1 to 5 ml sample) flowed through a flow cell and each fluorescent chain, colony, or cell triggered the digital camera. The combination of the size of the Nitex mesh, the size of the flow cell chamber, and the fluorescence trigger sensitivity limited the FlowCam detection range to particle sizes of 5 to 300 µm. Digital images were classified manually into pennate and centric diatom taxa, *Phaeocystis antarctica,* dinoflagellates, ciliates, small unidentified cells, and other.

Biovolume calculations are prone to error, as two-dimensional images are used to estimate the volume of a three-dimensional shape (Alvarez et al. 2012) and plankton cells captured by the camera can be singular or part of a chain or colony and in a variety of orientations (Jackobsen and Carstensen 2011). For all taxonomic categories other than *P. antarctica*, biovolume calculations were made using geometric shape equations following Menden-Deur and Lessard (2000) and Jackobsen and Carstensen (2011). *P. antarctica* cells per image within a *P. antarctica* colony were estimated using a multiple linear regression model ($R^2 = 0.95$, $p < 0.001$) based on the following FlowCam image parameters: area-based diameter ($B = 8.402 \times 10^{-3}$, $p < 0.001$) and convex perimeter ($B = 8.235 \times 10^{-2}$, $p < 0.001$), which were selected using results from a best subsets model analysis (Bayesian Information Criteria) of 1000 images. To evaluate model skill,

a separate set of images (1000) was tested against the predicted values (Appendix A6). Colony volume calculations were made from cell number estimations following Mathot et al. (2000). We did not assess single-celled *P. antarctica* because we could not distinguish between small *P. antarctica* cells and other unidentifiable small cells. Taxonomic composition is presented in the results and discussion from FlowCam analysis as relative abundance, estimated from biovolume.

3.3 Results

3.3.1 Physical and Chemical Ice Environment

The ice stations were characterized by many small pancake ice floes (diameter ≈ 3 to 6 m) ranging in thickness from 0.42 to 1.18 m (mean 0.73 ± 0.28 m) that were sometimes rafted and covered by thick snow (Table 3.1). Freeboard, the height of the ice floe above sea level, ranged from -0.05 to 0.08 m, suggesting that 95% or greater of the ice floe was submerged at all ice stations (Table 3.1). Mean snow depth at each station ranged from 0.06 to 0.35 m with 75% of stations exceeding 0.10 m of snow cover. Ice floe surfaces consisted of snow, slush, and/or ice, with surface temperatures ranging from -6°C to the melting point. Mean bulk salinities ranged from 5 to 10 in non-slush layers and 9 to 15 in slush layers within ice cores (Table 3.1).

The vertical distributions of bulk nutrient concentrations were highly variable throughout the sea ice across the WAP, ranging from 0.09 to 13.42 μM NO_3^-, 0.17 to 3.14 μM PO_4^{3-}, and 0 to 28.28 uM $Si(OH)_4$ (Figure 3.2A-C). The ratios of observed nutrient concentrations to those expected by conservative mixing with seawater show where nutrients may be biologically elevated or depleted throughout the core profile (Figure 3.2D-F). Conservative mixing ratios for bulk NO_3^- and $Si(OH)_4$ were often <1, indicating net drawdown (Figure 3.2D and F), while PO_4^{3-} ratios were often >1, indicating enhanced remineralization or the presence of large algal intracellular phosphate pools within the sea ice (Figure 3.2E).

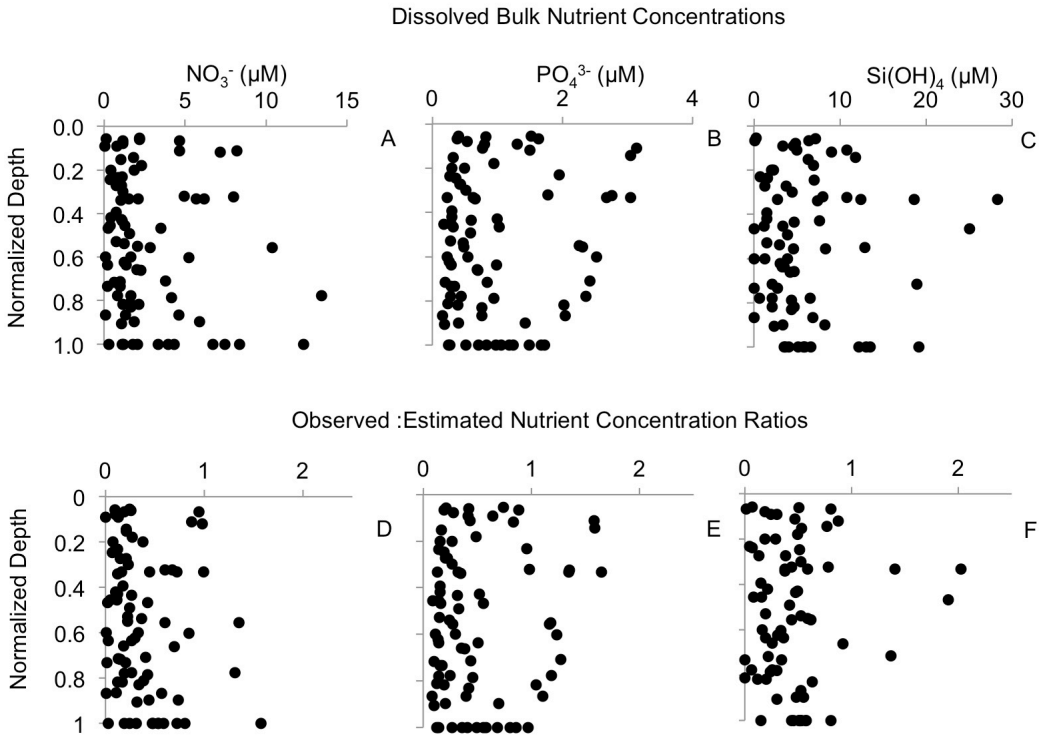

Figure 3.2 Ice core bulk nutrient profiles (A – C) distributed through the normalized ice core depth (1.0 is the ice-ocean interface). Profiles of (D – F) observed to estimated (assuming conservative mixing with seawater) nutrient concentration ratios distributed through the normalized ice core depth.

3.3.2 The Ice Algal Bloom

Biomass. Depth-integrated Chl *a* for all sea ice stations ranged from 5 to 120 mg m^{-2}, averaging 38 ± 34 mg m^{-2} (Table 3.2). Depth-integrated POC and PON ranged from 2.8 to 15.6 g C m^{-2} and 0.3 to 1.9 g C m^{-2}, respectively (Table 3.2). POC and PON were positively correlated ($y=6.87x+1182$, $R^2 = 0.90$, $p < 0.05$; Appendix A7) with an average POC:PON ratio of 9.1 ± 1.8 (Table 3.2). In contrast, POC and Chl *a* were not correlated, with POC:Chl *a* ratios ranging from 59.0 to 843.3, with a median of 168.4 (Table 3.2). Depth-integrated biomass proxies (Chl *a,* POC, PON) were not significantly correlated with snow depth, ice thickness, or ice temperature.

Table 3.2 Depth-integrated biomass of ice algae (mg m^{-2}) and photosynthesis-irradiance parameters (PvE) of high biomass layers in the ice core. (-) no data

Station	Biomass			PvE Parameters		
	Chl a	POC	PON	P*m	a*	Ek
24	18	-	-	-	-	-
50	20	6898	665	0.83	0.006	133
54	5	2850	260	0.19	0.013	15
58	27	4467	446	0.05	0.001	49
62	14	3433	279	-	-	-
66	120	15561	1726	0.31	0.005	58
68	67	6102	600	0.79	0.010	77
71	23	2791	331	0.53	0.015	35
75	87	5121	692	0.14	0.009	16
78	36	3117	433	3.79	0.033	115
94	14	12019	1920	0.28	0.003	101
98	26	4820	538	0.75	0.028	27

P^*_m, mg C mg^{-1} Chl *a* h^{-1}
α* mg C mg^{-1} Chl a h^{-1} (μmol photon m^2 s^{-1})$^{-1}$
Ek μmol photon m^2 s^{-1}

Biomass was vertically divided into surface (top 0.1 m at ice-snow interface), interior (non-slush layers between the surface and bottom of the ice core), bottom (0.1 m at ice-ocean interface) or slush layers (identified from visual inspection). Often biomass was concentrated in thick slush layers (>0.1 m) that were brown in color and sometimes divided into multiple slush layers within an ice core (Figure 3.3). Our biomass measurements of the slush layer are conservative because sample collection resulted in some unquantified dilution with ambient seawater. Mean slush layer Chl *a* (8.8 ± 1.9 mg m^{-2} [72 ± 11 mg m^{-3}]) and PON (136 ± 75 mg m^{-2} [1368 ± 641 mg m^{-3}]) concentrations were two to three times higher than those in the non-slush layers of the core, which included the mean of surface, interior, and bottom communities (3.2 ± 0.9 mg Chl *a* m^{-2} [34 ± 7 mg m^{-3}] and 56 ± 3 mg PON m^{-2} [651 ± 63 mg m^{-3}]) (Figure 3.3). In contrast, differences between slush and non-slush mean POC were small. Slush layers were characterized by lower POC:Chl *a* (136 ± 45) and POC:PON (7 ± 0.5) ratios relative to the rest of the core (300 ± 24 POC:Chl *a*, 10 ± 0.4 POC:PON) (Table 3.3).

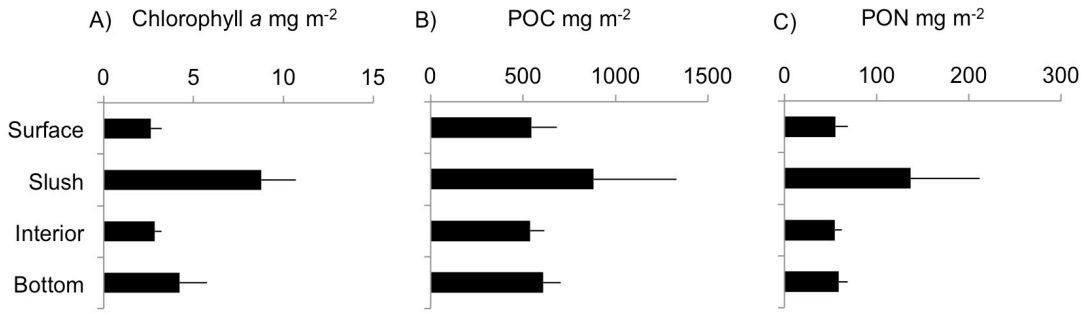

Figure 3.3 Mean ± Standard Error (SE) depth profiles of biomass (mg m^{-2}) for the surface, slush, interior, and bottom layers of the sea ice: (A) chlorophyll a (Chl *a*), (B) particulate organic carbon (POC), and (C) particulate organic nitrogen (PON). Ice core profiles are divided into: surface (0.1 m; ice-snow interface), slush (visually identified), interior (layers between the top and bottom), bottom (0.1 m; ice-ocean interface) layers.

Photophysiological state. Algae living within slush communities exhibited different photophysiological parameters than those in non-slush layers (surface, interior, and bottom) of the core (Table 3.3). The P^*_m of ice algal communities ranged from 0.03 (interior layer, data not shown) to 3.14 mg C mg^{-1} Chl *a* h^{-1} (high biomass slush layer, Table 3.2). Within that range, mean P^*_m of slush communities (1.19 ± 0.34 mg C mg^{-1} Chl *a* h^{-1}) was eight times greater than the rest of the core (0.15 ± 0.04 mg C mg^{-1} Chl *a* h^{-1}; Table 3.3). The photosynthetic efficiency (α^*) of ice algal communities ranged from <0.001 (interior layer, data not shown) to 0.043 mg C mg Chl a^{-1} (µmol photon m^{-2} s^{-1})$^{-1}$ (Table 3.2). The slush community mean α^* (0.021 ± 0.004 mg C mg Chl a^{-1} (µmol photon m^{-2} s^{-1})$^{-1}$) was an order of magnitude greater than that of the rest of the core (0.002 ± 0.001 mg C mg Chl a^{-1} (µmol photon m^{-2} s^{-1})$^{-1}$) (Table 3.3). Despite the differences in P^*_m and α^* between the slush and non-slush communities, the mean photoacclimation levels (E_k) for the non-slush (89 ± 24 µmol photon m^{-2} s^{-1}) and slush (55 ± 9 µmol photon m^{-2} s^{-1}) communities were not significantly different (Table 3.3). Overall, E_k ranged from 16 to 274 µmol photon m^{-2} s^{-1} between the ice communities.

There were no significant differences between slush and non-slush layer PS_{II} parameters. Overall, F_v/F_m was low for slush layers and non-slush layers (0.344 ± 0.027 and 0.306 ± 0.013, respectively) and the mean absorption cross-sections (σ_{PSII}, $Å^2$ $quanta^{-1}$) were similar (830 ± 37 and 897 ± 18 $Å^2$ $quanta^{-1}$, respectively) (Table 3.2). Photoprotective carotenoid pigment (PPC) to Chl *a* ratios were also similar (Table 3.2). Diadinoxanthin + diatoxanthin composed 95% of the PPC pigments in both slush and non-slush ice algal and communities.

Table 3.3 Mean (± SE) ice algal community parameters for non-slush (n=9) and slush layers (n=11). Non-slush layers include those sampled from bottom, interior, and surface communities.

		Slush	± SE	Non-slush	± SE
Biomass and Physiology Parameters					
POC:Chl *a* [1]	g:g	136	45	300	24
POC: PON [1]	g:g	7	0.5	10	0.4
P*m [1]	mg C mg^{-1} Chl a h^{-1}	1.19	0.34	0.15	0.04
α* [1]	mg C mg^{-1} Chl a h^{-1} (µmol photon m^2 $s^{-1})^{-1}$	0.021	0.004	0.002	0.001
Ek	µmol photon m^2 s^{-1}	55	9	89	24
Fv/Fm		0.344	0.027	0.306	0.013
Sigma	Å2 $quanta^{-1}$	830	37	897	18
PPC:Chl *a*	g:g	0.18	0.02	0.20	0.01
Taxonomic Composition (Relative Abundance)					
Colonial P. antarctica		0.69	0.10	0.60	0.11
Diatoms		0.22	0.09	0.15	0.06
Other		0.09	0.03	0.25	0.11

[1] *t*-test p value <0.05

Ice algal community composition. Estimates of the relative proportions of dominant taxa (>50%) from FlowCam and CHEMTAX-HPLC analyses were in general agreement (Appendix A6B). Overall, CHEMTAX-HPLC analysis estimated lower relative abundance of *P. antarctica* compared to FlowCam analysis. FlowCam imaging indicated *P. antarctica* populations were largely colonial, rather than single-celled, and comparison of the two methods suggests *P. antarctica* was adequately counted. Both methods showed that diatoms and haptophytes (*P. antarctica)* dominated all samples, and CHEMTAX HPLC showed that prasinophytes, dinoflagellates, and cryptophytes composed <1% of the algal community.

The community composition of high-biomass layers in the slush and nonslush layers (bottom, interior, or surface) of the sea ice was consistently dominated by *P. antarctica* (estimated by biovolume, μm^3) (Figure 3.1, Table 3.3). Mean relative abundances of *P. antarctica* and diatoms in slush and non-slush layers were not significantly different (Table 3.3). In contrast to the majority of stations, ice algal communities at STNs 24 and 75 were dominated by diatoms rather than *P. antarctica.* Diatoms were primarily centrics (*Thalassiosira)*, followed by large pennate diatoms (*Fragilariopsis*) and small unidentified pennate diatoms. Other diatoms, including

Chaetoceros, Nitzchia, Pseudonitzschia, Proboscia, Rhizosolenia, and *Skeletonema,* composed a minor fraction of the total biovolume.

3.3.3 Growth Experiments

To understand how ice algae (post-ice melt) and phytoplankton respond to changes in their light environment, we exposed both communities to high and low light levels over six-day incubations (Exps 1-3). Exp 1 differed in initial community composition (mixed diatom-*P. antarctica*) and light condition (12:12 h) from Exps 2 and 3 (*P. antarctica* dominant, 24 h continuous light) and are treated separately.

Community composition.

12:12 h light cycle (Exp 1). Initial (T0) communities were mostly composed of centric diatoms. *P. antarctica* was also present and made up a higher percentage of the ice algal community than of the phytoplankton community (Figure 3.4A). Ice and phytoplankton centric diatom communities were predominantly made up of *Thalassiosira (>75%)*. *Corethron* also contributed 20% to the centric phytoplankton biomass. At T6, relative abundance (estimated by biovolume) of *P. antarctica* had increased and diatoms decreased in all treatments (Figure 3.4A).

24 h light cycle (Exps 2 and 3). While diatoms dominated the T0 communities of Exp 1, the T0 communities of Exp 2 (24 h light conditions) consisted of a mix of diatoms and *P. antarctica* (Figure 3.4B). Similar to Exp 1, *P. antarctica* made up a larger percentage of the ice algae (67%) than the phytoplankton community (40%) in Exp 2. There were greater differences between the diatom communities of the ice algae and phytoplankton in Exp 2 than in Exp 1. Ice algae diatoms were composed of *Fragilariopsis* (12%) and *Thalassiosira* (17%), while phytoplankton diatoms were predominantly made up of *Thalassiosira* (45%)*, Chaetoceros* (9%), and *Corethron* (19%). In contrast to Exps 1 and 2, in Exp 3 *P. antarctica* dominated the initial ice algae (94%) and phytoplankton (92%) communities. Within both communities, *Thalassiosira* represented the majority of diatoms in Exp 3 (Figure 3.4C). At T6, in both Exps 2 and 3, relative abundance of *P. antarctica* had increased and diatoms decreased in all treatments (Figure 3.4B,C)

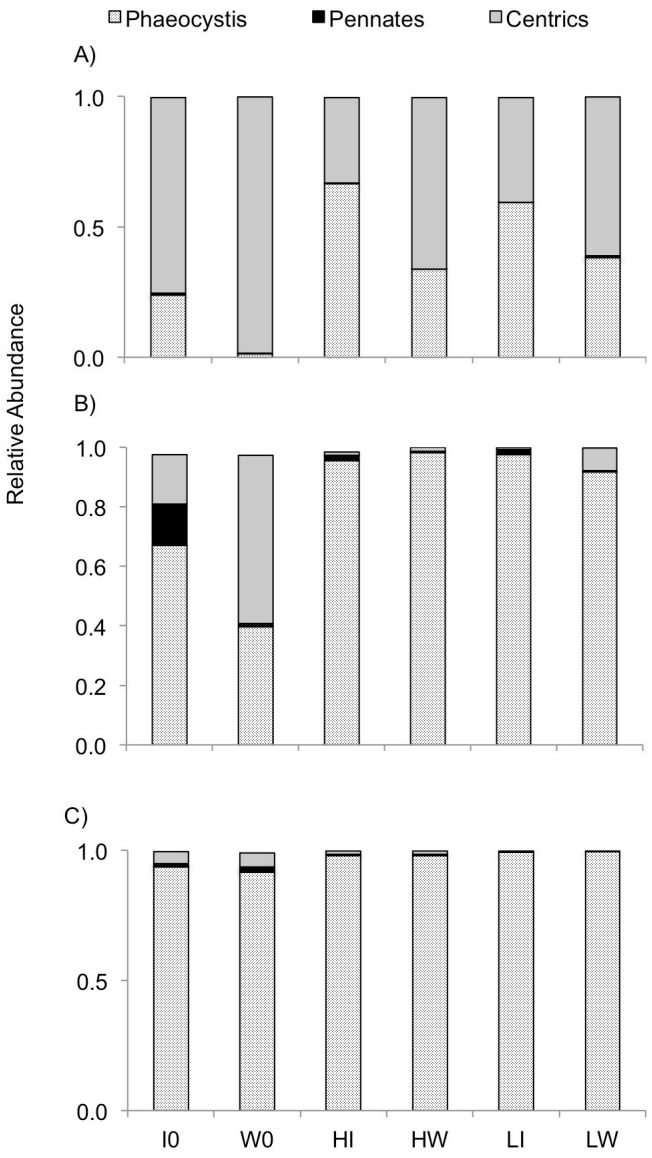

Figure 3.4 Taxonomic composition of ice algal (I) and phytoplankton (W) communities in high (H) and low (L) light treatments at day 0 and day 6 of growth experiment incubations. Relative abundance *of Phaeocystis antarctica* and diatoms is estimated from biovolume measurements with FlowCam for growth experiments (Exp): (A) Exp 1, (B) Exp 2, and (C) Exp 3.

Growth and Physiology Parameters

12:12 h light cycle (Exp 1). Phytoplankton tended to grow faster than ice algae under 12:12 h light, indicated by Chl *a*-based (two-way ANOVA, $p < 0.001$) and POC-based growth estimates (Table 3.4). Furthermore, phytoplankton were more sensitive to light treatments than ice algae, growing faster in high light (1.18 d^{-1}) than all other treatments (Tukey HSD, $p < 0.05$). At T0, ice

algae were acclimated to higher light levels (E_k : 84 µmol photon m^{-2} s^{-1}) than phytoplankton (E_k 47 µmol photon m^{-2} s^{-1}). At T6, E_k in these communities was similar, within 10 µmol photon m^{-2} s^{-1} for both light treatments (Figure 3.5A). Despite similarities in photoacclimation level (E_k), ice algae and phytoplankton exhibited differences in α^* and P^*_m, depending on light level (Figure 3.5B-C). At T6 in high light, ice algae had higher α^* (0.03 mg C mg^{-1} Chl *a* h^{-1} (µmol photon m^{-2} $s^{-1})^{-1}$) and P^*_m (1.95 mg C mg^{-1} Chl *a* h^{-1}) than phytoplankton (0.016 mg C mg^{-1} Chl *a* h^{-1} (µmol photon m^{-2} $s^{-1})^{-1}$, 1.03 mg C mg^{-1} Chl *a* h^{-1}). In low light at T6, trends were opposite those of high light conditions: ice algae had lower α^* (0.04 mg C mg^{-1} Chl *a* h^{-1} (µmol photon m^{-2} $s^{-1})^{-1}$) and P^*_m (1.92 mg C mg^{-1} Chl *a* h^{-1}) than phytoplankton (0.05 mg C mg^{-1} Chl *a* h^{-1} (µmol photon m^{-2} $s^{-1})^{-1}$ and 2.33 mg C mg^{-1} Chl *a* h^{-1}, respectively).

Initially ice algae had lower F_v/F_m and σ_{PSII} than phytoplankton (Figure 3.5D and E). From T0 to T6, phytoplankton maintained higher F_v/F_m than ice algae, but under both light levels F_v/F_m of ice algae increased (two-way ANOVA, $p < 0.001$; *t*-test, $p < 0.05$). Both communities decreased σ_{PSII} (*t*-test, $p < 0.05$) to similar values at T6. Ice algae and phytoplankton also had similar PPC:Chl *a* ratios at T6 (Figure 3.5F). T0 comparisons of photoprotective pigment to Chl *a* (PPC:Chl *a*) ratios were not available.

Table 3.4 A two-way analysis of variance was conducted on the influence of two independent variables (Light level +, Type *) on community growth parameters (mean (standard deviation)) for phytoplankton (W) and sea ice algae (I) communities. Significant main effects are designated by + (Light) and * (Type). When the interaction term (light x type) was significant, a Tukey HSD was performed on all combinations. Differences from the Tukey HSD are represented by letters: a,b,c.

Experiment	Light Level	Type	Chl a (d^{-1}) exponential eq.	POC (d^{-1}) exponential eq.
Exp 1	HIGH	W	1.18 (0.08) a	0.62 (0.10)
		I	0.47 (0.01) b	0.53 (0.06)
(12:12 h)	Low	W	0.80 (0.06) c	0.74 (0.07)
		I	0.46 (0.11) b	-
Exp 2	HIGH	W	0.62 (0.03)	0.75 (0.01)
		I	0.76 (0.09)	0.88 (0.06)
(24 h)	Low	W	0.73 (0.20)	0.61 (0.10)
		I	0.81 (0.09)	0.89 (0.18)
Exp 3	HIGH	W	0.54 (0.03) *	0.64 (0.07)
		I	1.26 (0.50) *	0.89 (0.03)
(24 h)	Low	W	0.63 (0.07) *	0.76 (0.14)
		I	0.94 (0.09) *	1.14 (0.25)

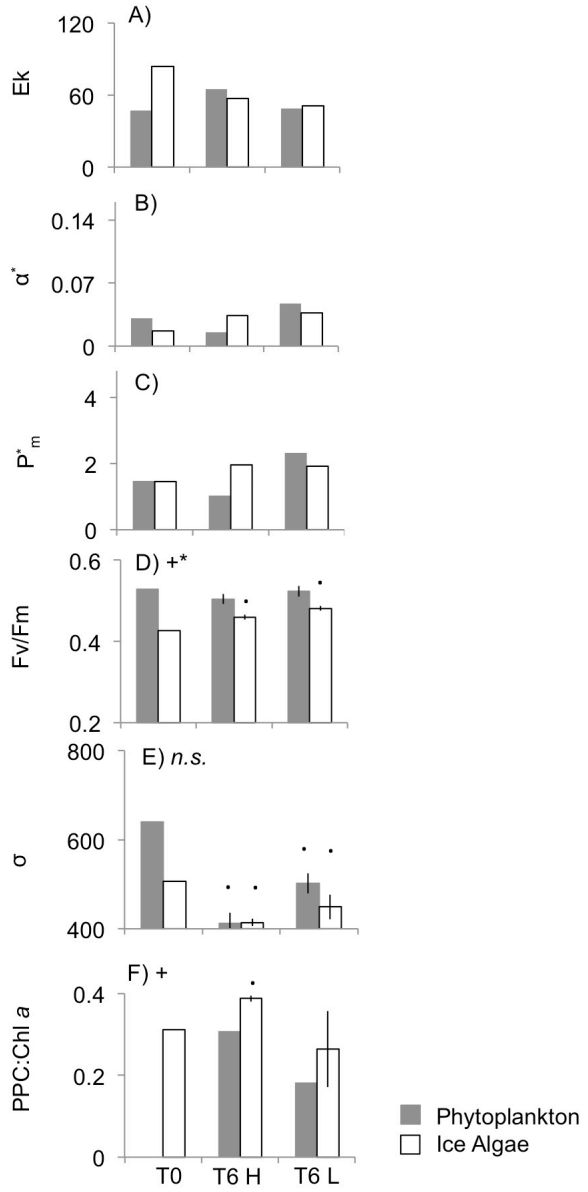

Figure 3.5 Photophysiology parameters of ice algae (I) and phytoplankton (W) for Experiment (Exp) 1 (12:12 h) at T0 and T6 incubated under high (H) and low (L) light levels: (A) photoacclimation parameter (Ek, µmol photon $m^2 s^{-1}$), (B) photosynthetic efficiency (α^*, mg C mg^{-1} Chl *a* h^{-1} (µmol photon $m^2 s^{-1})^{-1}$), (C) maximum photosynthetic rate (P^*_m, mg C mg^{-1} Chl *a* h^{-1}), (D) Photosystem II efficiency (Fv/Fm), (E) functional absorption cross-section ($\sigma_{PSII,}$ Å^2 $quanta^{-1}$), and (F) photoprotective pigment (PPC):Chl *a* ratios. A two-way analysis of variance was conducted on the influence of two independent variables (Light level +, Type *) on Fv/Fm, σ (Å^2 $quanta^{-1}$), and pigment ratios . A paired t-test (˙ $p<0.05$) was used to assess the change between T0 and T6.

24 h light cycle (Exps 2 and 3). Ice algal communities grown under 24 h continuous light tended to have higher Chl *a*-based (Exp 3: two-way ANOVA, $p < 0.05$) and POC-based growth rates than phytoplankton (Table 3.4). At T0, ice algae exhibited higher E_k (Exp 2: 90 µmol photon m^{-2} s^{-1}) than phytoplankton (27 and 17 µmol photon m^{-2} s^{-1} for Exps 2 and 3, respectively) (Figure 3.6A and B). At T6, ice algae maintained a higher E_k than phytoplankton in both the high and low light treatments. Initially, ice algae α^* (Exp 2: 0.02 mg C mg^{-1} Chl *a* h^{-1} (µmol photon m^{-2} s^{-1})$^{-1}$) were lower than those of phytoplankton (Exp 2: 0.13 mg C mg^{-1} Chl *a* h^{-1} (µmol photon m^{-2} s^{-1})$^{-1}$) (Figure 3.6C). At T6, ice algae and phytoplankton α^* were similar (Figure 3.6C and D). Initial P^*_m tended to be lower for ice algae (Exp 2: 2.11 mg C mg^{-1} Chl *a* h^{-1}) than for phytoplankton (3.65 and 2.79 mg C mg^{-1} Chl *a* h^{-1} for Exps 2 and 3, respectively) (Figure 3.6E-F). At T6, ice algae had higher P^*_m than phytoplankton in all light treatments (Exps 2 and 3).

Initially, ice algae tended to have lower F_v/F_m (0.410 and 0.358) and σ_{PSII} (507 and 661 $Å^2$ $quanta^{-1}$) and higher PPC:Chl *a* ratios (0.25 and 0.26) than phytoplankton (F_v/F_m: 0.480 and 0.471; σ_{PSII}:717 and 617 $Å^2$ $quanta^{-1}$; PPC:Chl *a*: 0.08 and 0.10) for Exp 2 and 3, respectively (Figure 3.6G-L). By T6, ice algae and phytoplankton had similar F_v/F_m and σ_{PSII}. While ice algae and phytoplankton PSII parameters were similar, ice algae PPC:Chl *a* ratios were significantly lower than those of phytoplankton (two-way ANOVA, $p < 0.001$, $p < 0.001$ for experiment 2 and 3, respectively).

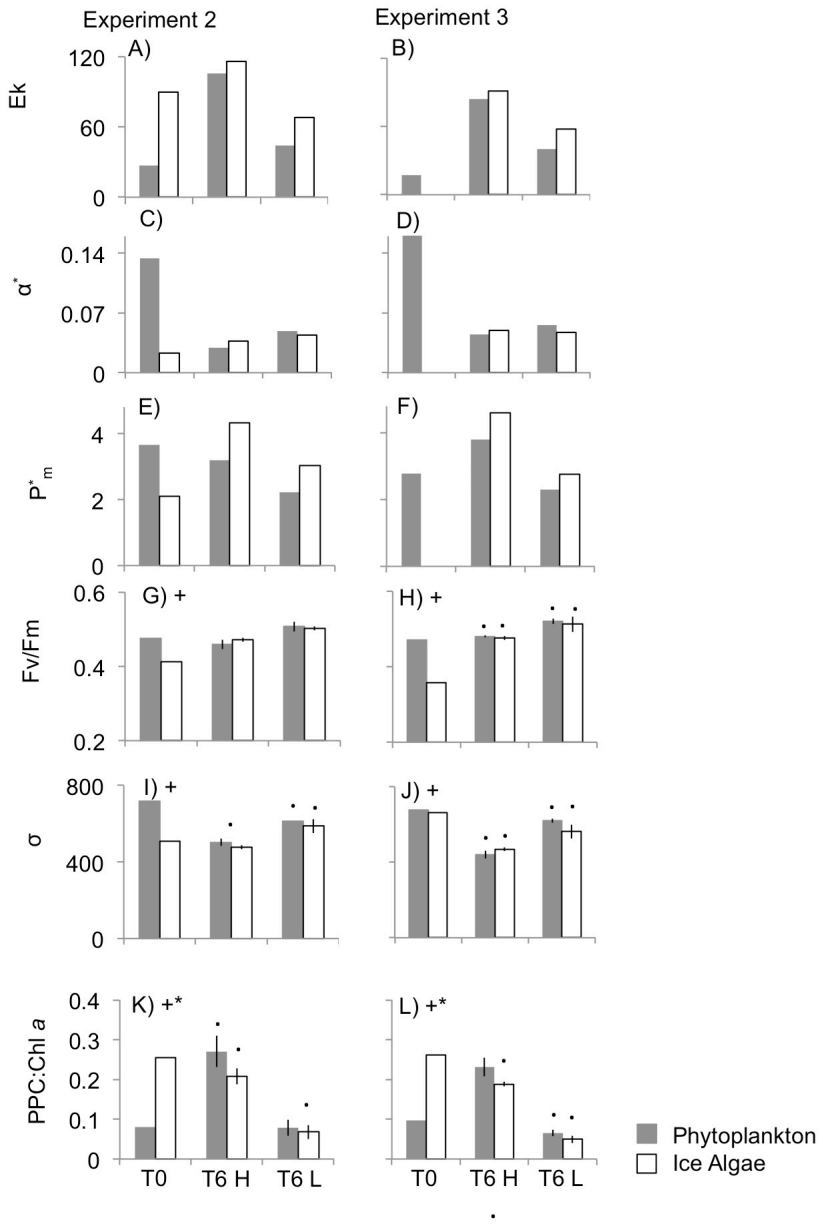

Figure 3.6 Photophysiology parameters of ice algae (I) and phytoplankton (W) for Experiment (Exp) 2 and 3 (24 h light) at T0 and T6 incubated under high (H) and low (L) light levels: (A-B) Photoacclimation parameter (Ek, µmol photon m^2 s^{-1}), (C-D) photosynthetic efficiency (α^*, mg C mg^{-1} Chl *a* h^{-1} (µmol photon m^2 s^{-1})$^{-1}$), (E-F) maximum photosynthetic rate (P^*_m, mg C mg^{-1} Chl *a* h^{-1}), (G-H) Photosystem II efficiency (Fv/Fm), (I-J) functional absorption cross-section ($\sigma_{PSII,}$ Å^2 $quanta^{-1}$) and (K-L) photoprotective pigment (PPC):Chl *a* ratios. A two-way analysis of variance was conducted on the influence of two independent variables (Light level +, Type *) on Fv/Fm, σ (Å^2 $quanta^{-1}$), and pigment ratios . A paired t-test (˙ $p < 0.05$) was used to assess the change between T0 and T6.

3.3.4 Settling Column Experiments

We also explored the role differential sinking may have on the contribution of ice algae to phytoplankton community composition through settling column experiments. Overall, ice algal communities had consistently higher sinking rates (0.22 ± 0.08 m d^{-1}) than phytoplankton (0.00 ± 0.09 m d^{-1}). Very low sinking rates for phytoplankton persisted over a wide range of settling times (Table 3.5). For ice algae, the highest sinking rate was observed after 4 h (STN 58; 1.11 m d^{-1}), compared to those after 24 h (STN 58; 0.28 m d^{-1}).

The taxonomic composition of the buoyant and sinking communities showed that when *P. antarctica* was present, it made up a disproportionately higher fraction of the settled biomass (estimated from biovolume) than would have been expected from an even distribution of communities throughout the settling column (Figure 3.7, STNs 40, 58, 66, and 71). Conversely, pennate diatoms were often buoyant, demonstrated by their low abundance in the settled biomass relative to their expected abundance based on an even distribution. The fate of centric and small, unidentified phytoplankton cells was less clear. These groups were more often found at the top and middle sections of the settling column than the bottom, indicating relatively slow sinking speeds over the length of the experiments (4 to 24 hrs).

Table 3.5 Sinking rates (m d^{-1}) of ice algae from the slush layer and phytoplankton communities from near surface waters (n=2,3).

Station #	Mean Sinking Rate (m d^{-1})	± SD
Phytoplanton		
2	0.06	0.00
15	0.13	0.03
38	-0.11	0.02
40	-0.10	0.06
44	0.00	0.01
48	0.03	0.00
Ice Algae		
50	0.17	0.02
58	0.38	0.69
62	0.18	0.04
66	0.24	0.07
68	0.18	0.04
71	0.22	0.01
78	0.17	0.01

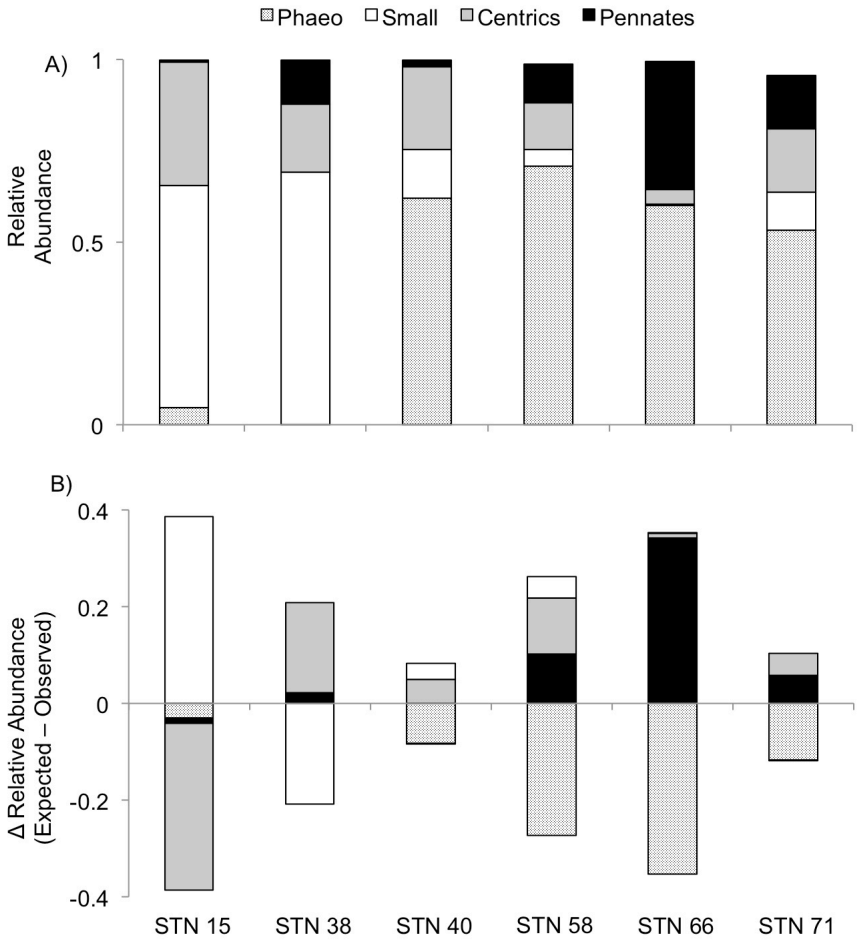

Figure 3.7 (A) Taxonomic composition of communities in settling column experiments (B) Change in relative abundance of taxa in bottom of settling columns from even distribution (expected even distribution – observed distribution of settled biomass): 0 would indicate there was no change from an expected even distribution. > 0 indicates taxa were + buoyant and ascended from the bottom to the middle and top portions of the settling column. < 0 indicates taxa were – buoyant and sank to the bottom of the settling column.

3.4 Discussion

3.4.1 The Magnitude of Spring Ice Algal Blooms

One study conducted on WAP ice ecosystems have qualitatively described the slush layer as *"gaps and holes and intensively brown layers on top of the underlying ice. Often these gaps were filled with slush ice that colored the whole broken ice brash a dark brown"* (Miller and Grobe 1996). Studies on WAP ice ecosystems have either been limited to Marguerite Bay (Massom et

al. 2006) or conducted outside of our study area, farther south in the Bellingshausen Sea (Miller and Grobe 1996, Boyd et al. 1995, Fritsen et al. 2011). Slush layer ice algal concentrations measured during our study were up to 3 times greater than observed earlier in spring in Marguerite Bay (71 mg m^{-3}; Massom et al. 2006), but integrated values from our study were three times lower than those of Massom et al. (2006; 309 mg m^{-2}). Differences were likely due to our thinner (0.39 – 1.18 m) dispersed ice pack compared to the rafted ice floes up to 10-15 m thick in Massom et al (2006). Depth-integrated biomass at most stations in our study was between 10 and 100 mg Chl *a* m^{-2} and the majority were in close agreement with estimates from the spring Bellingshausen Sea ASPeCt dataset (25-35 mg Chl *a* m^{-2} in Saenz and Arrigo 2014). Our ice biomass estimates are likely conservative because, similar to the challenging sample collection noted by Miller and Grobe (1996) during the ANT-XI/3 expedition, the slush was easily lost or diluted with seawater during collection. In other Antarctic regions, observations of Chl *a* within slush layers range from 80-244 mg m^{-2} (reviewed in Arrigo and Thomas 2004) and concentrations as high as 439 mg m^{-3} (Kattner et al. 2004) have been reported. In the Meiners et al. (2012) metadata analysis of ice communities across the Amundsen and Bellingshausen Seas, ice algal biomass was evenly distributed throughout the ice core, with surface (37.1%), interior (29.8%), and bottom habitats (33.2%) contributing almost evenly to depth-integrated Chl *a*. These observations agree with our first-ever mid to late spring measurements of sea ice algae along the LTER grid showing that elevated Chl *a* concentrations were contained in slush layers throughout the sea ice.

3.4.2 Ice Algal Community Physiology and Composition

Elevated irradiance and frequent seawater exchange through porous ice are associated with horizontal slush layers (Thomas et al. 1998) and support bloom-formation, as indicated by the lower POC:Chl *a* (Geider et al. 1997) and POC:PON ratios observed here and by Kattner et al. (2004). In our sea ice samples, nutrient concentrations were often high, and sometimes equal to or above expected values based on seawater exchange throughout the sea ice. High ice algal productivity has been observed within these slush layers, comparable to that of phytoplankton in other regions (Lizotte and Sullivan 1991), prompting the terms “biological soup” and “chemostat in ice” (Thomas et al. 1998). We also observed the highest values for P^*_m and α^* in the slush layer, indicating high maximal growth rates. Ice algae in the slush layer must maintain large numbers of PSII reaction centers to sustain the observed high P^*_m and α^* with low PSII reaction center efficiencies (F_v/F_m; Murchie and Lawson 2013). These results suggest that slush layers provide a very favorable combination of light and nutrients for growth relative to other ice habitats.

Despite significant differences in photosynthetic parameters (P^*_m and α^*) between communities living in the slush layer and other habitats of the sea ice, there were no consistent differences in community composition as *P. antarctica* dominated communities throughout the sea ice. High connectivity of porous sea ice and the motility of some phytoplankton, such as the flagellate stage of *P. antarctica,* may explain the absence of algal zonation with respect to community composition throughout sea ice (Syvertsen and Kristiansen 1993). In previous studies, *P. antarctica* has been observed in both single cell and colonial forms in sea ice, but it has rarely been dominant (Garrison and Buck 1989, Syvertsen and Kristiansen 1993, Arrigo et al. 2003), although Arrigo et al. (2003) observed high *P. antarctica* biomass in newly-formed sea ice. Haptophytes, such as *P. antarctica*, have been observed at low relative abundances in infiltration and surface sea ice communities in the Weddell Sea (Syvertsen and Kristiansen 1993) and Eastern Antarctic region (Trevena et al. 2000) and in bottom ice communities in the Bellingshausen Sea (Fritsen et al. 2011). More often, pennate diatoms such as *Nitzschia* (Garrison and Buck 1989, Thomas et al. 1998, Syvertsen and Kristiansen 1993), *Amphiprora* (Thomas et al. 1998, Guglielmo et al. 2000), and *Fragilariopsis* (Thomas et al. 1998) have dominated slush layers and other habitats in the sea ice.

The dominance of colonial *P. antarctica* blooms we observed in slush layers has the potential to influence upper trophic levels, particularly along the WAP. In other regions of the Antarctic, swarms of juvenile krill removed 3 to 4 cm of ice algal layers from the slush community within 30 minutes (Syvertsen and Kristiansen 1993), suggesting these layers can be a rich food source for krill. However, other field and laboratory studies have shown that krill (*Euphausia superba*) do not readily graze *P. antarctica* (Haberman et al. 2002), especially in colonial form (Haberman et al. 1993). Krill prefer to feed on diatoms, such as the common ice genus *Nitzschia*, as suggested by selective grazing experiments that showed higher grazing rates on diatoms (Haberman et al. 2003). The mucus matrix of *P. antarctica* may clog the feeding apparatus of zooplankton (Schnack 1985) or prevent ingestion (Hansen et al. 1994). Interestingly, we only observed swarms of krill feeding in the slush layer at the northern-most ice station (STN 24, Exp 1), which was one of the few ice stations dominated by diatoms. Massom et al. (2006) found that despite heavy ice conditions and high ice algal biomass in slush layers, krill recruitment was low along the WAP, although no phytoplankton taxonomic information was available in that study. These findings, paired with our anecdotal field observations, hint at the potential roles the physical structure of the sea ice may play in shaping lower and upper trophic level dynamics of the ocean ecosystem.

3.4.3 Ice algal and phytoplankton community responses to simulated ice melt.

Prior to simulated melt out, ice algal communities within the sea ice were acclimated (E_k) to light levels representative of mid to late spring MLs in the Southern Ocean (Smith and van Hilst 2003) and those defined as low light conditions in our growth experiments (90 μmol photon m^{-2} s^{-1}). These levels of light acclimation are similar to those measured previously in ice algal communities near Palmer station during late spring (> 80 μmol photon m^{-2} s^{-1}; Prezelin 1998). Therefore, our low light treatments simulated the transition of ice algal communities from the sea ice to the water column under mid to late spring ML conditions. High light treatments simulated the transition of ice algal communities from the sea ice to the water column under higher light conditions representative of stratified summer ML conditions (Smith and van Hilst 2003, Mills et al. 2010).

In contrast to ice algae, phytoplankton beneath sea ice in our study were acclimated to much lower light levels (17 to 47 μmol photon m^{-2} s^{-1}) prior to growth experiment incubations. Therefore, growth experiments simulate phytoplankton transitioning from a deeply mixed low light environment beneath the sea ice to ice-free waters with spring ML (low light treatment) and a summer MLs (high light treatment).

Photoacclimation of P. antarctica and diatoms. The initial phytoplankton and ice algal communities in our experiments were dominated by chain-forming diatoms, a well-documented bloom-forming group across the WAP (Prezelin et al. 2000 and Garibotti et al. 2003) and colonial *P. antarctica*. These taxa are thought to employ different adaptive strategies to variable (Van Leeuwe and Stefels 2007, Mills et al. 2010) and stable (Moisan et al. 1998, van Leeuwe and Stefels 1998, Moisan and Mitchell 1999, Arrigo et al. 2010) light conditions that persist during the spring transition period. Cullen and MacIntyre (1998) proposed the terms "mixers" and "layer-formers" to describe phytoplankton adapted to a variable light field under mixing conditions and a stable light field under stratified conditions, respectively. Field and laboratory studies have identified *P. antarctica* as a mixer based on its ability to utilize the maximum, rather than the average, irradiance experienced in the water column (Mills et al. 2010) and its observed dominance in blooms that form in deeply mixed conditions of the Ross Sea (Arrigo et al. 1999, 2010). Conversely, the diatom *Fragilaropsis cylindrus* was suggested to be more of a layer-former, adapted to higher and less variable light (Arrigo et al. 2010, Mills et al. 2010).

In the 12:12 h growth experiment (Exp 1), phytoplankton Chl *a* and POC-based growth rates were higher than those of ice algae, suggesting that under these light conditions, phytoplankton growth would outpace ice algal growth when released from the ice into the water column. Despite the dominance of diatoms at T6 in the Exp 1 phytoplankton communities, *P. antarctica* increased

and diatoms decreased in relative abundance over the six-day experiment, suggesting that *P. antarctica* has a competitive advantage over diatoms in both high and low light conditions. Similarly, in the high and low light ice algal communities, *P. antarctica* increased in abundance relative to diatoms, and in this instance, was the dominant taxa by T6. Arrigo et al. (2010) and Mills et al. (2010) showed that *P. antarctica* growth rates exceeded those of the diatom species *F. cylindrus* at irradiances <250 μmol photon m^{-2} s^{-1}. These light levels are within the range of our study, which simulates spring (low light) and summer (high light) mixed layer depth (MLD) scenarios. Comparison of mixed community (*P. antarctica* – diatoms) photoacclimation at T6 from our study (Exp 1, 12:12 h) showed that communities with higher proportions of *P. antarctica* had higher maximum photosynthesis rates in high light. This result is in agreement with others (Arrigo et al. 2010, Mills et al. 2010) showing that under high light, *P. antarctica* maximizes its growth potential rather than optimizing energy capture and utilization.

If cells capture energy faster than they can process it, the excess energy can damage reaction centers within the photosystem, which slows growth (Long et al. 1994). Taxonomically mixed communities (Exp 1, 12:12 h) with a greater proportion of *P. antarctica* had lower values for F_v/F_m, potentially indicative of damaged photosystems. Alternatively, community differences in F_v/F_m may be a result of the different photoprotective strategies employed by diatoms and *P. antarctica*. Laboratory studies show that both *P. antarctica* and diatoms employ rapid xanthophyll cycling to dissipate excess energy as heat and protect the reaction center from photodamage (Moisan et al. 1998, van Leeuwe and Stefels 2007, Kroupenske et al. 2009); however, comparative studies have suggested this is a dominant photophysiology strategy in diatoms, but not *P. antarctica* (Kroupenske et al. 2009, Arrigo et al. 2010, van de Poll et al. 2011). Rather, *P. antarctica* invests in the slower photoacclimation mechanism of D1 protein repair following photodamage (Kroupenske et al. 2009). While *P. antarctica* may be more susceptible to photodamage, as suggested by Kroupenske et al. (2009) and Mills et al. (2010), *P. antarctica* increased in relative abundance in all experiments. These results suggest that ice-derived and non-ice-derived *P. antarctica* were able to compensate for any photodamage incurred and has the potential to outcompete other taxa under high and low light conditions.

Variability within P. antarctica-dominated communities. Our growth experiments suggest that light history can also affect the response of ice algal or phytoplankton communities dominated by *P. antarctica* to changes in the light environment. In Exps 2 and 3, ice algal growth rates were higher than those of phytoplankton, suggesting that ice algal seeding and subsequent growth would outpace that of phytoplankton growth. PvE parameters indicate that phytoplankton were initially acclimated to lower light levels than ice algae. Our results from the growth

experiments suggested that deeply-mixed under-ice phytoplankton communities (E_k: 17 to 24 µmol photon m^2 s^{-1}) experience a 5-fold increase in light when transitioning to a mid to late spring ML (low light condition; 91 ± 25 µmol photon m^{-2} s^{-1}). In contrast, the light environment experienced by ice algal communities transitioning from sea ice to a deeply-mixed open water environment (low light environment) remains unchanged. At T6, ice algae remained acclimated to higher light levels, driven by their higher maximum photosynthetic rates (P^*_m) and higher growth rates than phytoplankton. Phytoplankton employed higher photoprotective pigment to Chl *a* ratios (PPC:Chl *a*) than ice algae in order to adjust to the order of magnitude increase in their light environment. While light history affected carbon fixation and photoprotective pigment composition, it appeared to have no effect on F_v/F_m or σ_{PSII} in either sea ice or phytoplankton communities. Others have noted species composition, rather than environment, often controls the variability observed in PSII parameters (Moore et al. 2005, 2006). Our results suggest that light history has a lasting effect on photoacclimation parameters, including carbon fixation and pigment composition, but not on the potentially community composition-driven PSII parameters in *P. antarctica*-dominant communities.

The contrasting light environments of the ice and water column may support the variety of *P. antarctica* populations we observed along the coastal WAP in spring. Gaebler-Schwarz et al. (2015) found that within Antarctic regions, bloom-forming *P. antarctica* were genetically diverse and distinctly different across regions (e.g., Ross Sea, Antarctic Circumpolar Current, Antarctic Peninsula). Gaebler-Schwarz et al. (2015) also found that geographically close, rather than genetically close, isolates responded similarly to environmental changes, further suggesting that environmental conditions of the ice or the water column in spring may influence population responses post-ice melt.

3.4.4 *P. antarctica* along the WAP.

Our experimental results suggest that, while colonial *P. antarctica* communities from the sea ice and the water column vary in their immediate responses to changes in their light environment, they have the potential to increase in abundance relative to other taxa and dominate the community within a week of acclimation. However, their success in utilizing resources may be balanced by their rate of sinking relative to other taxa, especially in stratified conditions. We observed that, when present, *P. antarctica* made up a larger fraction of the sinking community than diatoms (neutral or positively buoyant), suggesting that *P. antarctica* colonies have higher sinking rates than other taxa. Others have also reported rapid export of *P. antarctica* blooms (DiTullio et al. 2000) and *P. antarctica-Nitzschia* ice algal aggregates (Riebesell et al. 1991). However, Riebesell et al. (1991) noted that ice algae from the slush layer, relative to other ice

habitats, did not form aggregates and had lower sinking rates. Additionally, Becquevort and Smith (2001) observed that diatoms and dinoflagellates had higher sinking rates than *P. antarctica*. The sinking and export rates of *P. antarctica* relative to other taxa remain unclear and may be related to their respective metabolic activity (Waite et al. 1997) or cell density (Peperzak et al. 2003), both of which are beyond the scope of this study. Our data suggest that ice algal communities have faster sinking rates than phytoplankton communities and that *P. antarctica* from both the ice and the water column sink disproportionately more than other taxa along the WAP. The absolute magnitudes of sinking rates measured in this study are likely underestimates, as indicated by the error associated with sinking rates calculated after <24 h (higher sinking rates) and 24 h (lower sinking rates), as discussed in Bienfang (1981).

Studies suggest that colonial *P. antarctica* can be prevalent in sea ice and is sometimes dominant, co-occuring in late spring with diatoms in coastal surface waters of the Bellinghausen Sea (Savidge et al. 1995), Gerlache Strait (Varela et al. 2002, Rodriguez et al 2002), and the WAP (this study, Arrigo et al. *in review*). However, dominance of *P. antarctica* may be a spring phenomenon, because this dominance does not persist into summer phytoplankton blooms recorded in long-term data sets along the WAP. Garibotti et al. (2003) suggested that the seasonal succession of phytoplankton is tied to the timing of ice retreat where near-shore phytoplankton blooms associated with the ice edge are diatom-dominated. *P. antarctica* is often present, but not dominant, in these early summer communities (Varela et al. 2002, Rodriguez et al 2002, Garibotti et al. 2003, Annett et al. 2010). Observations of higher *P. antarctica* concentrations are generally limited to near-shore regions such as Marguerite Bay (Garibotti et al. 2003, Kozlowski et al. 2011) or Bransfield Strait (Trimborn 2015). Following the diatom bloom, Garibotti et al. (2003, 2005) suggested that communities shift to dominance by small unidentified flagellates and then by cryptophytes.

Elevated irradiance along the WAP in summer could explain the shift from either mixed or *P. antarctica* dominated communities in spring to observed diatom dominance in summer (Garibotti et al. 2003, 2005). Culture studies show that the diatom *F. cylindrus* has a competitive advantage when grown under irradiances corresponding to a 7 m MLD (Mills et al. 2010), generally greater than those of our study. In spring, deep MLDs (60 m) at Palmer station (Ducklow et al. 2012) and across the WAP create low light conditions and are potentially conducive to higher *P. antarctica* abundance, as observed in northern Marguerite Bay (Rozema et al. 2017) and the WAP (Arrigo et al. 2017), but not further north at Palmer Station (Schofield 2017). Typically in coastal waters (<50 km from shore) in mid-December, the water column abruptly shifts from unstable to stratified (MLD of 10 to 15 m) conditions, creating a high and

stable light environment, which potentially favors the diatom-dominated blooms seen by Rozema et al. (2017) and observed in summer stratified conditions (Garibotti et al. 2003, Garibotti et al. 2005, Annett et al. 2010, Ducklow et al. 2012). The onset of stratification and, consequently, the potential for nutrient limitation and photoinhibition, make sinking losses a more important component of total loss processes for phytoplankton populations (Cullen and MacIntyre 1998). The combination of the lower growth rate of *P. antarctica* at high irradiance (Mills et al. 2010) and higher sinking rates than diatoms (this study) may explain the nearly ubiquitous absence of *P. antarctica* dominance along the coastal WAP in summer phytoplankton blooms. In contrast to highly stratified coastal waters, mid- and outer continental shelf and offshore waters have deeper MLs (Prezelin et al. 2000, Martinson et al. 2008, Vernet et al. 2008) Recent studies have observed that *P. antarctica* can compose 50% or greater of the phytoplankton community in off-shore waters in spring (Arrigo et al. 2017) and that these high relative abundances can persist into summer (Kozlowksi et al. 2011, Trimborn et al. 2015).

The combination of field survey and experiment results suggest that sea ice is a potential source of *P. antarctica* to the water column and that these ice-derived *P. antarctica* are viable under light conditions phytoplankton would experience from late spring through summer. A complimentary study (Arrigo et al. 2017) found that *P. antarctica* distributions in the phytoplankton were positively correlated with ice cover, further suggesting that the *P. antarctica* blooms in sea ice may seed the water column. The ability of *P. antarctica* to grow faster at low light levels (Kroupenske et al. 2009) and increase in abundance relative to other taxa (this study), may allow it to maintain its dominance through the ice-covered spring season, contributing to moderate spring phytoplankton blooms in variable sea ice cover (Arrigo et al. 2017). Potential coupling between the sea ice and ocean communities along the wAP has been suggested by similar qualitative observations by Massom et al (2006), who described large-scale intra-ice pack spring phytoplankton blooms associated with high biomass slush layers in the sea ice.

3.5 Conclusion

The WAP sea ice experiences enhanced and widespread surface flooding during late spring, leading to pronounced slush ice algal communities that are dominated by the bloom-forming colonial haptophyte *P. antarctica.* During spring, the ice algal and phytoplankton communities are highly interconnected, as suggested by their taxonomic composition. Our ship-board experiments suggest that ice algae, especially *P. antarctica,* from slush layers can contribute to phytoplankton communities during sea ice melt. This ice-ocean coupling along the WAP is likely driven by high rates of flooding and seawater exchange in spring. Sea ice and water column

populations of *P. antarctica* may give this taxa a unique advantage for dominance, by having multiple seed populations adapted to different light regimes. However, this contribution may be limited due to *P. antarctica's* enhanced sinking potential relative to other taxa. Ice algal biomass location (slush, surface, interior, or bottom layer), taxonomic composition, and its role in seeding phytoplankton blooms may have broader consequences for upper trophic levels. Furthermore, as the WAP experiences continued warming, the role sea ice plays in controlling light availability and stratification may alter the structure of phytoplankton blooms, particularly for *P. antarctica.*

Chapter 4

Conclusion

4.1 Bi-Polar Ice Algal-Phytoplankton Coupling

The sea ice environment of the Arctic and Southern Oceans are vastly different, and this results in different algal habitats within the sea ice. We observed in Chapter 1 that in our studied Arctic region, the Chukchi Sea, the sea ice had a higher freeboard (more of its volume is above the water) than that of our studied Antarctic region, the west Antarctic Peninsula in Chapter 3 (Selz et al. 2017, 2018). Negative freeboards often result in seawater flooding Antarctic sea ice, a phenomenon that does not occur in the Arctic (Perovich et al. 2004). Ice algae will bloom in the sea ice when light and nutrients are optimal for growth. In the Chukchi Sea, where seawater flooding is absent, the porous bottom skeletal layer of the sea ice is optimal for algal taxa to bloom due to exchange with nutrient-rich seawater and a stable light environment and these bottom ice algal blooms reach high concentrations and are prevalent across the Chukchi Sea in spring (Selz et al. 2017). Conversely, in the WAP, seawater floods the sea ice and creates slushy, highly porous layers at the surface (Perovich et al. 2004, Saenz and Arrigo 2014). Here, ice algal taxa can bloom much closer to the air-ice interface (Selz et al. 2018) compared to the bottom ice algal blooms observed in the Chukchi Sea (Selz et al. 2017). The physical differences in Arctic versus Antarctic sea ice, due to varying freeboard, lead to blooms developing in bottom versus slushy layer habitats observed in the sea ice in these two different polar regions (Selz et al. 2017, 2018). Interestingly, Arctic bottom ice and Antarctic slushy ice communities are often composed of different taxa (van Leeuwe et al. 2018). As observed in this study, flagellates, such as *P. antarctica*, often dominate algal blooms in slushy layers of sea ice (WAP) and pennate diatoms dominate algal blooms in the bottom of the sea ice (Chukchi Sea). The tendency for pennate diatoms to dominate the bottom of the sea ice has been attributed to their efficient nutrient uptake at low light levels (Hegseth 1992, Gradinger et al. 1999, Lizotte 2001), while flagellates are hypothesized to adapt to high and variable light levels near the air-snow-ice interface (van Leeuwe et al. 2018).

Physical features of the sea ice covering the Arctic and Southern Oceans not only impact the ice algae within the sea ice, but also impact the development of phytoplankton blooms in late spring and early summer. In the Chukchi Sea, melt ponds form on the surface of the sea ice and

allow light to be transmitted to the ocean, stimulating early under-ice phytoplankton blooms (Arrigo et al. 2014). Conversely, in the WAP, there is no melt pond formation. WAP phytoplankton bloom after the ice has melted and the water column has stratified, both of which increase light availability later in spring and summer (Ducklow et al. 2012). Therefore, the physical features of the sea ice impact the onset of ice melt or melt pond development and the timing of the start of the phytoplankton bloom.

During this melt period, sea ice-covered regions transition from a period where benthic and pelagic ecosystems are dependent on ice algae to ones that are dependent on phytoplankton as primary producers (Leu et al. 2015). While many studies show physical sea ice features impact phytoplankton bloom development during this transitional period for the Chukchi Sea (Arrigo et al. 2014, Lowry et al. 2018) and WAP regions (Garibotti et al. 2005, Venables et al. 2013, Montes-Hugo et al. 2009), this dissertation work contributes to our knowledge gap on how the loss of the sea ice algal community into the water column impacts phytoplankton bloom development. Here, after characterizing the ice algal blooms, I investigated ice algal-phytoplankton coupling mechanisms in two very different ice habitats (bottom versus slushy layer) dominated by different taxa (pennate diatoms versus *P. antarctica*) that have different relationships with the phytoplankton bloom. Pennate diatoms are generally not associated with phytoplankton blooms (Horner 1985), while *P. antarctica* are often observed as dominant taxa in phytoplankton blooms (Garrison et al. 1987, Lannuzel et al. 2013). Therefore, it may be expected that ice algal-phytoplankton coupling would be stronger in the Antarctic than the Arctic.

However, the major finding of this work showed that in both polar ocean regions, ice algae melting out of the sea ice briefly elevated phytoplankton concentrations in spring, but did not persist into summer phytoplankton blooms. Rather, ice-derived phytoplankton likely sank out of the surface mixed layer in both polar ocean studies, based on results from experimental sinking rate measurements (WAP, Chapter 3) and a combined field and modeling approach (Chukchi Sea, Chapter 1). Our similar findings in both poles in very different conditions that included the physical sea ice habitat (slush versus bottom layer), ice algal and phytoplankton communities (diatom- versus flagellate-dominated), and spring-time phytoplankton bloom dynamics (under-ice versus marginal ice zone or open water blooms) suggest that the links between ice algae and phytoplankton tend to be weak and separate from each other in both poles. Additionally, if ice algae are not seeding phytoplankton, they must either be linked to export to the sea floor or deep ocean, or linked to consumption by grazers in the benthic or water column environment.

Our understanding of the physiology of taxa that dominate ice algae versus phytoplankton blooms further support our findings that a large proportion of the ice algal blooms

sink out of the surface layer in polar oceans. Extracellular polymeric substances (EPS), which are hypothesized to make sea ice more habitable to micro-organisms, as well as late-stage bloom, low-nutrient, sea ice melt conditions support the formation of aggregates of algal taxa (Riebesell et al. 1991, Kuosa et al. 1992). These aggregates observed in both our field settings potentially explain the higher sinking rates that were measured (Chapter 3) or inferred (Chapter 1) from experiments and modeling studies. In addition, field experiments show that previous light history of the algal community is important to the competitiveness of algal taxa following ice melt (Chapter 3). Other field observations demonstrate phytoplankton communities are acclimated to high light intensities, meaning the phytoplankton are ready to bloom as soon as light increases above a certain threshold (Lewis et al. in review), giving them a significant advantage over those taxa acclimated to the sea ice. Our results in the context of our understanding of ice algal versus phytoplankton physiology suggest that regardless of the sea ice habitat or the ice algal taxa, ice algal physiology related to sinking rate or light-acclimation leads to the export of ice algal taxa to the sea floor or deep ocean in both polar regions.

4.2 Broader significance and implications

While the fate of ice algae may be similar in the Chukchi Sea and WAP region, the resulting significance of the export of ice algae to the pelagic and benthic ecosystems differ on regional scales. In the WAP, the dominant spring ice algal taxa, *P. antarctica* is not palatable to upper trophic levels **(**Schnack 1985, Hansen et al. 1994, Haberman et al. 2003**)**, produces dimethylsulfide, impacting the sulfur cycle (van Leeuwe et al. 2018), and draws down a higher proportion of CO_2 relative to its biomass than other phytoplankton taxa, such as diatoms (Arrigo et al. 1999). *P. antarctica* is exported to the deep ocean (<1000m) in spring and succeeded by a summer phytoplankton bloom that is dominated by diatoms (Ducklow et al. 2012), a more palatable algal taxa that is readily eaten by grazers that are a critical link between lower and upper trophic levels (Michel 1996). Conversely in the Chukchi Sea, the ice algal bloom is composed of diatoms. In the Arctic, ice algal diatoms tend to be much higher in lipid content, which serves as a critical food source to early stages of various zooplankton and ice-associated grazers (reviewed in Kedra et al. 2015). Rather than being exported to the deep ocean, here the ice algal bloom is exported ~80 m to a shallow shelf region and serves as an early pulse of food, the only food source, to the benthic ecosystem prior to the development and export of the phytoplankton bloom in early spring. During this period, the timing of the pulse, as well as the quality of the pulse of export may impact benthic species composition and abundance (Ambrose and Renaud 1997).

It remains uncertain how these polar marine ecosystems will respond to environmental conditions as the snow and sea ice conditions continue to change in the Arctic and Southern Oceans. I demonstrated that even with large variability in snow and sea ice thickness, earlier sea ice melt in spring is driving significant declines in ice algal production over time (1980-2015; Chapter 2). Thinner snow packs may compensate for ice-melt driven ice algal production declines, but recent research cannot agree on whether we can expect a more (Bintanja and Selton 2014) or less (Hezel et al. 2012) snowy future due to uncertainties in sea ice dynamics and precipitation falling as rain versus snow. I showed that, for my study year, the seeding of sea ice algae do not impact the development of phytoplankton blooms. Therefore, if these field observations from spring 2014 apply to all years, changes in ice algal production will not impact phytoplankton bloom development. Instead, ice algal biomass that likely sinks to the sea floor, provides the only source of food early in the spring to benthic consumers (Kedra et al. 2015). While one study suggested that earlier export of ice algae would result in higher amounts of biomass exported to the benthos (Gradinger 1995); declines or northward shifts in benthic consumer biomass have been linked to changes in sea ice extent (Grebmeier et al. 2015, 2016). Additionally, modeling studies have shown that reduced export of ice algal and/or phytoplankton biomass can lead to significant shifts and complete loss of some dominant benthic consumers (Lovvorn et al. 2016) in subpolar regions. Our modeling results suggest declines in sea ice reduce the amount of ice algal biomass available for export, and others have suggested reductions in sea ice extent also results in reduced phytoplankton export due to shifts in community composition, increased grazing, and/or recycling of organic matter in surface waters (Renaud et al. 2008, Moran et al. 2012). Therefore, the benthic consumers that rely on the export of the ice algae, as well as the phytoplankton, may be negatively impacted by the continued decline and potential complete loss of sea ice in spring (Kedra et al. 2015).

4.3 Future research directions

Can this understanding of the Chukchi Sea and the Western Antarctic Peninsula be applied to the broader Arctic and Southern Ocean? My study covered two systems: (1) a shallow shelf region that transitioned from a bottom sea ice pennate diatom bloom to an under-ice phytoplankton centric diatom bloom and (2) a deeper coastal region that transitioned from a slushy ice flagellate bloom to an open water phytoplankton diatom bloom. A review of ice algal diversity found that our study is similar to general trends in the sea ice communities: pennate diatoms bloom in bottom sea ice in the Arctic and when slushy layers are present, flagellates bloom in slushy Antarctic sea ice (van Leeuwe et al. 2018). The general understanding of ice

algal and phytoplankton physiology that impacts light adaptation and buoyancy (discussed above) is in agreement with my studies findings that suggest the majority of ice algae sink to the sea floor or the deep ocean. However, the lack of interannual coupled ice algal-phytoplankton studies and the heterogeneity of the ice-covered Arctic and Southern Oceans suggest that these systems are too complex with many exceptions to generalize our findings across the polar oceans over time.

4.3.1 Arctic

Our results in the context of other coupled ice algal-phytoplankton Arctic studies (discussed in Chapter 1) suggest that the timing and rate of ice algal release to the water column, relative to processes controlling phytoplankton growth (i.e. water column stratification/light availability), impact the coupling between the ice algal and phytoplankton communities. For instance, delays in phytoplankton bloom development relative to ice melt in the Bering Sea resulted in ice algae seeding the water column with taxa that dominate phytoplankton blooms and in this instance potentially "primed" the system for a bloom (Syzmanski et al. 2016). Interannual variability within one region may also impact ice algal-phytoplankton coupling. For example, field observations from the Canadian Archipelago (Galindo et al. 2014) showed that under gradual melt conditions (similar to that observed in our study), the phytoplankton community was dominated by taxa common to phytoplankton blooms. However, for another year in the same region, rapid ice melt conditions resulted in a phytoplankton bloom dominated by ice algal taxa impacting both the timing and magnitude of the under-ice phytoplankton bloom (Galindo et a. 2014).

A comparison of these studies raises the question – *How do physical conditions (i.e. rapid sea ice melt, or mixing/stratification conditions) that vary interannually and impact ice algal and phytoplankton bloom phenology impact ice algal-phytoplankton coupling on regional scales?* Continued paired studies of ice algae, phytoplankton, and benthic trap community composition (similar to Syzmanski et al. 2017) coupled with experiments that investigate the sinking rates and physiology of ice-derived phytoplankton (similar to Selz et al. 2018) would enhance our understanding of what factors drive ice algal-phytoplankton coupling (or lack thereof) from year to year across the heterogeneous Arctic Ocean. In addition these paired observational and experimental studies would also address questions about the export versus consumption in the water column of ice algae and examine the relative importance of ice algae versus phytoplankton as sources of food to pelagic and benthic communities in spring. Building a synthesis of these studies, comparing and contrasting results in areas with varying sea ice and ocean conditions, prone to under-ice versus open water phytoplankton blooms, would advance

our knowledge on how these complex factors affect the fate of Arctic ice algae, their coupling with the phytoplankton, and ultimately their impact on the benthic and pelagic ecosystems.

4.3.2 Antarctic

In the Antarctic, few comprehensive paired ice algal-phytoplankton studies exist to put our WAP study into a broader ice-algal phytoplankton coupling understanding on broader temporal or spatial scales. For the WAP, a long time-series exists for summer phytoplankton blooms that show diatoms, rather than the dominant observed ice-algal taxa *P. Antarctica,* dominate the phytoplankton (Ducklow et al. 2012). This comparison suggests that interannual variability in ice algal-phytoplankton coupling observed in Arctic studies is not present along the WAP. However, because this was the first study of spring ice algal blooms along the WAP region, it is unclear whether *P. antarctica* regularly bloom in slushy WAP sea ice over the long-term time series. Increasing the number of study years (1+) would advance our understanding of whether our observations of *P. antarctica* ice algal blooms are a rare versus a regular occurrence.

In addition to looking forward, another approach would be to look backward in time and ask the question – *Is P. antarctica present in spring prior to the collection of samples in the long-term time-series summer record?* Because flagellates, such as *P. Antarctica* are more often dominant in slushy sea ice layers, an assumption could be made that if slushy sea ice is present, *P. antarctica* is likely dominant. Therefore, the question becomes – *How has the fraction of slushy layers of sea ice changed across the WAP over time?* That question could be addressed by applying the Sea Ice Ecosystem State model (Saenz and Arrigo 2012, 2014) to the WAP for the long-term time series record, which illustrates what fraction of sea ice is flooded (i.e. slushy). Examining changes in physical conditions of the sea ice would yield more information on how ice environments optimal for flagellates (like *P. antarctica*) versus diatoms have changed over time. Results from these studies could yield more insight into how observations of alterations in WAP zooplankton communities (krill versus salp dominance), which have significant impacts on upper trophic levels (Ross et al. 2008, Ross et al. 2014, Steinberg et al. 2015), are linked to changes in the physical structure and inferred community composition of the ice algal blooms over time.

Beyond our understanding of the WAP region, *do ice-derived P. antarctica remain in the water column and seed phytoplankton blooms or sink to the deep ocean in regions of the Southern Ocean that are dominated by P. antarctica blooms?* In these regions, such as those of the Ross Sea, rapid export of *P. antarctica* blooms have been observed (DiTullio et al. 2000). Investigating ice algal-phytoplankton coupling questions using a combination of field surveys and ship-board experiments in regions that experience alternating diatom versus *P. antarctica* versus mixed *P.*

antarctica-diatom bloom communities, such as the Ross Sea (DiTullio et al. 2000) would build on our foundation of knowledge of how ice algal-phytoplankton coupling is impacted by various physical and biological factors in the Southern Ocean.

4.4 Final remarks

A combination of field observations, experiments, and modeling studies were employed to investigate the linkages between the ice algal and phytoplankton communities in two polar ocean regions. This required first developing an in-depth understanding of environmental drivers and biological characteristics of ice algal blooms in these two regions. This work extensively characterizes blooms in different sea ice habitats and suggests that regardless of ice algal bloom type (bottom vs. slush layer; pennate diatom vs. flagellate-dominated) or polar location (Arctic vs. Antarctic) ice algal blooms are more often separated from than coupled to phytoplankton blooms, sinking to the seafloor or deep ocean during ice melt. However, other studies discussed above contradict our findings in the Arctic and no Antarctic studies exist to compare to. Therefore, questions remain as to what physical or biological conditions determine the strength of ice algal – phytoplankton coupling in spring across the heterogeneous Arctic and Southern Oceans.

Appendices

A1 Distribution of taxonomic classes identified from Imaging FlowCytobot Images

Taxonomic Category	Images (#)
Chaetoceros	27,444
Small Unidentified	12,425
Nitzschia	6,596
Pyramimonas	4,015
Pennate diatom	2,985
Dinoflagellate	2,662
Detritus	1,771
Fragilariopsis	1,277
Thalassiosira	1,080
Pseudonitzschia	1,064
Cylindrotheca	904
Entomoneis	650
Large Unidentified	449
Navicula	373
Centric Unidentified	273
Skeletonema	218
Pleurosigma	181
Ciliate	171
Pinnularia	143
Eucampia	131
Leptocylindrus	81
Ephemera	61
Attheya	59
Phaeocystis	40
Haslea	36
Paralia	36
Bacterosira	21
Melosira	15
Detonula	14
Thalassionema	14
Dictyocha	9
Dinobryon	9
Euglena	6
Gyrosigma	4
Guinardia	3
Total	65,220

A2 Nutrients (μM) from sea ice cores (weighted means) and surface sea water collected from <5 m depth.

	Weighted-mean bulk ice nutrients				Sea Water Nutrients			
Station	NO_3	PO_4^3	$Si(OH)_4$	NH_4	NO_3	PO_4^3	$Si(OH)_4$	NH_4
Spring								
29	1.05	0.82	1.92	0.83	2.97	1.20	28.00	0.85
35	1.78	0.75	2.72	0.70	13.56	1.85	49.20	1.74
51	0.34	0.46	1.21	0.65	9.72	1.84	48.40	2.44
59	1.41	0.85	3.28	0.43	9.91	1.82	46.40	2.56
75	0.42	0.93	2.75	0.33	11.25	1.76	49.80	0.57
84	0.10	0.36	0.45	0.16	1.17	0.81	6.50	0.05
99	0.74	0.72	0.83	0.44	15.47	1.94	54.10	1.17
104	0.17	0.60	2.81	0.17	12.88	1.74	48.40	1.27
105	0.10	0.33	1.34	0.27	13.02	1.76	48.50	1.15
106	0.56	0.44	1.77	0.27	12.94	1.78	49.60	1.08
107	0.38	0.53	2.96	2.01	13.02	1.79	49.10	1.15
142	0.26	0.28	1.43	0.29	0.04	0.64	10.30	0.00
160	0.18	0.34	1.04	0.51	12.49	1.63	44.30	0.61
178	0.23	0.32	3.68	0.31	13.70	1.87	50.40	0.97
196	0.58	0.62	2.93	0.19	13.79	1.78	48.60	0.48
209	0.15	0.24	1.88	0.20	12.46	1.70	47.10	0.24
Summer								
33	0.04	0.12	0.61	0.73	0.01	0.65	1.08	0
68	0.29	0.12	0.40	0.74	0	0.52	0.39	0.12
55	0.04	0.08	0.46	0.05	0.07	0.66	15.46	0.05
69	0.80	0.10	0.37	0.47	0.05	0.72	2.64	0
56	0.00	0.08	0.38	0.26	0.03	0.92	20.93	0.04
57	0.06	0.07	0.26	0.35	0.06	0.64	3.43	0
90	0.18	0.06	0.43	0.16	0	0.62	2.94	0
100	0.13	0.07	0.16	0.14	0.02	0.72	3.92	0.09
101	0.89	0.11	0.52	0.26	0.02	0.73	4.11	0.08
109	0.22	0.08	0.47	0.33	0	0.7	2.94	0.13
100	0.13	0.07	0.16	0.14	0	0.58	2.45	0

A3 Mean community composition of clusters I-IX and their corresponding sampling location: station and depth. Ice (I) and phytoplankton (P) and mixed I and P (MIX) communities in spring (SP) and summer (S).

Cluster	SP-I I	SP-I II	SP-P III	SP-MIX IV	SP-MIX VIII	S-I VI	S-I IX	S-P V	S-P VII
Nitzschia	0.60	0.22	0.01	0.01	0.16	0.13	0.13	0.01	0.01
Unidentified Pennates	0.11	0.35	0.01	0.18	0.04	0.05	0.09	0.01	0.02
Entomoneis	0.05	0.04	0.01	0.08	0.00	0.00	0.01	0.00	0.00
Navicula	0.01	0.10	0.03	0.06	0.04	0.00	0.00	0.00	0.01
Fragilariopsis	0.03	0.03	0.40	0.15	0.14	0.02	0.09	0.04	0.00
Other pennates	0.04	0.12	0.01	0.05	0.00	0.02	0.00	0.07	0.01
Total Pennates	**0.83**	**0.86**	**0.48**	**0.53**	**0.37**	**0.23**	**0.32**	**0.14**	**0.05**
Chaetoceros	0.00	0.00	0.01	0.01	0.00	0.00	0.01	0.56	0.17
Thalassiosira	0.02	0.02	0.22	0.14	0.06	0.00	0.00	0.03	0.01
Other centrics	0.02	0.01	0.12	0.03	0.11	0.00	0.00	0.01	0.02
Melosira	0.00	0.00	0.02	0.02	0.08	0.00	0.00	0.00	0.01
Total Centrics	**0.04**	**0.03**	**0.36**	**0.21**	**0.25**	**0.01**	**0.01**	**0.59**	**0.20**
Small unidentifiable cells	0.05	0.02	0.04	0.12	0.17	0.14	0.25	0.18	0.61
Large unidentifiable cells	0.01	0.04	0.05	0.05	0.13	0.00	0.07	0.00	0.01
Pyramimonas	0.00	0.00	0.00	0.02	0.08	0.55	0.01	0.01	0.01
Dinoflagellates	0.01	0.02	0.00	0.01	0.00	0.03	0.32	0.02	0.06
Ciliates	0.00	0.00	0.00	0.00	0.00	0.02	0.00	0.00	0.01
Total Other	**0.07**	**0.08**	**0.09**	**0.20**	**0.37**	**0.74**	**0.65**	**0.21**	**0.70**
Ice	19, 101, 105, 106, 107, 196	99, 142, 160				35, 34, 100, 109	33, 56, 57, 68, 69		36, 67
Surface (≤10 m)	106		19, 142	142, 160,196	99, 106, 196			33, 56, 57, 67, 69, 100, 102, 108, 110	99, 102
Subsurface (>10 m)	106	99	19, 57, 142	99, 160, 196				33, 56, 57, 67, 100	69, 100, 102, 110

A4 Initial and final pigment ratios for CHEMTAX-HPLC analysis of ice algal communities in slush and non-slush layers.

Algal Pigments[1]	Per	19-But	Fuco	19-Hex	Chl c_3	Allo	Viola	Chl b
Initial Ratios								
Prasinophytes	0.00	0.00	0.00	0.00	0.00	0.00	0.03	0.72
Dinoflagellates	0.69	0.00	0.00	0.00	0.00	0.00	0.00	0.00
Cryptophytes	0.00	0.00	0.00	0.00	0.00	0.31	0.00	0.00
Haptophytes 1	0.00	0.05	0.23	0.65	0.10	0.00	0.00	0.00
Pelagophytes	0.00	0.20	0.15	0.25	0.10	0.00	0.00	0.00
Diatoms	0.00	0.00	0.56	0.00	0.00	0.00	0.00	0.00
Final Ratios (non-slush)[2]								
Prasinophytes	0.00	0.00	0.00	0.00	0.00	0.00	0.03	0.72
Dinoflagellates	0.69	0.00	0.00	0.00	0.00	0.00	0.00	0.00
Cryptophytes	0.00	0.00	0.00	0.00	0.00	0.31	0.00	0.00
Haptophytes1	0.00	0.01	0.24	0.53	0.18	0.00	0.00	0.00
Pelagophytes	0.00	0.20	0.15	0.25	0.03	0.00	0.00	0.00
Diatoms	0.00	0.00	0.68	0.00	0.00	0.00	0.00	0.00
Final Ratios (slush)[3]								
Prasinophytes	0.00	0.00	0.00	0.00	0.00	0.00	0.03	0.72
Dinoflagellates	0.69	0.00	0.00	0.00	0.00	0.00	0.00	0.00
Cryptophytes	0.00	0.00	0.00	0.00	0.00	0.31	0.00	0.00
Haptophytes1	0.00	0.01	0.23	0.52	0.18	0.00	0.00	0.00
Pelagophytes	0.00	0.20	0.15	0.25	0.14	0.00	0.00	0.00
Diatoms	0.00	0.00	0.65	0.00	0.00	0.00	0.00	0.00

[1] Peridinin (Per), 19-Butanoyloxyfucoxanthin (19-But), 19-Hexanoyloxyfucoxanthin (19-Hex), Fucoxanthin (Fuco), Alloxanthin (Allo), Violaxanthin (Viola), Chlorophyll b (Chl b)

[2] RMS Error = 0.051

[3] RMS Error = 0.103

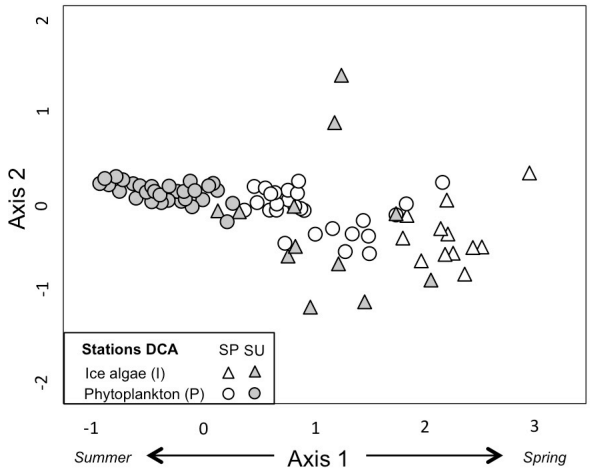

A5 Detrended correspondence analysis (DCA) including a Station DCA (site x taxa) of spring (open symbols) and summer (closed symbols) ice algal (triangles) and phytoplankton (circles) communities.

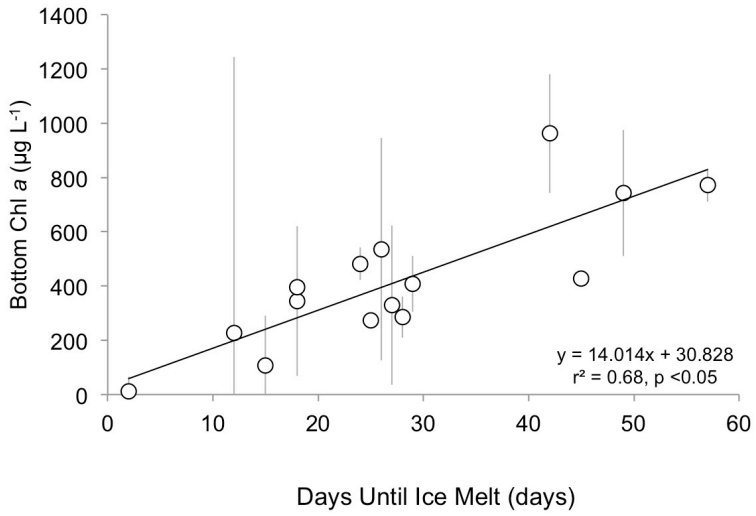

A6 Relationship between bottom ice chl *a* (µg L^{-1}) ± standard error versus days until ice melt (days) for spring (SUBICE, white circles).

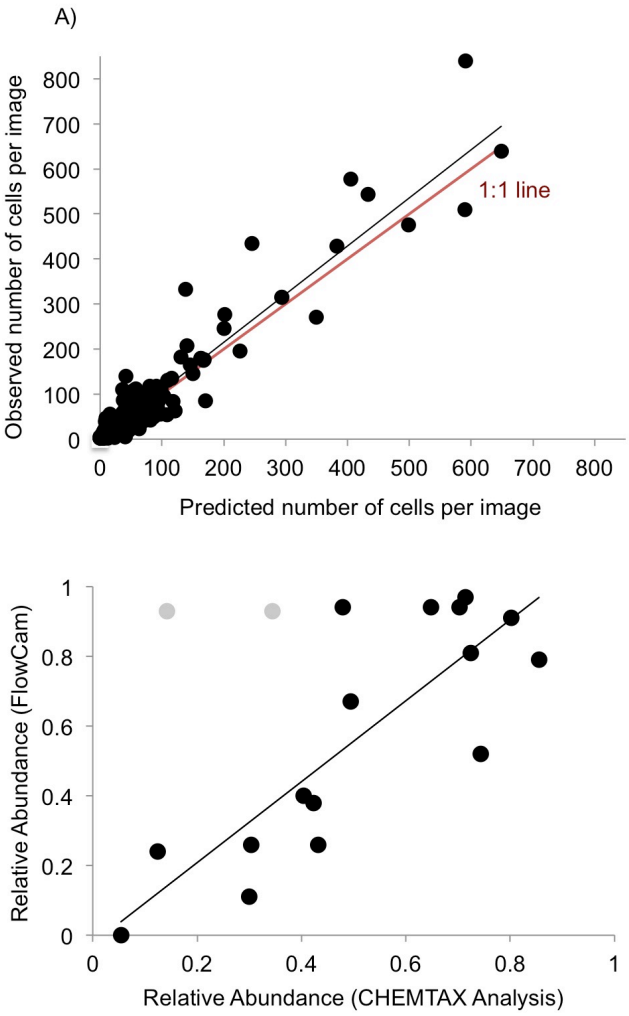

A7. Evaluation of methods to calculate relative abundance of *Phaeocystis antarctica* in ice algal communities: (A) Predicted versus observed *P. antarctica* cells per image in FlowCam test data set ($y = 1.07x + 1.41$, $R^2 = 0.91$, $p < 0.001$) and (B) Agreement between relative abundance estimates from FlowCam analysis and CHEMTAX analysis for *P. antarctica* (black circles, outliers in gray; $y = 1.16x - 0.02$, $R^2 = 0.69$).

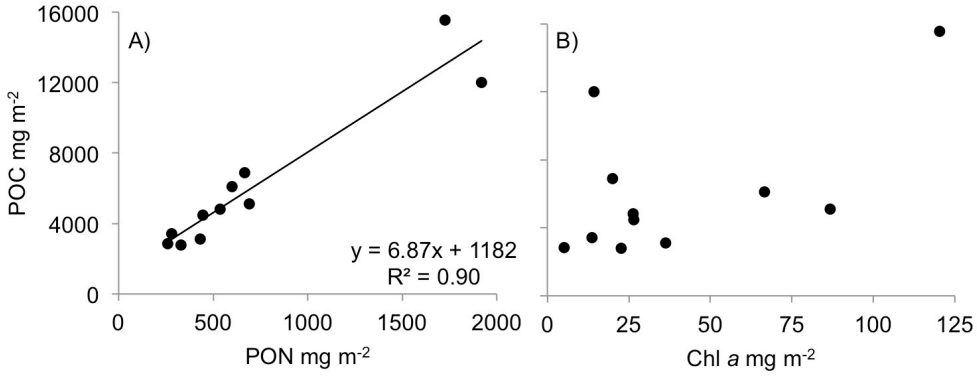

A8. Relationship between different proxies for biomass in sea ice (mg m^{-2}): (A) particulate organic carbon (POC) versus particulate organic nitrogen and (B) POC versus Chl *a.*

Bibliography

Ackley SF, Sullivan CW. 1994. Physical controls on the development and characteristics of Antarctic sea ice bio- logical communities — a review and synthesis. *Deep Sea Res I* 41:1583–1604

Ackley SF, Lewis MJ, Fritsen CH, Xie H. 2008. Internal melting in Antarctic sea ice: development of 'gap layers'. *Geophys Res Lett* 35:L11503

Alexander V. 1980. Interrelationships Between the Seasonal Sea Ice and Biological Regimes. *Cold Reg Sci Technol.* 2: 157–78. doi:10.1017/CBO9781107415324.004.

Alexander V and Chapman T 1981. The Role of Epontic Algal Communities in Bering Sea Ice, p. 773-80. In D.W. Hood and J.A. Calder (eds.), The Eastern Bering Sea Shelf: Oceanography and Resources II. University of Washington Press.

Alou-Font E, Mundy CJ, Roy S, Gosselin M, and Agusti S. 2013. Snow Cover Affects Ice Algal Pigment Composition in the Coastal Arctic Ocean during Spring. *Mar Ecol Prog Ser.* 474: 89–104. doi:10.3354/meps10107.

Álvarez E, López-Urrutia Á, Nogueira E. 2012. Improvement of plankton biovolume estimates derived from image-based automatic sampling devices: application to FlowCAM. *J Plankton Res* 34:454-469.

Ambrose WG Jr. and Renaud PE. 1997. Does a pulsed food supply to the benthos affect polychaete recruitment patterns in the Northeast Water Polynya? Journal of Marine Systems 10, 483-495.

Ambrose WG, Quillfeldt CV, Clough LM, Tilney PVR, and Tucker T. 2005. The Sub-Ice Algal Community in the Chukchi Sea: Large- and Small-Scale Patterns of Abundance Based on Images from a Remotely Operated Vehicle. *Polar Biol.* 28: 784–95. doi:10.1007/s00300-005-0002-8.

Annett AL, Carson DS, Crosta X, Clarke A, Ganeshram RS. 2010. Seasonal progression of diatom assemblages in surface waters of Ryder Bay, Antarctica. *Polar biol 33*:13-29.

Apollonio, S. 1965. Chlorophyll in Arctic Sea Ice. *Arctic.* 18: 118–22.

Arrigo KR, Sullivan CW, Kremer JN. 1991. A bio-optical model of Antarctic Sea Ice. Journal of Geophys Res 96: 10581-10592.

Arrigo KR, Kremer JN, and Sullivan CW. 1993. A simulated Antarctic Fast Ice Ecosystem. *Journal of Geophysical Research*. 98: 6929-6946.

Arrigo KR, and Sullivan CW. 1994. A high resolution bio-optical model of microalgal growth: Tests using sea-ice algal community time-series data. *Limnol. Oceanogr.* 39: 609-631.

Arrigo KR, Robinson DH, Worthen DL, Dunbar RB, DiTullio GR, VanWoert M, Lizotte M.

1999. Phytoplankton community structure and the drawdown of nutrients and CO_2 in the Southern Ocean. *Science* 283: 365-367.

Arrigo KR, Robinson DH, Dunbar RB, Leventer AR, Lizotte MP. 2003. Physical control of chlorophyll *a*, POC, and TPN distributions in the pack ice of the Ross Sea, Antarctica. *J Geophys Res* 108: 3316.

Arrigo KR, Thomas DN. 2004. Large-scale importance of sea ice biology in the Southern Ocean. *Antarct Sci* 16:471-486.

Arrigo KR, Mock T, and M. P. Lizotte. 2009. Primary Producers and Sea Ice, p. 283-325. In D. N. Thomas and G. S. Dieckmann (eds.), Sea Ice. Wiley-Blackwell.

Arrigo KR, Mills MM, Kropuenske LR, van Dijken GL, Alderkamp AC, and Robinson DH. 2010. Photophysiology in Two Major Southern Ocean Phytoplankton Taxa: Photosynthesis and Growth of Phaeocystis Antarctica and Fragilariopsis Cylindrus under Different Irradiance Levels. *Integr Comp Biol.* 50: 950–66, doi:10.1093/icb/icq021.

Arrigo KR. and others. 2012. Massive phytoplankton blooms under Arctic sea ice. *Science*. 336, 1408.

Arrigo KR. 2013. The Changing Arctic Ocean. *Elementa: Science of the Anthropocene* 1: 000010, doi:10.12952/journal.elementa.000010.

Arrigo KR and others. 2014. Phytoplankton Blooms beneath the Sea Ice in the Chukchi Sea. *Deep-Sea Res Pt II.* 105: 1–16, doi:10.1016/j.dsr2.2014.03.018.

Arrigo KR, Mills MM, van Dijken GL, Lowry KE, Pickart RS, Schlitzer R. 2017. Late spring nitrate distributions beneath the ice-covered Chukchi Shelf. *Journal of Geophysical Research Biogeosciences*, doi:10.1002/2017JG003881.

Arrigo KR, Van Dijken GL, Alderkamp AC, Erikson ZK and others. 2017. Early spring phytoplankton dynamics in the western Antarctic Peninsula. *J Geophys Res Oceans* 122

Becquevort S, Smith WO. 2001. Aggregation, sedimentation and biodegradability of phytoplankton-derived material during spring in the Ross Sea, Antarctica. *Deep Sea Res II* 48: 4155-4178.

Belchansky GI, Douglas DC, Alpatsky IV, Platonov NG, et al. 2004. Duration of the Arctic sea ice melt season: Regional and interannual variability, 1979–2001, *J. Clim.*, 17, 67–80.

Bengtsson L, Hodges KI, Koumoutsaris S, Zahn M and Keenlyside N. 2011. The changing atmospheric water cycle in Polar Regions in a warmer climate. *Tellus A*, 63: 907–920.

Bergmann MA, Welch HE, Butler-Walker JE, and Siferd TD. 1991. Ice Algal Photosynthesis at Resolute and Saqvaqjuac in the Canadian Arctic. *Journal Marine Syst.* 2: 43–52,

doi:10.1016/0924-7963(91)90012-J.

Bernard KS, Steinberg DK, Schofield OME. 2012. Summertime grazing impact of dominant macrozooplankton off the western Antarctic Peninsula, *Deep Sea Res A, Oceanogr Res Pap* 62: 111-122.

Bienfang PK. 1981. SETCOL – A technologically simple and reliable method for measuring phytoplankton sinking rates. *Can J. Fish. Aquat. Sci.* 38:1289-1294.

Bintanja R and Selton FM. 2014. Future increases in Arctic precipitation linked to local evaporation and sea-ice retreat. Nature, 509: 479 – 482.

Booth JA. 1984. The Epontic Algal Community of the Ice Edge Zone and Its Significance to the Davis Strait Ecosystem. *Arctic* 37: 234–43. doi:10.1063/1.463189.

Boyd PW, Robinson C, Savidge G, LeB Williams PJ. 1995. Water column and sea-ice primary production during Austral spring in the Bellingshausen Sea. *Deep-Sea Res II* 42: 1177-1200.

Brandini FP and Baumann MEM. 1997. The Potential Role of Melted Brown Ice as Sources of Chelators and Ammonia to the Surface Waters of the Weddell Sea, Antarctica. *Proc. NIPR Symp. Polar Biol.* 10: 1–13.

Briegleb BP, and Light B. 2007. A Delta-Eddington Multiple Scattering Parameterization for Solar Radiation in the Sea Ice Component of the Community Climate System Model. NCAR Technical Note NCAR/TN-472+STR, doi:10.5065/D6B27S71

Campbell K, Mundy CJ, Barber DG, and Gosselin M. 2015. Characterizing the Sea Ice Algae Chlorophyll a-Snow Depth Relationship over Arctic Spring Melt Using Transmitted Irradiance. *J of Marine Syst.* 147: 76–84, doi:10.1016/j.jmarsys.2014.01.008.

Carey AG, and Boudrias MA. 1987. Feeding Ecology of *Pseudalibrotus* (=Onisimus) *Litoralis Kryer* (Crustacea: Amphipoda) on the Beaufort Sea Inner Continental Shelf. *Polar Biol.* 8: 29–33, doi:10.1007/BF00297161.

Connell PE, Michel C, Meisterhans G, Arrigo KR, Caron DA (in revision) Phytoplankton and bacterial dynamics on the Chukchi Sea Shelf during the spring-summer transition. Submitted to *Mar. Ecol. Prog. Ser*.

Conover RJ, Mumm N, Bruecker P, and MacKenzie S. 1999. Sources of Urea in Arctic Seas: Seasonal Fast Ice. *Mar Ecol Prog Ser.* 179: 55–69.

Cota GF, Prinsenberg SJ, Bennet EB, Loder JW, Lewis MR, Anning JL, Watson NHF, and Harris LR. 1987. Nutrient Fluxes During Extended Blooms of Arctic Ice Algae. *J Geophys Res.* 92: 1951–1962.

Cota GF, and Horne EPW. 1989. Physical Control of Arctic Ice Algal Production. *Mar Ecol Prog*

Ser. 52: 111–21, doi:10.3354/meps052111.

Cota GF, Anning JL, Harris LR, Harrison WG, and Smith REH. 1990. Impact of Ice Algae on Inorganic Nutrients in Seawater and Sea Ice in Barrow Strait, NWT, Canada during Spring. *Can J Fish Aquat Sci.* 47:1402–1415.

Cota GF, Legendre L, Gosselin M, and Ingram RG. 1991. Ecology of Bottom Ice Algae: I. Environmental Controls and Variability. *J of Marine Syst.* 2: 257–77, doi:10.1016/0924-7963(91)90036-T.

Cota GF, and Smith REH. 1991. Ecology of Bottom Ice Algae: II. Dynamics, Distributions and Productivity. *J Marine Syst.* 2: 279–95, doi:10.1016/0924-7963(91)90037-U.

Croft MV, and Chow-Fraser P. 2007. Use and Devolopement of the Wetland Macrophyte Index to Detect Water Quality Impairment in Fish Habitat of Great Lakes Coastal Marshes. *J Great Lakes Res.* 33:172-197, doi: http://dx.doi.org/10.3394/0380-1330(2007)33[172:UADOTW]2.0.CO;2

Cullen JJ, and MacIntyre JG. 1998. Behavior, physiology, and the niche of depth-regulating phytoplankton. In Anderson DM, Cembella AD, Hallegraeff GM (eds) Physiological Ecology of Harmful Algal Blooms. Springer-Verlag.

Cullen JJ, and Davis RF. 2003. The Blank Can Make a Big Difference in Oceanographic Measurements. *Limnol and Oceanogr.* 12: 29–35. http://citeseerx.ist.psu.edu/viewdoc/summary?doi=10.1.1.134.2271.

Daly KL, and Macaulay MC. 1988. Abundance and distribution of krill in the ice edge zone of the Weddell Sea, austral spring 1983. *Deep Sea Res A, Oceanogr Res Pap* 35: 21-41.

Daly KL. 1990. Overwintering development, growth, and feeding of larval *Euphausia superba* in the Antarctic marginal ice zone. *Limnol. and Oceanogr.* 35: 1564-1576.

Deal C, Jin M, Elliot S, Hunke E, Maltrud M, and Jeffrey N. 2011. Large-scale modeling of primary production and ice algal biomass within arctic sea ice in 1992. *Journal of Geophysical Research*, 116: C07004.

Dinniman MS, Klinck JM. 2004. A model study of circulation and cross-shelf exchange on the west Antarctic Peninsula continental shelf. *Deep Sea Research Part II: Topical Studies in Oceanography*, 51: 2003-2022.

Dinniman MS, Klinck JM, Smith WO. 2011. A model study of Circumpolar Deep Water on the West Antarctic Peninsula and Ross Sea continental shelves. *Deep Research II*, 58, 1508-1523.

DiTullio GR, Grebmeier JM, Arrigo KR, Lizotte MP, Robinson DH, Leventer A, Barry JP,

VanWoert ML, Dunbar RB. 2000. Rapid and early export of Phaeocystis Antarctica blooms in the Ross Sea, Antarctica. *Nature* 404:595 - 597

DiTullio GR, Garcia N, Riseman SF, Sedwick PN. 2007. Effects of iron concentration on pigment composition in *Phaeocystis antarctica* grown at low irradiance. *Biogeochemistry* 83: 71-81.

Duarte P, Meyer A, Olsen LM, Kauko HM, Assmy P, Rosel A, Itkin P, Hudson SR, Granskog MA, Gerland S, Sundfjord A, Steen H, Hop H, Cohen L, Peterson AK, Jeffery N, Elliot SM, Hunke EC, and Turner AK. 2017. Sea ice thermohaline dynamics and biogeochemistry in the Arctic Ocean: Empirical and model results. *JGR: Biogeosciences,* 122:1632-1654.

Dupont F. 2012. Impact of sea-ice biology on overall primary production in a biophysical model of the pan-Arctic Ocean, *J. Geophys. Res*., 117, C00D17, doi:10.1029/2011JC006983.

Ducklow HW, Baker K, Martinson DG, Quetin LB, Ross RM, Smith RC, Stammerjohn SE, Vernet M, Fraser W. 2007. Marine pelagic ecosystems: the West Antarctic Peninsula. *Phil. Trans. R. Soc. B* 362: 67-94.

Ducklow HW, Clarke A, Dickhut R, Doney SC, Geisz H, Huang K, Martinson DG, Meredith MP, Moeller HV, Montes-Hugo M, Schofield O, Stammerjohn SE, Steinberg D, Fraser W. 2012. The Marine System of the Antarctic Peninsula. In Rogers AD, Johnston NM, Murphy EJ, Clarke A (eds), Antarctic Ecosystems: An extreme environment in a changing world. Blackwell Publishing.

Ducklow HW, Fraser WR, Meredith MP, Stammerjohn SE, Doney SC, Martinson DG, Sailley SF, Schofield OM, Steinberg DK, Venables HJ, and Amsler CD. 2013. West Antarctic Peninsula: An ice-dependent coastal marine ecosystem in transition. *Oceanography* 26: 190 – 203.

Dunton KH, Goodall JL, Schonberg SV, Grebmeier JM, and Maidment DR. 2005. Multi-Decadal Synthesis of Benthic-Pelagic Coupling in the Western Arctic: Role of Cross-Shelf Advective Processes. *Deep-Sea Res Pt II.* 52: 3462–77, doi:10.1016/j.dsr2.2005.09.007.

Durbin EG, and MC Casas. 2013. Early Reproduction by Calanus Glacialis in the Northern Bering Sea: The Role of Ice Algae as Revealed by Molecular Analysis. *J Plankton Res* 36: 523–541, doi:10.1093/plankt/fbt121.

Ebert EE, Schramm JL, and Curry JA. 1995. Disposition of Solar Radiation in Sea Ice and the Upper Ocean. *J Geophys Res*. 100: 15965-15975, doi: 10.1029/95JC01672.

Fritsen CH, Ackley SF, Kremer JN, Sullivan CW. 1998. Flood-freeze cycles and

microalgal dynamics in Antarctic pack ice. *Antarct Res Ser* 73: 1-21.

Fritsen CH, Coale S, Neenan D, Gibson A, Garrison D. 2001. Biomass, production and microhabitat characteristics near the freeboard of ice floes in the Ross Sea, Antarctica, during the austral summer. *Ann Glaciol* 33:280-286.

Fritsen CH, Wirthlin ED, Momberg DK, Lewis MJ, Ackley SF. 2011. Bio-optical properties of Antarctic pack ice in the early austral spring. *Deep-Sea Res II* 58: 1052-1061.

Fortier M, Fortier L, Michel C, and Legendre L. 2002. Climatic and Biological Forcing of the Vertical Flux of Biogenic Particles under Seasonal Arctic Sea Ice. *Mar Ecol Prog Ser.* 225: 1–16, doi:10.3354/meps225001.

Gaebler-Swartz S, Davidson A, Assmy P, Chen J, Henjes J, Nothig E-M, Lunau M, Medlin L. 2015. A new cell stage in the haploid-diploid life cycle of the colony-forming haptophyte *Phaeocystis antarctica* and its ecological implications. *J Phycol* 46:1006-1016

Gaebler-Swartz S, Medlin LK, Leese F. 2015. A puzzle with many pieces: the genetic structure and diversity of Phaeocystis Antarctica Karsten (Prymnesiophyta). *Eur J Phycol* 50:112-124.

Galindo V. and others. 2014. Biological and Physical Processes Influencing Sea Ice, Under-Ice Algae, and Dimethylsulfoniopropionate during Spring in the Canadian Arctic Archipelago. *J Geophys Res-Oceans.* 119: 3746–66, doi:10.1002/2013JC009497.

Garribotti IA, Vernet M, Kozlowski WA, Ferrario ME. 2003. Composition and biomass of phytoplankton assemblages in coastal Antarctic waters: a comparison of chemotaxonomic and microscopic analyses. *Mar Ecol Prog Ser*. 247:27-42.

Garribotti IA, Vernet M, Ferrario ME, Smith RC, Ross RM, Quetin LB. 2003. Phytoplankton spatial distribution patterns along the western Antarctic Peninsula (Southern Ocean). *Mar Ecol Prog Ser.* 261: 21-39.

Garribotti IA, Vernet M, Ferrario M. 2005. Annually recurrent phytoplanktonic assemblages during summer in the seasonal ice zone west of the Antarctic Peninsula (Southern Ocean). *Deep-Sea Res I*. 52: 1823-1841.

Garribotti IA, Vernet M, Smith RC, Ferrario ME. YEAR Interannual variability in the distribution of the phytoplankton standing stock across the seasonal sea-ice zone west of the Antarctic Peninsula. *Journal of Plankton Research*, Volume 27, Issue 8, 1 August 2005, Pages 825–843, https://doi.org/10.1093/plankt/fbi056

Garrison DL, Ackley SF, and Buck KR. 1983. A Physical Mechanism for Establishing Algal Populations. *Nature.* 306: 363–65.

Garrison DL, Buck KR, Fryxell GA. 1987. Algal assemblages in Antarctic pack ice and in ice-edge plankton. *J. Phycol* 23: 564-572.

Garrison DL, and Buck KR. 1989. The Biota of the Antarctic Pack Ice in the Weddell Sea and Antarctic Peninsula Regions. *Polar Biol*, 10: 211-219.

Geider RJ, MacIntyre HL, Kana TM. 1997. Dynamic model of phytoplankton growth and acclimation: responses of the balanced growth rate and chlorophyll *a*: carbon ratio to light, nutrient-limitation and temperature. *Mar Ecol Prog Ser* 148:187-200.

Geisenhagen HC, Detmer AE, de Wall J, Weber A, Gradinger RR, Jochem FJ. 1999. How are Antarctic planktonic microbial foodwebs and algal blooms affected by melting sea ice? Microcosm simulations. *Acquat Microb Ecol*, 20:183-201.

Gradinger R, Spindler M, and Henschel D. 1991. Development of Arctic Sea-Ice Organisms under Graded Snow Cover. *Polar Res.* 10: 295–307. doi:10.1111/j.1751-8369.1991.tb00655.x.

Gradinger R. 1995. Climate change and biological oceanography of the Arctic Ocean. Philosophical Transactions of the Royal Society of London Series A 352, 277-286.

Gradinger R, and Ikävalko J. 1998. Organism Incorporation into Newly Forming Arctic Sea Ice in the Greenland Sea. *J Plankton Res.* 20: 871–86, doi:10.1093/plankt/20.5.871.

Gradinger, R. 1999. Vertical fine structure of algal biomass and composition in Arctic pack ice. Mar Biol 133: 745-754.

Gradinger, R, Friedrich, D and Spindler, M. 1999. Abundance, biomass and composition of the sea ice biota of the Greenland Sea pack ice. *Deep Sea Res II* 46: 1457–1472. DOI: https://doi.org/10.1016/ S0967-0645(99)00030-2.

Gradinger, R. 2009. Sea-Ice Algae: Major Contributors to Primary Production and Algal Biomass in the Chukchi and Beaufort Seas during May/June 2002. *Deep-Sea Res Pt II:* 56: 1201–12, doi:10.1016/j.dsr2.2008.10.016.

Grainger EF. 1977. The Annual Nutrient Cycle in Sea Ice, p. 285-299. In M.J. Dunbar (ed.), *Polar Oceans*. The Arctic Institute of North America.

Grebmeier JM, Cooper LW, Feder HM, and Sirenko BI. 2006. Ecosystem Dynamics of the Pacific-Influenced Northern Bering and Chukchi Seas in the Amerasian Arctic. *Prog Oceanogr.* 71: 331–61, doi:10.1016/j.pocean.2006.10.001.

Grebmeier JM, Cooper LW, Moore SE. 2016. The Bering Strait Region: A Window into Changing Benthic Populations in Response to Varying Subarctic-Arctic Connectivity and Ecosystem Dynamics. American Geophysical Union, Ocean Sciences Meeting #HE41A-07.

Grebmeier JM., Bluhm BA, Cooper LW, Denisenko SG, Iken K, Kędra M, and Serratos C. 2015. Time-series benthic community composition and biomass and associated environmental characteristics in the Chukchi Sea during the RUSALCA 2004–2012 Program. *Oceanography* 28(3):116–133, http://dx.doi.org/10.5670/ oceanog.2015.61.

Gregg WW, and Carder KL. 1990. A simple spectral solar irradiance model for cloudless maritime atmospheres, *Limnol. Oceanogr*., 35,1657– 1675.

Grenfell TC, and Maykut GA. 1977. The Optical Properties of Snow in the Arctic Basin. *Journal of Glaciology*. 18:445-463, doi: https://doi.org/10.3198/1977JoG18-80-445-463

Gosselin M, Legendre L, Demers S, and Ingram RG. 1985. Responses of Sea-Ice Microalgae to Climatic and Fortnightly Tidal Energy Inputs (Manitounuk Sound, Hudson Bay). *Can J Fish and Aquat Sci*. 42:999-1006, doi: 10.1139/f85-125.

Gosselin M, Legendre L, Therriault J-C, Demers S, and Rochet M. 1986. Physical Control of the Horizontal Patchiness of Sea-Ice Microalgae. *Mar Ecol Prog Ser.* 29: 289–98, doi:10.3354/Meps029289.

Gosselin M, Legendre L, Therriault J-C, and Demers S. 1990. Light and Nutrient Limitation of Sea-Ice Microalgae (Hudson Bay, Canadian Arctic). *J Phycol*. 26:220-232, doi:10.1016/S0198-0254(06)80482-6.

Gosselin M, Levasseur M, Wheeler PA, Horner RA, Booth BC. 1997. New measurements of phytoplankton and ice algal production in the Arctic Ocean. *Deep-Sea Res PT II*. 44: 1623-1644.

Guglielmo L, Carrada GC, Catalano G, Dell'Anno A, Fabiano M, Lazzara L, Mangoni O, Pusceddu A, Saggiomo V. 2000. Structural and functional properties of sympagic communities in the annual sea ice at Terra Nova Bay (Ross Sea, Antarctica), *Polar Biol*, 23:137-146.

Haas C*,* Pfaffling A*,* Hendricks S*,* Rabenstein L*,* Etienne J-L*, and* Rigor I. 2008. Reduced Ice Thickness in Arctic Transpolar Drift Favors Rapid Ice Retreat*, Geophys. Res. Lett.* 35*: L17501, doi:*10.1029/2008GL034457.

Haberman KL, Ross RM, Quetin LB. 1993. Palmer LTER: Grazing by the antarctic krill *Euphausia superba* on *Nitzschia sp*. and *Phaeocystis sp*. monocultures*, Antarct. JUS* 28: 217-219.

Haberman KL, Ross RM, Quetin LB, Vernet M, Nevitt GA, Kozlowski W. 2002. Grazing by Antarctic krill *Euphausia superba* on *Phaeocystis antarctica*: an immunochemical approach. *Mar Ecol Prog Ser* 241: 139-149.

Haberman KL, Ross RM, Quetin LB. 2003. Diet of the Antarctic krill (*Euphausia superba* Dana): II. Selective grazing in mixed phytoplankton assemblages. *J Exp Mar Biol Ecol* 283: 97-113.

Hayashida H, Steiner N, Monahan A, Galindo V, Lizotte M, and Levasseur M. 2017. Implications of sea-ice biogeochemistry for oceanic production and emissions of dimethyl sulfide in the Arctic, *Biogeosciences*, 14: 3129 – 3155.

Hansen B, Verity P, Falkenhaug T, Tande KS, Norrbin F. 1994. On the trophic fate of Phaeocystis pouchetti (Harriot). V. Trophic relationships between Phaeocystis and zooplankton: an assessment of methods and size dependence. *J Plankton Res* 16: 487-511.

Hameedi, M. J. 1978. Aspects of Water Column Primary Productivity in the Chukchi Sea During Summer. *Mar Biol.* 46: 37–46.

Hegseth, EN. 1992. Sub-ice algal assemblages of the Barents Sea – species composition, chemical composition, and growth rates. *Polar Biol* 12: 485–496. DOI: https://doi.org/10.1007/BF00238187

Hezel PJ, Zhang X, Bitz CM, Kelly BP, and Massonnet F. 2012. Projected decline in spring snow depth on Arctic sea ice caused by progressively later autumn open ocean freeze-up this century, *Geophys. Res. Lett.,* 39*, L17505, doi:*10.1029/2012GL052794.

Holm-Hansen O, Lorenzen CJ, Holmes RW, and Strickland JDH. 1965. Fluorometric Determination of Chlorophyll. *ICES J Mar Sci.* 30: 3-15, doi:10.1093/icesjms/30.1.3.

Horner RA, and Alexander V. 1972. Algal Populations in Arctic Sea Ice : An Investigation of Heterotrophy. *Limnol and Oceanogr.* 17: 454-58, doi:10.4319/lo.1972.17.3.0454.

Horner RA. 1982. Do Ice Algae Produce the Spring Phytoplankton Bloom in Seasonally Ice-covered Waters. *In 7th International Diatom-Symposium,* 401-409.

Horner RA, and Schrader GC. 1982. Relative Contributions of Ice Algae, Phytoplankton, and Benthic Microalgae to Primary Production in Nearshore Regions of the Beaufort Sea. *Arctic.* 35: 485-503, doi:10.14430/arctic2356.

Horner RA and others. 1992. Ecology of Sea Ice Biota. *Polar Biol.* 12: 417–27.

Horner RA. 1996. Ice Algal Investigations: Historical Perspective. *Proceedings of the NIPR Symposium- Polar Biol.* 9:1-12.

Horvat C, Jones DR, Iams S, Schroeder D, Flocco D, Felham D. 2017. The frequency and extent of sub ice phytoplankton blooms in the Arctic Ocean. *Science Advances*, *3:e1601191.*

Jackobsen HH, Carstensen J. 2011. FlowCAM: Sizing cells and understanding the impact

of size distributions on biovolume of planktonic community structure, *Aquat Microb Ecol* 65: 75-87.

Jeffries MO, Morris K, Weeks WF, and Worby AP. 1997. Seasonal variations in the properties and structural composition of sea ice and snow cover in the Bellinghausen and Amundsen Seas, Antarctica. *J Glaciol* 43:138-151.

Ji R, Jin M, Varpe O. 2013. Sea ice phenology and timing of primary production pulses in the Arctic Ocean. *Global Change Biology*, 19: 734 – 741.

Jin M, Deal CJ, Wang J, Shin K-H, Tanaka N, Whitledge TE, Lee SH, and Gradinger R. 2006. Controls of the land fast ice-ocean ecosystem offshore Barrow, Alaska. *Attn. Glaciol*, 44: 63 – 72.

Jin M, Deal CJ, Wang J, Alexander V, Gradinger R, Saitoh S, Lida T, Wan Z, and Stabeno P. 2007. Ice-associated phytoplankton blooms in the southeastern Bering Sea, *Geophys Res Lett*, 34: L06612.

Jin M, Deal C, Lee SH, Elliot S, Hunke E, Maltrud M, and Jeffrey N. 2012. Investigation of Arctic sea ice and ocean primary production for the period 1992 – 2007 using a 3-D global ice-ocean ecosystem model. *Deep-Sea Res II*, 81-84: 28-35.

Johnson TO, and Smith Jr WO. 1986. Sinking rates of phytoplankton assemblages in the Weddell Sea marginal ice zone. *Mar Ecol Prog Ser* 33: 131-137.

Juhl AR, and Krembs C. 2010. Effects of snow removal and algal photoacclimation on growth and export of ice algae. *Polar Biol*. 33: 1057–1065. doi:10.1007/s00300-010- 0784-1.

Kattner G, Thomas DN, Haas C, Kennedy H, Dieckmann GS. 2004. Surface ice and gap layers in Antarctic sea ice: highly productive habitats. *Mar. Ecol. Prog. Ser.* 277: 1-12.

Kavanaugh, MT, Abdala FN, Ducklow HW, Glover DM, Fraser WR, Martinson DG, Stammerjohn SE, Schoefeild OME, Doney SC. 2015. Effect of continental shelf canyons on phytoplankton biomass and community composition along the western Antarctic Peninsula, *Marine Ecological Progress Series,* 524, 11-26.

Kędra M, Moritz C, Choy ES, David C, Degen R, Duerksen S, Ellingsen I, Górska B, Grebmeier JM, Kirievskaya D, and others. 2015. Status and trends in the structure of Arctic benthic food webs. *Polar Research* 34: 23775, http://dx.doi.org/10.3402/polar.v34.23775.

Kirchman DL, Hill V, Cottrell M.T., Gradinger R., Malmstrom R.R., and Parker A. 2009. Standing Stocks, Production, and Respiration of Phytoplankton and Heterotrophic Bacteria in the Western Arctic Ocean. *Deep-Sea Res Pt II*. 56:1237-1248.

Kirst GO and Wiencke C. 1995. Ecophysiology of polar algae. *Journal of Phycology* 31(2): 181–

199. DOI: https://doi.org/10.1111/j.0022-3646.1995.00181.x

Kolber ZS, Prasil O, and Falkowski PG. 1998. Measurements of Variable Chlorophyll Fluorescence Using Fast Repetition Rate Techniques: Defining Methodology and Experimental Protocols. *BBA - Bioenergetics* 1367: 88-106. doi:10.1016/S0005-2728(98)00135-2.

Kottmeier ST, Grossi SM, Sullivan CW. 1987. Sea ice microbial communities VIII. Bacterial production in annual sea ice of McMurdo Sound, Antarctica. *Mar. Ecol. Prog. Se*r. 35: 175-186.

Kozlowski WA, Deutschman D, Garibotti I, Trees C, Vernet M (2011) An evaluation of the application of CHEMTAX to Antarctic coastal pigment data. Deep-Sea Res I 58:350−368

Krembs C, Gradinger R, and Spindler M. 2000. Implications of Brine Channel Geometry and Surface Area for the Interaction of Sympagic Organisms in Arctic Sea Ice. *J Exp Mar Biol and Ecol.* 243: 55-80, doi:10.1016/S0022-0981(99)00111-2.

Krembs C, Eicken H, and Deming JW. 2011. Exopolymer Alteration of Physical Properties of Sea Ice and Implications for Ice Habitability and Biogeochemistry in a Warmer Arctic. *P Natl Acad Sci USA.* 108: 3653-58, doi:10.1073/pnas.1100701108.

Kroupenske LR, Mills MM, Van Dijken GL, Bailey S, Robinson DH, Welschmeyer NA, Arrigo KR. 2009. Photophysiology in two major Southern Ocean phytoplankton taxa: Photoprotection in *Phaeocystis antarctica* and Fragilariopsis cylindrus. *Limnol Oceanogr* 54:1176-1196.

Kuosa H, Norrman B, Kivi K, Brandini F. 1992 Effects of Antarctic sea ice biota on seeding as studied in aquarium experiments. *Polar Biology* 12:333-339.

Kwok R, and Rothrock DA. 2009. ″Decline in Arctic sea ice thickness from submarine and ICESat records: 1958–2008. *Geophys. Res. Lett.* 36*: L15501, doi: 1-/1029/2009GL039035.*

Laney SR, and Sosik HM. 2014. Phytoplankton Assemblage Structure in and around a Massive under-Ice Bloom in the Chukchi Sea. *Deep-Sea Res Pt II.* 105: 30-41, doi:10.1016/j.dsr2.2014.03.012.

Lannuzel D, Schoemann V, Dumont I, Content M, De Jong J, Tison J.-L., Delille B, Becquevort S. 2013. Effect of melting Antarctic sea ice on the fate of microbial communities studied in microcosms. *Polar Biol* 36: 1483-1497.

Lavoie D, Denman K, Michel C. 2005. Modeling ice algal growth and decline in a seasonally

ice-covered region of the Arctic (Resolute Passage, Canadian Archipelago). J*ournal of Geophysical Research*, 110:C11009.

Lavoie D, Macdonald RW, and Denman K. 2009. Primary productivity and export fluxes on the Canadian shelf of the Beaufort Sea: A modeling study. *J Mar Syst*, 75: 17-32.

Legendre L, Ingram RG, and Poulin M. 1981. Physical Control of Phytoplankton Production under Sea Ice (Mannitouk Sound. Hudson Bay). *Can J Fish and Aquat Sci* 38: 1385–92.

Legendre L, Ackley SF, Dieckmann GS, Gullicksen B, Horner R, Hoshiai T, Melnikov IA, Reburgh WS, Spindler M, and Sullivan CW. 1992. Evology of sea ice biota: Part 2. Global Significance. Polar Biol, 12: 429 – 444.

Legendre, P. 2015. lmodel2: Model II Regression. R package version 1.7-2

Leu E, Mundy CJ, Assmy A, Campbell K, Gabrielsen TM, Gosselin M, Juul-Pedersen T, and Gradinger R. 2015. Arctic Spring Awakening - Steering Principles behind the Phenology of Vernal Ice Algal Blooms. *Prog Oceanogr.* 139: 151–70, doi:10.1016/j.pocean.2015.07.012.

Lewis MR, and Smith JC. 1983. A Small Volume, Short- Incubation-Time Method for Measurement of Photosynthesis as a Function of Incident Irradiance. *Mar. Ecol. Prog. Ser*. 13: 99–102, doi:10.3354/meps013099.

Light B, Grenfell TC, Perovich DK. 2008. Transmission and absorption of solar radiation by Arctic sea ice during melt season. Journal of Geophysical Research, 113: C03023.

Liu J, Curry JA, Martinson DG. 2004. Interpretation of recent Antarctic sea ice variability. *Geophys Res Lett* 31*: L02205*

Lizotte MP, and Sullivan SW. 1991. Photosynthesis-irradiance relationships in microalgae associated with Antarctic pack ice: evidence for in situ activity. *Mar. Ecol. Prog. Ser.* 71: 175-184.

Lizotte MP. 2001. The contributions of Sea Ice Algae to Antarctic marine primary production. *Amer Zool* 41: 57–73. DOI: https://doi.org/10.1093/icb/41.1.57

Lowry KE, Pickart RS, Selz V, Mills MM, Pacini A, Lewis KM, … Arrigo KR. 2018. Under‐ice phytoplankton blooms inhibited by spring convective mixing in refreezing leads. *Journal of Geophysical Research: Oceans*, 123, 90–109. https://doi.org/10.1002/2016JC012575

Loeb V, Siegel V, Holm-Hansen O, Hewitt R, Fraser W, Trivelpiece W, and Trivelpiece S. 1997. Effects of sea-ice extent and krill or salp dominance on the Antarctic food web. *Nature* 387: 897-900.

Long SP, Humphries S, and Falkowski PG. 1994. Photoinhibition of photosynthesis in nature. *Ann. Rev. Plant Physiol. Plant Mol. Biol.* 45: 633-662.

Loose BA, Miller LA, Elliot S, Papakyriakou T. 2011. Sea ice biogeochemistry and material transport across the frozen interface, *Oceanography*, 24(3), 202-218.

Lovvorn JR, North CA, Kolts JM, Grebmeier JM, Cooper LW, Cui X. 2016. Projecting the effects of climate-driven changes in organic matter supply on benthic food webs in the northern Bering Sea. Mar Ecol Prog Ser 548:11-30. https://doi.org/10.3354/meps11651.

Lowry KE, van Dijken GL, and Arrigo KR. 2014. Evidence of under-ice phytoplankton blooms in the Chukchi Sea from 1998 to 2012. Deep-Sea Res Pt II. 105: 105–117, doi:10.1016/j.dsr2.2014.03.013.

Lowry KE, Pickart RS, Mills MM, Brown ZW, van Dijken GL, Bates NR, and Arrigo KR. 2015. The Influence of Winter Water on Phytoplankton Blooms in the Chukchi Sea. *Deep-Sea Res Pt II.* 118: 53–72, doi:10.1016/j.dsr2.2015.06.006.

Mackey MD, Higgins HW, Mackey DJ, and Wright SW. 1996. CHEMTAX – a program for estimating class abundances from chemical markers: application to HPLC measurements of phytoplankton. *Mar. Ecol. Prog. Ser.* **144:** 265–283.

Mangoni O, Saggiomo M, Modigh M, Catalano G, Zingone A, and Saggiomo V. 2009. The Role of Platelet Ice Microalgae in Seeding Phytoplankton Blooms in Terra Nova Bay (Ross Sea , Antarctica): A Mesocosm Experiment. *Polar Biol.* 32: 311-23, doi:10.1007/s00300-008-0507-z.

Marschall H-P. 1988. The overwintering strategy of Antarctic krill under the pack-ice of the Weddell Sea. *Polar Biol* 9: 129-135.

Marshall GJ, Lagun V, and Lachlan-Cope TA. 2002. Changes in Antarctic Peninsula tropospheric temperatures from 1956 to 1999: a synthesis of observations and reanalysis data. *Int. J. Climatol*. 22: 291–310.

Martinson DG, Stammerjohn SE, Smith RC, Iannuzzi RA. 2008. Palmer, Antarctica, Long-Term Ecological Research program first 12 years: physical oceanography, spatio-temporal variability. *Deep-Sea Res II* 55: 1964-1987.

Maslanik JA, Fowler C, Stroeve J, Drobot S, Zwally J, Yi D, and Emery W. 2007. A Younger, Thinner Arctic Ice Cover: Increased Potential for Rapid, Extensive Sea-Ice Loss. *Geophys. Res. Lett.* 34*: L24501, doi:*10.1029/2007GL032043.

Massom RA, Eicken H, Haas C, Jeffries MO, Drinkwater MR, Sturm M, Worby AP, Wu X, Lytle VI, Ushio S, Morris K, Reid PA, Warren SG, Allison I. 2001. Snow on Antarctic sea ice. *Rev of Geophys.* 39: 413-445.

Massom RA, Stammerjohn SE, Smith RC, Pook MJ, Iannuzzi RA, Adams N, Martinson DG,

Vernet M, Fraser WR, Quetin LB, Ross RM, Massom Y, Krouse HR. 2006. Extreme anomalous atmospheric circulation and its west Antarctic peninsula region in austral spring and summer 2001/02, and its profound impact on sea ice and biota. *J Clim* 19: 3544-3571.

Massom RA, Stammerjohn SE. 2010. Antarctic sea ice change and variability – Physical and ecological implications, *Polar Sci* 4: 149-186.

Mathot S, Smith WO, Carlson C, Garrison DL, Gowing MM, and Vickers CL. 2000. Carbon partitioning within *Phaeocystis antarctica* (prymnesiophyceae) colonies in the Ross Sea, Antarctica. *J. Phycol* 36: 1049-1056.

Maxwell K, and Johnson GN. 2000. Chlorophyll flourescence - a practical guide. *J exp bot*. 51: 659-668. doi: 10.1093/jexbot/51.345.659

Maykut GA. 1985. An Introduction to Ice in the Polar Oceans. Technical Report APL-UW 8510.

McCune B, and Grace JB. 2002. Data transformations, p. 67-89. In B. McCune, J. B. Grace, D. L. Urban (eds.), Analysis of Ecological Communities. MjM.

Meguro H, Ito K, and Fukushima H. 1966. Diatoms and the Ecological Conditions of Their Growth in Sea Ice in the Arctic Ocean. *Science.* 152: 1089–1090. doi:10.1126/science.152.3725.1090.

Meiners KM, Vancoppenolle M, Thanassekos S, Dieckmann GS, Thomas DN, Tison J-L, Arrigo KR, Garrison DL, McMinn A, Lannuzel D, Van Der Merwe P, Swadling KM, Smith Jr WO, Melnikov I, Raymond B. 2012. Chlorophyll a in Antarctic sea ice from historical ice core data, *Geophysical Research Letters*, 39:L21602

Melnikov IA. 1997. The Arctic Ice Ecosystem. Gordon and Breach Science Publishers, Amsterdam.

Menden-Deur S, and Lessard EJ. 2000. Carbon to volume relationships for dinoflagellates, diatoms, and other protest plankton. *Limnol. Oceanogr* 45: 569-579.

Meredith MP, and King JC. 2005. Rapid climate change in the ocean west of the Antarctic Peninsula during the second half of the 20th century. *Geophys Res Lett* 32: L19604

Michel C, Legendre L, Ingram RG, Gosselin M, and Levasseur M. 1996. Carbon budget of sea-ice algae in spring: Evidence of a significant transfer to zooplankton grazers, *J. Geophys Res*, 101:18,345-18,360.

Michel C, Ingram RG, Harris LR. 2006. Variability in oceanographic and ecological processes in the Canadian Arctic Archipelago. *Prog Oceanogr*, 71, 379 – 401.

Miller H, Grobe H. 1996. Die Expedition ANTARKTIS-XI/3 mit FS "Polarstern" 1994, (The

expedition ANTARKTIS-XI/3 of RV "Polarstern" in 1994). Berichte zur Polarforschung (Reports on Polar Research), Bremerhaven, Alfred Wegener Institute for Polar and Marine Research 188: 1-115.

Mills MM, Kropuenske LR, Van Dijken GL, Alderkamp AC, Berg GM, Robinson DH, Welschmeyer NA, Arrigo KR. 2010. Photophysiology in two Southern Ocean phytoplankton taxa: Phaeocystis Antarctica (prymnesiophyceae) and cylindrus (bacillariophyceae) under simulated mixed-layer irradiance. *J. Phycol* 46: 1114-1127.

Mills MM, and others. 2015. Impacts of Low Phytoplankton NO_3^-:PO_4^{3-} Utilization Ratios Over the Chukchi Shelf, Arctic Ocean. *Deep-Sea Res Pt II*. 118: 105-121, doi: http://dx.doi.org/10.1016/j.dsr2.2015.02.007.

Min S-K, Zhang X, and Zwiers F. 2008. Human-Induced Arctic Moistening. *Science*, 320: 518 - 520.

Moisan TA, Olaizola M, Mitchell BG. 1998. Xanthophyll cycling in *Phaeocystis antactica*: changes in cellular fluorescence. *Mar. Ecol. Prog. Ser.* 169: 113-121.

Moisan TA, Mitchell BG. 1999. Photophysiological acclimation of *Phaeocystis antarctica* Karsten under light limitation. *Limnol Oceanogr* 44: 247-258.

Montes-Hugo M, Doney SC, Ducklow HW, Fraser W, Martinson D, Stammerjohn SE, Schofield O. 2009. Recent changes in phytoplankton communities associated with rapid regional climate change along the western Antarctic Peninsula. *Science* 323: 1470

Montes-Hugo M, Vernet M, Martinson D, Smith R, Iannuzzi R. 2008. Variability on phytoplankton size structure in the western Antarctic Peninsula (1997-2006*). Deep-Sea Res II* 55: 2106-2117.

Moore CM, Lucas MI, Sanders R, Davidson R. 2005. Basin-scale variability of phytoplankton bio-optical characteristics in relation to bloom state and community structure in the Northeast Atlantic. *Deep-Sea Res I*. 52: 401-419.

Moore CM, Suggett DJ, Hickman AE, Kim Y-N, Tweddle JF, Sharples J, Geider RJ, Holligan PM. 2006. Phytoplankton accumulation and photoadaptation response to environmental gradients in a shelf sea. *Limnol Oceanogr*. 51: 936-949.

Moran S.B., Lomas M.W., Kelly R.P., Gradinger R., Iken K. & Mathis J.T. 2012. Seasonal succession of net primary productivity, particulate organic carbon export, and auto-trophic community composition in the eastern Bering Sea. Deep-Sea Research Part II: 6570-8497.

Mortenson E, Hayashida H, Steiner N, Monahan A, Blais M, Gale MA, Galindo V, Gosselin M, and others. 2017. A model-based analysis of physical and biological controls on ice algal

and pelagic primary production in Resolute Passage. *Elem Sci Anth,* 5: 39, DOI: https://doi.org/10.1525/elementa.229

Mundy CJ, Ehn JK, Barber DG, and Michel C. 2007. Influence of Snow Cover and Algae on the Spectral Dependence of Transmitted Irradiance Through Arctic Landfast First-Year Sea Ice. *J Geophys Res-Oceans*. 112: *C03007*, doi: 10.1029/2006JC003683

Mundy CJ, Gosselin M, Gratton Y, Brown K, Galindo V, Campbell K, Levasseur M, Barber D, Papakyriakou T, Bélanger S. 2014. Role of environmental factors on phytoplankton bloom initiation under landfast sea ice in Resolute Passage, Canada. *Marine Ecology Progress Series*, 497, 39-49.

Murchie EH, and Lawson T. 2013. Chlorophyll fluorescence analysis: a guide to good practices and understanding some new applications. *J Exp Bot* 64: 3983 - 3998.

Nelson DM, and Gordon LI. 1982. Production and Pelagic Dissolution of Biogenic Silica in the Southern Ocean. *Geochim Cosmochim Ac.* 46: 491–501.

Nicolaus M, Katlein C, Maslanik J, Hendricks S. 2012. Changes in Arctic sea ice result in increasing light transmittance and absorption, *Geophysical Research Letters,* 39*, L24501, doi:*10.1029/2012GL053738.

Niemi A, Michel C, Hille K, and Poulin M. 2011. Protist Assemblages in Winter Sea Ice: Setting the Stage for the Spring Ice Algal Bloom. *Polar Biol.* 34: 1803-1817, doi:10.1007/s00300-011-1059-1.

Oksanen, J. and others. 2016. vegan: Community Ecology Package. R package version 2.4-1.

Olson RJ, and Sosik HM. 2007. A Submersible Imaging-in-Flow Instrument to Analyze Nano- and Microplankton: Imaging FlowCytobot. *Limnol and Oceanogr-Methods* 5: 195-203, doi:10.4319/lom.2007.5.195.

Palmer MA, Saenz BT, Arrigo KR. 2014. Impacts of sea ice retreat, thinning, and melt pond proliferation on the phytoplankton bloom in the Chukchi Sea, Arctic Ocean, *Deep Sea Research II,* 105, 85-104.

Peperzak L, Colijn F, Koeman R, Gieskes WWC, Joordens JCA. 2003 Phytoplankton sinking rates in the Rhine region of freshwater influence. *J Plankton Res.* 25: 365–383.

Perovich DK, Elder BC, Claffey KJ, Stammerjohn S, Smith R, Ackley SF, Krouse HR, Gow AJ. 2004. Winter sea-ice properties in Marguerite Bay, Antarctica. *Deep Sea Res II* 51: 2023-2039.

Perovich DK, Polashenski C. 2012. Albedo evolution of seasonal Arctic sea ice, *Geophysical Research Letters*, *39*, L08501, doi*:*10.1029/2012GL051432.

Petrou K, Doblin MA, and Ralph PJ. 2011. Heterogeneity in the Photoprotective Capacity of

Three Antarctic Diatoms during Short-Term Changes in Salinity and Temperature. *Mar Biol.* 158: 1029–1041, doi:10.1007/s00227-011-1628-4.

Platt T, Gallegos CL, and Harrison WG. 1980. Photoinhibition of photosynthesis in natural assemblages of marine phytoplankton. *J Mar Res*. 38: 103-111.

Pogson L*,* Tremblay B*,* Lavoie D*,* Michel C*,* and Vancoppenolle M. 2011. Development and validation of a one-dimensional snow-ice algae model against observations in Resolute Passage, Canadian Arctic Archipelago, *J Geophys. Res*., 116*, C04010, doi:*10.1029/2010JC006119.

Polashenski C, Perovich D, Courville Z. 2012. The mechanisms of sea ice melt pond formation and evolution. *Journal of Geophysical Research*, 117, C01001

Polashenski, C. and others. 2015. Physical and Morphological Properties of Sea Ice in the Chukchi and Beaufort Seas during the 2010 and 2011 NASA ICESCAPE Missions. *Deep-Sea Res Pt II.* 118: 7–17, doi:10.1016/j.dsr2.2015.04.006.

Pomeroy JW, Brun E. 2001. Physical properties of snow. In: Snow Ecology: An Interdisciplinary Examination of Snow-Covered Ecosystems (eds Jones HG, Pomeroy JW, Walker DA, HohamRW), pp. 45–126. Cambridge University Press, Cambridge.

Prezelin BB, Moline MA, Matlick HA. ICECOLORS '93: Spectral UV radiation effects on Antarctic frazil ice algae. 1998. *Antarct. Res. Ser*. 73: 45-83.

Prezelin BB, Hofmann EE, Mengelt C, Klink JM. 2000. The linkage between upper circumpolar deepwater (UCDW) and phytoplankton assemblages on the west Antarctic Peninsula continental shelf. *J Mar Res.* 58: 165-202.

Prezelin BB, Hofmann EE, Moline MM, Klinck JM. 2004. Physical forcing of phytoplankton community structure and primary production in continental shelf waters of the Western Antarctic Peninsula, 62, 419 – 460.

Quillfeldt CHV, Ambrose WG Jr, and Clough LM. 2003. High number of diatom species in first year ice from the Chukchi Sea. *Polar Biol. 26: 806 - 818.*

R Core Team. 2013. R: A language and environment for statistical computing. R Foundation for Statistical Computing, Vienna, Austria. ISBN 3-900051-07-0, URL http://www.R-project.org/.

Ramette, A. 2007. Multivariate analyses in microbial ecology. *FEMS Microbiol Ecol*. 62: 142-160, doi:10.1111/j.1574-6941.2007.00375.x.

Renaud PE, Carroll ML, Ambrose WG Jr. 2008. Effects of global warming on Arctic sea-floor communities and its consequences for higher trophic levels. In C.M. Duarte (ed.): Impacts of global warming on polar ecosystems. Pp. 139 175. Bilbao: Fundacio´n BBVA.

Riebesell U, Schloss I, and Smetacek V. 1991. Aggregation of algae released from melting sea ice: implications for seeding and sedimentation. *Polar Biol* 11: 239.

Rodriguez F, Varel M, Zapata M. 2002. Phytoplankton assemblages in the Gerlache and Bransfield Straits (Antarctic Peninsula) determined by light microscopy and CHEMTAX analysis of HPLC pigment data. *Deep Sea Res II* 4-5: 723-747.

Ross RM, Quetin LB, Martinson DG, Iannuzzi RA, Stammerjohn SE, Smith RC. 2008. Palmer LTER: Patterns of distribution of five dominant zooplankton species in the epipelagic zone west of the Antarctic Peninsula, 1993-2004. *Deep Sea Res II* 55: 2086-2105.

Ross RM, Quetin LB, Newberger T, Shaw CT, Jones JL, Oakes SA, Moore KJ. 2014. Trends, cycles, interannual variability for three pelagic species west of the Antarctic Peninsula 1993-2008. *Mar Ecol Prog Ser* 515: 11-32.

Rozema PD, Venables HJ, Van de Poll WH, Clarke A, Meredith MP, and Buma AGJ. 2017. Interannual variability in phytoplankton biomass and species composition in northern Marguerite Bay (West Antarctic Peninsula) is governed by both winter sea ice cover and summer stratification. *Limnol Oceanogr* 62: 235-252.

Rózańska M, Gosselin M, Poulin M, Wiktor JM, and Michel C. 2009. Influence of Environmental Factors on the Development of Bottom Ice Protist Communities during the Winter-Spring Transition. *Mar Ecol Prog Ser.* 386: 43-5, doi:10.3354/meps08092.

Rysgaard, S., M. Kühl, R. N. Glud, and J. W. Hansen. 2001. Biomass, Production and Horizontal Patchiness of Sea Ice Algae in a High-Arctic Fjord (Young Sound, NE Greenland). *Mar Ecol Prog Ser.* 223: 15-26, doi:10.3354/meps223015.

Saenz BT and Arrigo KR. 2012. Simulation of a sea ice ecosystem using a hybrid model for slush layer desalination. *J Geophys Res*. 117

Saenz BT and Arrigo KR. 2014. Annual primary production in Antarctic sea ice during 2005 2006 from a sea ice state estimate. *J Geophys Res:Oceans*. 119: 3645-3678.

Saito K and Taniguchi A. 1987. Phytoplankton Communities in the Bering Sea and Adjacent Seas II. Spring and Summer Communities in Seasonally Ice-Covered Areas. *Astarte.* 11:27-35.

Savidge G, Harbour D, Gilpin LC, Boyd PW. 1995. Phytoplankton distributions and production in the Bellingshausen Sea, Austral spring 1992. *Deep Sea Res II 42*: 1201-1224.

Serebrennikova YM, Fanning KA. 2004. Nutrients in the Southern Ocean GLOBEC region: variations, water circulation, and cycling. *Deep Sea Research Part II: Topical Studies in Oceanography*, *51*(17), 1981-2002.

Schandelmeier L, and Alexander V. 1981. An Analysis of the Influence of Ice on Spring

Phytoplankton Population Structure in the Southeast Bering Sea. *Limnol and Oceanogr.* 26: 935-43, doi:10.4319/lo.1981.26.5.0935.

Schnack SB. 1985. Feeding by *Euphausia superba* and copepod species in response to varying concentrations of phytoplankton. In: Siegfried WR, Condy PR, Laws RM (ed) Antarctic nutrient cycles and food webs, Springer, Verlag Berlin Heidelberg

Schofield O, Saba G, Coleman K, Carvalho F, Couto N, Ducklow H, Finkel Z, Irwin A, Kahl A, Miles T, Montes-Hugo M, Stammerjohn S, Waite N (2017) Decadal variability in coastal phytoplankton community composition in a changing West Antarctic Peninsula. *Deep-Sea Res I* 124: 42-54.

Screen JA, Simmonds I, and Keay K. 2011. Dramatic inter‐annual changes of perennial Arctic sea ice linked to abnormal summer storm activity, J. Geophys. Res., 116, D15105,

Serreze, M. C., M. M. Holland, and J. C. Stroeve. 2007. Perspectives on Arctic's Shrinking Sea Ice Cover. *Science.* 315: 1533–37.

Sharma S, and Jackson DA. 2007. Fish Assemblages and Environmental Conditions in the Lower Reaches of the Northeastern Lake Erie Tributaries. *J Great Lakes Res*. 33:15-27, doi http://dx.doi.org/10.3394/0380 1330(2007)33[15:FAAECI]2.0.CO;2.

Sherr EB, Sherr BF, and Hartz AJ. 2009. Microzooplankton grazing impact in the Western Arctic Ocean. *Deep-Sea Res PT II.* 56 (17): 1264–1273.

Sherr EB, Sherr BF, and Ross C. 2013. Microzooplankton grazing impact in the Bering Sea during spring sea ice conditions. *Deep-Sea Res PT II*. 94: 57–67.

Smith REH, Gosselin M, and Taguchi S. 1997. The Influence of Major Inorganic Nutrients on the Growth and Physiology of High Arctic Ice Algae. *J Marine Syst.* 11: 63-70, doi:10.1016/j.dsr2.2011.06.005.

Smith REH, Harrison WG, Harris LR, and Herman AW. 1990. Vertical fine structure of particulate matter and nutrients in sea ice of the high Arctic, *Can J. Fish. Aquat. Sci*, 47: 1348-1355.

Smith WO, and van Hilst CM. 2003. Effects of assemblage composition on the temporal dynamics of carbon and nitrogen uptake in the Ross Sea. In: DiTullio GR, Dunbar RB (eds) Biogeochemistry of the Ross Sea. *Antarct Res Ser* 78:197–208.

Stabeno PJ, Schumacher JD, Davis RF, and Napp JM. 1998. Under-ice Observations of Water Column Temperature, Salinity, and Spring Phytoplankton Dynamics. *J of Mar Res*. 56: 239-255.

Stambler N, Lovengreen C, and Tilzer MM. 1997. The Underwater Light Field in the Bellingshausen and Amundsen Seas (Antarctica). *Hydrobiologia.* 344: 41–56,

doi:10.1023/A:1002993925441.

Stammerjohn SE, Martinson DG, Smith RC, Iannuzzi RA. 2008. Sea ice in the western Antarctic Peninsula region: Spatial-temporal variability from ecological and climate change perspectives. *Deep Sea Res II* 55: 2041-2058.

Stammerjohn S, Massom R, Rind D, Martinson D. 2012. Regions of rapid sea ice change: An interhemispheric seasonal comparison, Geophysical Research Letters, 39: L06501.

Steinberg DK, Ruck KE, Gleiber MR, Garzio LM, Cope JS, Bernard KS, Stammerjohn SE, Schofield OME, Quetin LB, Ross RM. 2015. Long term (1993-2013) changes in macrozooplankton off the Western Antarctic Peninsula. *Deep-Sea Res* I 101: 54-70.

Stroeve JC, Markus T, Boivert L, Miller J, and Barrett A. 2014. Changes in Arctic Melt Season and Implications for Sea Ice Loss. *Geophys Res Lett.* 41: 1216–1225, doi:10.1002/2013GL058951.

Stroeve J, Holland MM, Meier W, Scambos T, and Serreze M. 2007. Arctic sea ice decline: Faster than forecast, *Geophys Res. Lett*, 34: L09501.

Stroeve JC, Markus T, Boisvert L, Miller J, and Barrett A. 2014. Changes in Arctic melt season and implications for sea ice loss. *Geophys. Res. Lett*., 41, 1216–1225, doi:10.1002/2013GL058951.

Sukhanova IN, Flint MV, Pautova LA, Stockwell DA, Grebmeier JM, Sergeeva VM. 2009. Phytoplankton of the western Arctic in the spring and summer of 2002: Structure and seasonal changes. *Deep-Sea Res PT II. 56:* 1223-1236.

Syvertsen EE. 1991. Ice algae in the Barents Sea: types of assemblages, origins, fates, and role in the ice-edge phytoplankton bloom. *Polar Res.* 10:277-287.

Syvertsen EE, Kristiansen S. 1993. Ice algae during EPOS, leg 1: assemblages, biomass, origin, and nutrients. *Polar Biol* 13: 61-65.

Szymanski A, and Gradinger R. 2016. The Diversity, Abundance and Fate of Ice Algae and Phytoplankton in the Bering Sea. *Polar Biol.* 39: 309–325, doi:10.1007/s00300-015-1783-z.

Taniguchi A, Saito K, Koyama A, and Fukuchi M. 1976. Phytoplankton Communities in the Bering Sea and Adjacent Seas I. Communities in Early Warming Season in Southern Areas. *Journal of Oceanographical Society of Japan.* 32: 99-106.

Tedesco L, Vichi M, Haapala J, and Stipa T. 2009. An enhanced sea-ice thermodynamic model applied to the Baltic Sea. *Boreal Environment Research*. 14:68-80.

Tedesco L, Vichi M, Haapala J, and Stipa T. 2010. A dynamic Biologically Active Layer for numerical studies of the sea ice ecosystem. *Ocean Modelling*. 35: 89-104,

https://doi.org/10.1016/j.ocemod.2010.06.008.

Tedesco L, Vichi M, Haapala J, and Thomas DN. 2012. Process studies on the ecological coupling between sea ice algae and phytoplankton. *Ecological Modelling*. 226:120-138, https://doi.org/10.1016/j.ecolmodel.2011.11.011.

Tedesco L, and Vichi M. 2014. Sea Ice Biogeochemistry for Modellers. PLOS one. 9: e89217

Ter Braak CJF. 1985. Correspondence Analysis of Incidence and Abundance Data: Properties in Terms of a Unimodal Response Model. *Biometrics. 41*:859-873, doi:10.2307/2530959.

Ter Braak CJF, and Prentice IC. 1988. A Theory of Gradient Analysis. *Adv Ecol Res*. 18: 271-317, doi: http://dx.doi.org/10.1016/S0065-2504(08)60183-X

Ter Braak CJF, and Verdonoschot PFM. 1995. Canonical Correspondence Analysis and Related Multivariate Methods in Aquatic Ecology. *Aquat Sci*. 57: 255-289, doi:10.1007/BF00877430.

Thomas DN, Lara JN, Haas C, Schnack-Schiel SB, Dieckmann GS, Kattner G, Nothig E.-M., Mizdalski E. 1998. Biological soup within decaying summer sea ice in the Amundsen Sea, Antarctica, *Antarct Res Ser* 73: 161-171.

Timcoe GW and Frederking RMW. 1996. A review of sea ice density. *Cold Reg Sci and Technol.* 24:1-6.

Tison JL, Brabant F, Dumont I, and Stefels J. 2010. High resolution DMS and DMSP time series profiles in decaying summer first-year sea ice at ISPOL (Western Weddell Sea, Antarctica), *J Geophys Res 115*: G04044.

Tremblay C, Runge JA, and Legendre L. 1989. Grazing and Sedimentation of Ice Algae during and Immediately after a Bloom at the Ice-Water Interface. *Mar Ecol Prog Ser.* 56: 291-300, doi:10.3354/meps056291.

Tremblay J.-E., Michel C, Hobson KA, Gosselin M, and Price NM. 2006. Bloom dynamics in early opening waters of the Arctic Ocean. *Limnol and Oceanogr*. 51*:900-912 doi: 10.4319/lo.2006.51.2.0900.*

Trimborn S, Hoppe CJM, Taylor BB, Bracher A, Hassler C. 2015. Physiological characteristics of open ocean and coastal phytoplankton communities of Western Antarctic Peninsula and Drake Passage waters. *Deep-Sea Res I.* 98:115-124.

Trevena AJ, Jones GB, Wright SW, Van den Enden RL. 2000. Profiles of DMSP, algal pigments,nutrients, and salinity in pack ice from eastern Antarctica*, J Sea Res* 43: 265-273.

Turner J, Colwell SR, Marshall GJ, Lachlan-Cope TA, Carleton AM, Jones PD,

Lagun V, Reid PA, and Iagovkina S (2005) Antarctic climate change during the last 50 years. *Int J Climatol* 25: 279–294.

Vancoppenolle M, Meiners KM, Michel C, Bopp L, Brabant F, Carnat G, Delille B, Lannuzel D, Madec G, Moreau S, Tison JL, Van den Merwe P. 2013. Role of sea ice in global biogeochemical cycles: emerging views and challenges. *Quarternary Science Reviews* 79: 207-230.

Van de Poll WH, Lagunas M, de Vries T, Visser RJW, Buma AGJ. Non-photochemical quenching of chlorophyll fluorescence and xanthophyll cycle responses after excess PAR and UVR in *Chaetoceros brevis*, *Phaeocystis antarctica* and coastal Antarctic phytoplankton. *Marine Ecology Progress Series* 426: 119-131.

Van Heukelem L, Thomas CS (2001) Computer-assisted high performance liquid chromatography method devel- opment with applications to the isolation and analysis of phytoplankton pigments. *J Chromatogr A* 910:31−49.

Van Leeuwe MA and Stefels J. 1998. Effects of iron and light stress on the biochemical composition of Antarctic *Phaeocystis* sp. (Prymnesiophyceae). II. Pigment Composition, *J. Phycol*, 34, 496-503.

Van Leeuwe MA and Stefels J. 2007. Photosynthetic responses in *Phaeocystis antarctica* towards varying light and iron conditions. *Biogeochemistry* 83: 61-70.

Varela M, Fernandez E, Serret P (2002) Size-fractionated phytoplankton biomass and primary production in the Gerlache and south Bransfield Straits (Antarctic Peninsula) in Austral summer 1995 – 1996. Deep Sea Res II 49:749−768

Vaughan D G, Marshall GJ, Connolley WM, Parkinson C, Mulvaney R, Hodgson DA, and King JC. 2003. Recent rapid regional climate warming on the Antarctic Peninsula. *Climatic Change*, 60, 243-274.

Venables HJ, Clarke A, Meredith MP. 2013. Wintertime controls on summer stratification and productivity at the western Antarctic Peninsula. *Limnol and Oceanogr* 58*: 1035-1047.*

Vernet M, Martinson D, Iannuzzi R, Stammerjohn S, Kozlowski W, Sines K, Smith R, Garibotti I. 2008. Primary production within the sea-ice zone west of the Antarctic Peninsula: I- Sea ice, summer mixed layer, and irradiance *Deep-Sea ResII* 55: 2068-2085.

Wadhams P, Lange MA*,* Ackley SF. 1987. The ice thickness distribution across the Atlantic sector of the Antarctic Ocean in midwinter. *J Geophys Res* 92*:* 14535–14552.

Waite A, Fisher A, Thompson PA, Harrison PJ. 1997. Sinking rate versus cell volume relationships illuminate sinking rate control mechanisms in marine diatoms. *Mar Ecol Prog Ser*. 157: 97-108.

Wakatsuchi M, and Ono N. 1983. Measurements of Salinity and Volume of Brine Excluded from Growing Sea Ice. J Geophys Res. 88: 2943–2951, doi:10.1029/JC088iC05p02943.

Watanabe E, Onodera J, Harada N, Aita MN, Ishida A, and Kishi MJ. 2015. Wind-driven interannual variability of sea ice algal production in the western Arctic Chukchi Borderland. *Biogeosciences*, 12, 6147–6168.

Webster MA, Rigor IG, Nghiem SV, Kurtz NT, Farrell SL, Perovich DK, and Sturm M. 2014. Interdecadal changes in snow depth on Arctic sea ice, J. Geophys. Res. Oceans, 119, 5395– 5406, doi:10.1002/2014JC009985.

Welch HE, and Bergmann MA. 1989. Seasonal Development of Ice Algae and Its Prediction from Environmental Factors near Resolute, N.W.T. *Can J Fish Aquat Sci.* 46: 1793-1804, doi: 10.1139/f89-227

Welch HE, Legault JA, and Bergmann MA. 1987. Effects of Snow and Ice on the Annual Cycles of Heat and Light in Saqvaqjuac Lakes. *Can J Fish Aquat Sci.* 44: 1451-1461, doi:10.1139/f87-174.

Wiktor J. 1999. Early Spring Microplankton Development under Fast Ice Covered Fjords of Svalbard, Arctic. *Oceanologia.* 41: 51–72.

Zapata M, Rodriguez F, and Garrido JL. 2000. Separation of Chlorophylls and Carotenoids from Marine Phytoplankton: A New HPLC Method Using a Reversed Phase C_8 Column and Pyridine-Containing Mobile Phases. *Mar Ecol Prog Ser.* 195: 29-45, doi:10.3354/meps195029.

Zeebe RE, Eicken H, Robinson DH, Wolf-Gladrow D, and Dieckmann GS. 1996. Modeling the Heating and Melting of Sea Ice through Light Absorption by Microalgae. *J Geophys Res.* 101: 1163, doi:10.1029/95JC02687.

Zhang Q, Gradinger R, and Spindler M. 1998. Dark Survival of Marine Microalgae in the High Arctic (Greenland Sea). *Polarforschung.* 65: 111–16.

Zhang Q, Gradinger R, Spindler M. 1999. Experimental study on the effect of salinity on growth rates of Arctic-sea-ice algae from the Greenland Sea. *Boreal Environ Res*. 4:1-8.

Zhou, Q., P. Wang, C. Chen, J. Liang, B. Li, and Y. Gao. 2015. Influences of Sea Ice on Eastern Bering Sea Phytoplankton. *Chinese J of Oceanol and Limnol.* 33: 458–67, doi:10.1007/s00343-015-3367-8.